THE ADSORPTION OF WATER VAPOUR ON IONIC CRYSTALS

by

Peter Gill Hall, B.Sc.

A thesis submitted for the Degree of
Doctor of Philosophy in the
University of London

Department of Physical and Inorganic Chemistry,
Imperial College of Science and Technology,
London, S.W.7.

September, 1961

ABSTRACT

The adsorption of water vapour on ionic crystals has been investigated, mainly at temperatures between 0°C and -45°C, using a thermistor pressure gauge technique. Adsorption isotherms were obtained at different temperatures, enabling the isosteric heats and entropies of adsorption to be determined. Krypton was used for measurements of surface area.

With vacuum deposited films of KCl, the isosteric log plots at low coverage showed a break at about -25°C, indicating a higher heat of adsorption at the higher temperature, and the proposed mechanism for this was based on a phase change involving the solubility of the adsorbent. The heats of adsorption at the higher temperature showed no significant variation with coverage, while those at the lower temperature increased sharply from 3 kcal per mole to a constant level corresponding to the heat of liquefaction of water. The value of 3 kcal per mole was shown theoretically to correspond to adsorption above the lattice cell centre where the electrostatic field is zero.

The silver halides and PbF_2 gave an inflexion in the early stages of the isosteric heat curve. This could be explained, semi-quantitatively, on the basis of lateral interactions between square arrays of adsorbed molecules. However, with CaF_2 and PbI_2, the crystal structure of the adsorbent seemed to be the dominant feature in determining the adsorptive properties. Two-dimensional

condensation occurred on CaF_2 and a mechanism of adsorption by hydrogen-bonding was proposed. The heats of adsorption at various stages of the photochemical decomposition of AgBr were tentatively explained, following considerations of the entropy and approximately calculated heat of adsorption, in terms of adsorption in surface cation vacancies.

The effect of lateral interactions between water molecules adsorbed on some of the insoluble adsorbents was also reflected by activation energy plots of the rates of adsorption.

ACKNOWLEDGMENTS

I wish to express my thanks to Professor R.M. Barrer, for providing research facilities, and to my supervisor, Professor F.C. Tompkins, for his valuable guidance and assistance throughout this work.

I should also like to thank my fellow students and colleagues, in particular Drs. P.M. Gundry and F.V. Allan, for their stimulating discussions and advice.

My thanks are due to the College Technical Staff for their assistance and co-operation.

I am indebted to the United States Air Force for the provision of a Fellowship.

P.G. Hall

CONTENTS

Table of figures

1. Introduction

1.1. General Introduction

The object of this study has been to initiate work on the adsorption of polar vapours by crystalline heteropolar solids. This is of interest in as much as it can provide information on the mechanism of the primary step in the process of heterogeneous nucleation of a condensed phase from the vapour. In serving as a foreign nucleus it seems reasonable that any particle must first act as an adsorbent in an adsorption process consisting of the formation of a monolayer, then multilayers, and finally involving bulk condensation. From this standpoint, it would be expected that the formation of several layers at low relative pressures would characterise whether an adsorbent could function as an efficient nucleating agent. Water as the adsorbate is of considerable practical importance in view of artificial stimulation of rainfall (1). Since silver iodide, which has an ice-like crystalline structure, is a good nucleating agent for water vapour, it has been suggested (2) that, in general, structural similarity between the nucleating agent and the condensed phase of the adsorbate is a prerequisite for the growth of the seed crystal. The validity of this generalisation is open to question and it is therefore desirable to investigate the adsorption of water vapour on a range of solids, both known nucleating agents and others. The general approach to the problem has been to study the effect on adsorption isotherms and adsorption thermodynamics, of varying the crystal lattice parameters and crystal type. The heteropolar adsorbents studied are divided into three groups, namely,

a) KCl; vacuum deposited films.

b) Silver Halides, AgCl, AgBr and AgI; precipitated powders.

c) Lead Halides, PbI_2, PbF_2; precipitated powders.

In addition, a homopolar adsorbent, CaF_2, was investigated. Since the heterogeneous nucleation of water usually takes place at temperatures below the freezing point, the present study was largely confined to low temperatures: and, in view of the relative insensitivity of thermodynamic measurements in the multilayer region, the experiments were mainly concerned with the monolayer region.

1.2. Review of Previous Work

Durau (3) was one of the first to study quantitatively adsorption on ionic crystals. He obtained isotherms at 18°C for a variety of adsorbates on NaCl. Generally the adsorption was small and the high pressures employed prevented the attainment of great accuracy. In the case of water vapour, solubility of the surface complicated the adsorption process and it was not possible to obtain reliable results.

Frazer (4) used an optical method due to Rayleigh, involving the measurement of the ellipticity of light reflected from the surface of polished and freshly cleaved samples of rock salt. Exposure to a water vapour pressure less than that of a saturated solution of NaCl produced no permanent change in the surface. This was not so, however, for polished surfaces, which showed the effect at a much lower pressure. It was concluded that the thickness of the adsorbed film at room temperature was limited to about 6×10^{-8} cm. i.e., at the most, two layers.

Uhara and Nakamura (5) measured the adsorption of water vapour on KBr at room temperature by a simple gravimetric method and obtained an isotherm corresponding to Type III of the Brunauer classification (6), in which the curve is convex to the pressure axis. They also measured the electrical conductance in the surface layer and showed that this was negligible up to a relative pressure of about 0.75, at which the conductance increased markedly. These effects were interpreted in terms of the mobility of ions in the adsorbed layer. It was suggested that, at small adsorptions, the complete hydration of ions was impossible and the ions could not be separated from the surface. However, for a large number of adsorbed layers the surface ions possessed considerable freedom and mobility. Since ions are known to be negatively adsorbed at the surface of an aqueous solution the same may also be true for adsorbed water films, from which it follows that surface conductance would not be observed until the layer reached a certain thickness.

The adsorption of water vapour by silver iodide has been reported by Coulter and Candella (7), who obtained isotherms at 16°C, 34°C and 50°C. The results were complicated by the anomalous shape of the isotherms which was attributed to the hydration of a surface impurity. After allowing for this, by subtraction of the amount of water taken up by the phase transition, Type III isotherms were obtained. There was little indication of affinity of the adsorbent for the adsorbate, a result which was difficult to understand in view of the known nucleating efficiency of AgI. It was suggested that the anomaly may

be in part due to the higher temperature and that the surface may have been different from the uncondensed smoke of silver iodide used for nucleation. The AgI used for this particular experiment was prepared by precipitation, followed by solution in anhydrous ammonia and removal of the ammonia in vacuo. Surface areas calculated from the adsorption data by the B.E.T., Harkins-Jura and Hüttig methods (section 1.3.) were all less than 0.1 $m^2 g^{-1}$. Heats of adsorption calculated from the B.E.T. equation were 0.4 to 1 kcal per mole greater than the heat of liquefaction whilst the isosteric heats were about 1 kcal per mole less.

Type III isotherms have also been obtained by Birstein (8) who studied the adsorption of water vapour on commercial, laboratory prepared and aerosol samples of silver iodide and lead iodide at temperatures of -20°C and +25°C. To obtain sufficiently high surface areas for the McBain-Bakr (9) gravimetric method to be employed, the commercial and laboratory prepared samples were milled to a mean particle size diameter of 1 to 2 microns. The isosteric heats of adsorption at low coverage were about 18 kcal per mole for AgI and 22 kcal per mole for PbI_2, decreasing exponentially towards the heat of liquefaction as more layers were adsorbed. In contrast with the results of Coulter and Candella, it was shown that as many as 200 layers could be adsorbed without formation of the liquid phase. Even at a coverage of 50 layers the heat of adsorption was greater than the heat of liquefaction. Since under ordinary conditions the Van der Waals forces acting from the surface fall off with the cube of

the distance, it would be expected that the influence of the surface would not extend beyond the first few layers, and the general conclusion was that the silver iodide surface produced oriented water molecules which themselves transmitted forces through comparatively large distances by a polarisation mechanism.

At this point it is relevant to describe the work of Halsey (10) who developed a new technique for examining the multilayer region, with the idea of overcoming the difficulty of examination of adsorption at pressures approaching the condensation pressure. This consisted of first depositing one or more layers of a more condensible gas ('pre-freezing') before determining an isotherm of a less condensible gas. An example of this was the adsorption of argon on pre-frozen xenon on carbon, anatase and silver iodide. It was shown that distinguishable stepwise isotherms, a necessary characteristic of a uniform surface (11), were obtained up to six layers of pre-adsorbed xenon on carbon, showing that surface forces were still operative at this distance: thereafter the isotherms were indistinguishable. In the case of anatase and silver iodide, however, the steps were less evident and the isotherms coincident after two pre-frozen layers. It thus seemed that the structure of the underlying solid was important, and that with these particular ionic adsorbents only a few layers of xenon could be stabilised, thicker layers being unstable both with respect to the bulk solid and thinner layers. In a later publication (12) Karasz, Champion and Halsey applied the same procedure to pre-frozen layers of ice on anatase and silver iodide. The argon isotherms were indistinguishable after

three ice layers on anatase and one layer on silver iodide. From the latter fact they concluded that the growth of layers of ice on AgI did not take place under equilibrium conditions and that the two surfaces were energetically incompatible.

A rather more extensive investigation of the adsorption of water vapour on AgI has recently been made by Russian workers (13). They obtained Type II isotherms at four temperatures between -20 and +20°C. Results also given for AgCl were similar, but in the case of the iodide the isosteric heat of adsorption below 0°C was greater than that above 0°C, indicating a phase change in the adsorbed layer (section 1.7.). Below 0°C the heat of adsorption decreased slightly with increasing coverage towards the heat of liquefaction, but above 0°C the trend was reversed. Jenkins (14) obtained water isotherms on NaCl at 0°C and 10°C using a McBain-Bakr type of quartz fibre helical spring balance. The results at -23°C, however, were ambiguous, and it was concluded that three factors were responsible:

a) slow adsorption on the glass walls,

b) slow adsorption on the salt,

c) slow attainment of the water vapour-ice equilibrium.

The isosteric heat of adsorption increased from about 4 kcal per mole at low coverage to about 10 kcal per mole at higher coverages, thus approaching the heat of liquefaction of water. From the B.E.T. plot of the water vapour isotherms, the effective surface area of the water molecule was shown to be 28.5 A^2, consistent with a model of single water molecules adsorbed above the centres of lattice squares.

Infra red studies, at both room and liquid air temperatures, of water adsorbed on alkali halides were made by Price, Sherman and Wilkinson (15). Pressed discs formed from finely powdered chlorides, bromides and iodides of Na, K, Rb and Cs acted as matrices of large surface area on which thin films of adsorbed water could be studied. Electron micrographs showed that the discs were mosaics of tiny crystals about one micron in diamter packed together. Plots of frequency of the strongest band (corresponding to a modified asymmetrical stretching vibration of the water molecule) in the 3000 to 3500 cm^{-1} region versus unitary displacement of the negative halogen ion gave straight lines for each common metal ion. The greatest shift in frequency relative to the free molecule was produced by the lattice with the halogen of greatest electronegativity and the metal ion of lowest electropositive character. This indicated that the water was attached by hydrogen bonding to the negative ions. It was claimed that this was supported by considerations of the relative size of the ions: the positive ions, particularly those of sodium and potassium, being smaller, tend to be buried in the structure by the negative ions and are relatively inaccessible from the outside. Certain bands visible in the spectrum of a thin layer of water adsorbed on caesium iodide showed extreme sharpening on going to liquid air temperature. These bands were only obtained with caesium and thallium halides, and were presumed to be associated with the positive ion of the body-centred cubic lattice, to which bonding would be through the oxygen of the water. With

larger amounts of adsorbed water, bands appeared in the 2000 to 2200 cm^{-1} region. These corresponded to bands which in water and ice have been interpreted as a molecular deformation plus a libration of the molecule against the forces of association with the other molecules. Their frequencies in a caesium chloride disc were 2110 and 1977 cm^{-1} compared with 2243 and 2041 cm^{-1} in ice, and probably corresponded to 'frozen-in' states of the hydrated ions.

Papée and Laidler (16) have used a Tian-Calvert (17) type of microcalorimeter to measure the heats of adsorption of water vapour at 25°C on microcrystals of NaCl, the rate of heat production being followed as a function of time. A special apparatus of two interconnecting cells, one containing the salt and the other containing the water, allowed measurements to be made of both the heat evolved in the salt cell and of the heat absorbed in the water cell. The amount of water taken up by the salt could be calculated, knowing the heat of vaporisation of water. Microcrystals of salt were produced by the technique of Young and Morrison (18) in which vapour was swept from the surface of molten NaCl in a turbulent stream of nitrogen and carried into an electrostatic precipitator, where the small particles were collected. With crystals of surface area between 1 and 15 square metres per gram, it was found that three distinct processes occurred in the following order: a) simple adsorption of water on the surface, b) decrease in the surface area, and c) penetration of water into the lattice. During the second stage no adsorption could be detected.

On crystals of larger surface area there was considerable overlapping of the three phenomena, but the general mechanisms appeared to be the same. The heat of adsorption during stage a) was about 36 kcal per mole which is too large to correspond to simple physical adsorption; it was presumed that some change in the surface was occurring at the same time although the amount of water adsorbed at this stage was only about one twelfth of that required to form a monolayer.

Detailed studies of the surface enthalpies of NaCl have been made by Benson (19) who measured the heat evolved on the solution in water of NaCl crystals of high surface area. The plot of heat of solution versus surface area gave a straight line of slope equal to the surface enthalpy. Papée's results (16) similarly gave straight line plots corresponding to surface enthalpies of about the same magnitude as those obtained by Benson. This was regarded as further evidence that the stages a) and b) above were not sharply separated from one another, although it would appear that all the surface had been broken down by the end of stage b).

Papée (20) has further investigated the adsorptive properties of 'blue' NaCl obtained by 'straining' the surface of microcrystals in a high frequency discharge. Following exposure to water vapour at 25°C and unit relative pressure, the surface area was measured as a function of time and compared with the sintering rate of the normal unstrained surface. Induction periods were found in both cases, indicating surface adsorption, but the 'blue' sample sintered much more slowly

than normal NaCl. The heat of adsorption (21) on the 'blue' NaCl was several times greater than previously found for normal NaCl, and the process appeared to consist of two overlapping stages instead of three. Stage A, corresponding to the adsorption of water vapour and breaking down of the surface, released about twice as much heat with the blue salt as with the normal chloride, and the amount of water adsorbed was almost twice as large. Stage B represented the penetration of water into the lattice and reaction with colloidal sodium and F centres in the first strata. The process took much longer to reach completion than with stage A, and the heat released and amount absorbed were about ten times more than for uncoloured NaCl. This confirmed the expected reactivity of the blue particles to water vapour. Measurements of the potential of the crystals suggested that the hydration of the blue salt resulted in the possible build up of electrical charges on the surface, which would favour clustering of water molecules around a nucleus.

Microcalorimetry has also been used in the case of lead iodide (22) with particular reference to the effect of surface sintering by water vapour. Heats of sintering were calculated by comparing the results with earlier work (23) relating to the kinetic process of surface sintering. The decrease of the PbI_2 surface with time upon hydration followed a first order pattern according to the equation:

$$\log (S - S_{\infty}) = -.245t + A$$

S = specific surface at time t

S_{∞} = specific surface of the product after long exposure to water vapour

A = constant.

The same sintering characteristics were found for preheated and unheated samples, but the heated product adsorbed more water than the original salt. However, the heats of adsorption were about 14.5 kcal per mole for the unheated salt and 3.0 kcal per mole for PbI_2 heated to between 50 and 150°C. For lead monoiodide, PbI, obtained by thermal decomposition of the di-iodide, the pattern of heat evolution with time of exposure was different, and the overall process required more water to reach completion than with the di-iodide. The heat of adsorption was about 18 kcal per mole, although the actual heats evolved in the salt cell and absorbed in the water cell were much greater, probably partly due to the reaction of the water with the surface. In no case did the number of adsorbed water layers exceed 2.4, a result which was in complete disagreement with the earlier work of Birstein (8). Papée has pointed out that the thermal stability of the microcalorimeter to within 10^{-5} °C over long periods would necessarily detect any experimental abnormalities to which the discrepancy might be due, and suggests that small temperature differences between the source of water vapour and the salt in Birstein's system could be responsible.

Various results for the adsorption of water vapour on other ionic solids have been published. Many of these are not extensive, but some will be reviewed insofar as they illustrate the energetics of the process, possible mechanisms or interesting techniques.

Law (24) employed an unusual experimental technique with germanium oxide. After allowing the solid to attain equilibrium with water vapour at a particular temperature, the adsorbed water was desorbed at 350°C, as water plus hydrogen, into a calibrated volume where its pressure was measured. Isosteric heats of adsorption were observed to fall with increasing coverage from about 14.5 kcal per mole at low monolayer coverage to near the heat of liquefaction after two layers had been adsorbed. The thermodynamics of the system was discussed in terms of theories of multilayer adsorption.

Theimer (25) examined adsorption on $BaSO_4$ in the region of 0°C and obtained Type II isotherms. The isosteric heat, calculated from three temperatures, showed a secondary maximum of 13.0 kcal per mole at a point, derived from B.E.T. and Huttig isotherms, corresponding to completion of the monolayer.

The isosteric heat of adsorption of water at room temperature on molybdenum disulphide (26) decreased uniformly from about 10 kcal per mole to 4 kcal per mole as the first layer filled, and thereafter increased to about 6 kcal per mole at which it remained constant. Zettlemoyer (26) commented that this behaviour was almost identical for water adsorbed on graphon, thereby suggesting cluster adsorption. His interpretation was based on the fact that the B.E.T. monolayer coverage obtained from water isotherms was about 1/1500 of the B.E.T. monolayer coverage from nitrogen adsorption. The second layer began to form when only a small fraction of the total surface was filled. It was presumed that the hydrophobic graphon surface contained some

hydrophilic sites of high but non-uniform energy. After adsorption on these sites, a second layer formed in preference to adsorption on the surrounding hydrophobic area. Thus, it was not surprising that the heat of adsorption was found to be less than the heat of liquefaction, since, on this picture, the adsorbed molecules were isolated on the surface and the possibility of normal hydrogen bonding, which contributes largely to the high heat of liquefaction of water, was precluded.

Amphlett (27) investigated the effect of heating commercial samples of calcium fluoride on the water vapour adsorption characteristics at 25°C. When samples were repeatedly cycled through adsorption-desorption sequences involving heating to 100°C and above, the amount of water adsorbed was reduced and the monolayer volume decreased. After several such cycles there was no further change, suggesting that the heat treatment had de-activated some of the more active parts of the adsorbent surface.

Mays and Brady (28) used the nuclear magnetic resonance absorption method for water adsorption on titanium dioxide. At low coverage the adsorbed layer was shown to be mobile at temperatures as low as 77°K, but the energy of adsorption was still sufficiently strong to prevent the formation of clusters. Near the monolayer coverage, the adsorbed molecules became immobilised and the resonance had a breadth appropriate to that of ice.

The adsorption of water vapour on diamond and zinc blende is of some interest in view of the similarity of these structures to silver iodide and ice. Bowden and Throssel (29) measured the thicknesses of adsorbed water films by means of the Rayleigh optical method. It was shown that only a few layers were adsorbed, and there was no evidence of heavy adsorption even when the vapour was 90 per cent saturated.

It has been proposed that with certain solids, notably ionic oxides, the adsorbed water may be linked to the adsorbent by means of hydrogen bonds. Thus for water adsorbed on bauxite at $-80^{\circ}C$ there is evidence (30) for the structure:

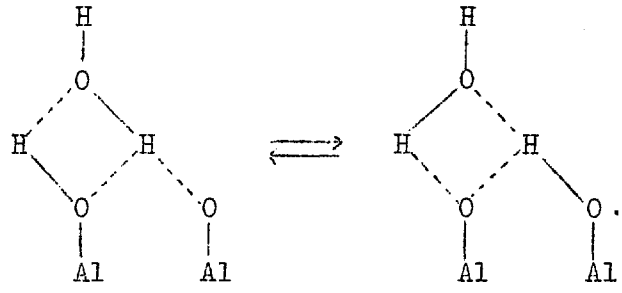

The differential heat of adsorption of water on Al_2O_3 at $18^{\circ}C$ to $35^{\circ}C$ (31) is about equal to the heat of liquefaction, which would be expected for two hydrogen bonds, each of energy 6 kcal per mole, per adsorbed molecule. Hickmott and Selwood (32) have investigated the effect further by means of proton relaxation time measurements on water, alcohols and n-hexane adsorbed on γ-Al_2O_3 at room temperature. The substrate was much more effective in lowering the relaxation time of protons in the associated liquids than in n-hexane. This

was explained qualitatively on the grounds of proton exchange between labile hydrogens in the associated liquids and lattice vacancies and protons incorporated in the alumina during preparation.

Ethyl alcohol is a polar molecule and, like water, although to a lesser degree, is capable of forming hydrogen bonds. Pearce and Rice (33) determined isotherms of water and alcohol on four ionic adsorbents at 99.4°C. At 140 mm pressure, zirconium dioxide was the best adsorbent for alcohol but the poorest for water, both on a volume or weight basis. On the volume basis, the order of the adsorbents for water was ThO_2, Al_2O_3, WO_3 and ZrO_2, whereas for alcohol it was exactly the reverse. Brunauer (6) considered that this was a clear example of 'specificity' in physical adsorption and was related to the stronger ion-dipole interaction energy between the surface and adsorbed water. In support of this he pointed out that the dipole moment (section 1.9.) of water per unit surface is almost two and a half times as large as that of alcohol.

During the last decade several workers (34) have studied the dielectric properties of water adsorbed on high surface area solids, particularly powdered silica gel. The technique usually involved the determination of the dielectric constant ε', and the relaxation time, τ, which is related to the frequency f_{max} at which the dielectric loss is a maximum. For water adsorbed on silica gel coated with a thin layer of NaCl, deposited by drying the gel after soaking in a solution of the salt, Kurosaki (35) showed that the value of f_{max} was the same as for water adsorbed on the uncoated gel. The interpretation was

that the stage 3 (see below) adsorbed water was in a more solid state than ordinary liquid water, and possessed characteristics approaching those of ice. This was based on the fact that, if any evolution of the salt had occurred, the specific conductivity, and hence the dielectric polarisation, would be altered. For the uncoated gel the curve of dielectric constant versus amount adsorbed showed three definite breaks corresponding to three stages of the process. Stage 1 corresponded to the region of low adsorption, stage 2 to multilayer adsorption, and stage 3 to capillary condensation.

1.3. The Adsorption Isotherm

The following section deals with the various theories or models for adsorption. The adsorption isotherm is the most convenient form in which to obtain and plot experimental data, and is usually the starting-point for theoretical treatments. One important restriction then for any valid theory of adsorption is that it predicts correctly the experimental isotherm. This however, in itself, is an insufficient test: further considerations of how the energy and entropy of adsorption vary with the amount adsorbed must be taken into account.

1.3.1. Langmuir adsorption

The Langmuir equation is perhaps the most important single equation in the field of adsorption. Although there are other isotherm equations that fit experimental data over a wider range, in most cases the starting point in their derivations is the Langmuir

equation, i.e.,

$$v = \frac{v_m bp}{1 + bp} \qquad \ldots\ldots\ldots\ldots\ldots\ldots\ldots \quad (1)$$

where v_m = the volume adsorbed when the surface is covered with a complete unimolecular layer, and b, the adsorption coefficient, is given by the original kinetic derivation of (1) by Langmuir (36) as,

$$b = \frac{\alpha_0 \exp\left(\frac{q}{kT}\right)}{k_0 (2\pi mkT)^{\frac{1}{2}}} \qquad \ldots\ldots\ldots\ldots\ldots\ldots\ldots \quad (2)$$

α_0 = condensation coefficient on the bare surface,

$$k_0 = \frac{\nu}{\exp\left(\frac{-q}{kT}\right)} ,$$

ν = rate of evaporation of molecules from the surface,

q = heat of adsorption.

In addition to the kinetic derivation of eqn.(1), similar forms have been derived thermodynamically by Volmer (37) and statistically by Fowler (38).

The principal postulates of the Langmuir isotherm can be summarised as:

a) The energy of adsorption is constant (which implies uniform sites and no interactions between adsorbate molecules).

b) The adsorption is on localised sites (which implies no translational motion of adsorbate molecules in the plane of the surface).

c) The maximum adsorption possible corresponds to a complete monomolecular layer.

Langmuir-type isotherms are characterised by having a linear low pressure region and an approach to saturation at high pressures. Many representative examples are given by Brunauer (6) and Schwab (39). The data are generally plotted according to the linear form and the constants b and v_m evaluated from the best fitting straight lines.

The Langmuir equation can be applied to the case of unimolecular adsorption on a heterogeneous surface, by assuming a certain type of distribution (40) of the heats of adsorption. The result is the well known empirical Freundlich equation:

$$v = kp^{\frac{1}{n}} \qquad \ldots\ldots\ldots\ldots\ldots\ldots \qquad (3)$$

where n is generally greater than 1. The Freundlich equation can also be obtained (41) by assuming that the adsorption is multimolecular, and that each adsorbed layer obeys a separate Langmuir equation with different constants.

1.3.2. <u>The potential theory</u>

A rather different approach to adsorption was made by Polanyi (42), who considered the potential field at the surface of the adsorbent, into which adsorbate molecules 'fall'. The adsorbed layer is most compressed at the surface of the solid and decreases in density outwards.

The potential of the adsorbent at a point i is given by:

$$\varepsilon_i = \int_{p}^{p_0} \left(\frac{RT}{p}\right) dp = RT \ln \frac{p_0}{p} \qquad \ldots\ldots\ldots\ldots \qquad (4)$$

where p_0 is the saturation pressure of the gas. The potential of the

molecule is thus equated to the work done in the isothermal compression of the gas from p to p_0. This is equivalent to assuming that the forces operative in the adsorption process are of the same nature and magnitude as between molecules in the gas phase, which may not be true if ion-dipole forces are important.

Corresponding to ε_i is a volume ϕ_i which represents the volume enclosed by the adsorbent and the equipotential surface, ε_i, and given by the ratio of mass adsorbed to liquid density at the isotherm temperature. The plot of ϕ_i versus ε_i is known as the characteristic curve and should be independent of temperature. The testing of the potential theory consists of the calculation of the characteristic curve from an experimental isotherm, and the calculation of other isotherms from the characteristic curve. Examples of the successful application of this to polar molecules such as CO_2 and CS_2 adsorbed on charcoal are given by Brunauer (6). However, Barrer and Brook (43) found in sorption by chabazite that the more polar the sorbate, the poorer the agreement with the Polanyi theory.

Bering and Serpinsky (44) have more recently attempted to use the potential theory to calculate the heats of adsorption from single isotherms, but their assumptions included a neglect of any net entropy change on adsorption. This is equivalent to assuming that the adsorbate is liquid, which probably restricts the method to near the capillary condensation region (45).

In general, the potential theory is very successful in accounting for the temperature dependence of physical adsorption, both uni- and

multimolecular, on heterogeneous surfaces. But it does not attempt to formulate an isotherm equation, therefore the scope of information obtainable is rather limited. Moreover, the available evidence suggests that the application to molecules as strongly polar as water would be even more limited.

1.3.3. The B.E.T. theory

Brunauer, Emmett and Teller (46) showed how to extend Langmuir's approach to multilayer adsorption, and their equation:

$$\frac{p}{v(p_o - p)} = \frac{1}{v_m C} + \frac{C - 1}{v_m C}\,\frac{p}{p_o} \qquad \ldots\ldots\ldots\ldots \qquad (5)$$

has had considerable success as a general method of obtaining surface areas from adsorption data.

The basic assumption was that the Langmuir equation applied to each layer, with the added postulate that for the first layer the heat of adsorption, E_1, had a special value, whereas for all succeeding layers it was equal to the heat of liquefaction, E_L, of the liquid adsorbate. A further assumption was that evaporation and condensation could occur only from or on exposed surfaces. As in the Langmuir model, the B.E.T. equation can also be derived from statistical mechanics.

Surface areas are obtained from the values of v_m, which is given by the slope $\left(\frac{1}{v_m C}\right)$ and intercept $\left(\frac{C - 1}{v_m C}\right)$ of the linear plot of $\frac{p/p_o}{v(1 - p/p_o)}$ against p/p_o. Since $v_m = v_o A/N\sigma_o$, the specific surface area, A, can be calculated by choosing some reasonable value

for the actual area, σ_0, per molecule.

The constant C is given by:

$$C = \frac{a_1 b_2}{b_1 a_2} \exp\left(\frac{E_1 - E_L}{RT}\right) \quad \ldots\ldots\ldots\ldots\ldots\ldots \quad (6)$$

where $\frac{a_1 b_2}{b_1 a_2} \simeq 1$.

The theory has several limitations. At low pressures it reduces to the Langmuir equation, consequently all the criticism that has been levelled against the Langmuir theory can be directed equally well against the B.E.T. theory in the low pressure region of the isotherm. The most active parts of the surfaces of most adsorbents are markedly heterogeneous with strongly varying heats of adsorption, therefore the Langmuir equation is not obeyed. For most adsorbents the B.E.T. theory applies only in the range $p/p_0 = 0.05$ to 0.30. Below $p/p_0 = 0.05$ the potential theory is probably the only theory which can deal successfully with physical adsorption.

Perhaps the outstanding fault of the B.E.T. model is the neglect of horizontal interactions. Hill (47) has taken this into account approximately, correcting the B.E.T. theory in the desired direction of reducing the amount of adsorption (above a monolayer) for a given relative pressure, and Halsey (48), from a somewhat more qualitative treatment of horizontal interactions, has concluded that adsorption in steps would occur on an ideally uniform surface. The effect of horizontal interactions is discussed more fully in section 1.6.

It may be mentioned that Hűttig (49) has derived a modified form of the B.E.T. equation by assuming that the rate at which the number of uncovered first layer molecules decreases is proportional, not to the number of uncovered second layer molecules as in the original B.E.T. derivation, but to the total number of molecules in the second layer. However, Hill (50) considers that although the equation may be sound empirically, the theoretical basis is open to doubt.

1.3.4. Use of krypton for surface area measurement

Since the work of Brunauer, Emmett and Teller (46) surface areas of solids have been determined most frequently from measurements of adsorption of gases at temperatures near their boiling points, preferably of nitrogen at -196°C. However, if the solid has a small surface area, e.g. less than 1 m^2/g, the use of a temperature below the boiling point is advantageous; in this way the quantity of gas in the dead space is reduced, permitting the volume adsorbed to be obtained more accurately. Krypton at -196°C is commonly used and Rosenberg (51) has employed the thermistor method to measure accurately, to less than 1 per cent, isotherms on powders of area as low as 50 cm^2. Beebe (52) previously used krypton with success to measure specific surfaces of about 400 cm^2. Making use of an anatase sample, the surface area of which had been measured by the absolute method of Harkins and Jura (53), he estimated the area occupied by the krypton atom in the monolayer to be 19.5 A^2, which is considerably higher than would be predicted on the assumption that the atoms in the monolayer formed a close packed liquid monolayer. This value is generally accepted nowadays.

Beebe also found that the equilibrium saturation pressure, p_0, for solid krypton at -196°C ranged from 1.8 to 2.62 mm, indicating a temperature variation for commercial liquid nitrogen of -194°C to -196°C. His extrapolated value for the liquid ranged from 2.63 to 3.72 mm. Emmett (52) suggested the use of the liquid value for p_0 because the isotherms for krypton at -196°C behaved as though they were governed by the vapour pressure of the supercooled liquid rather than of the solid.

1.3.5. Isotherms based on the equation of state of the adsorbate

If the adsorbate is regarded as a two-dimensional film analogous to those found with monolayers on liquid substrates, then straightforward application of the Gibbs equation gives:

$$\text{spreading pressure } \pi = \frac{RT}{v_0 A} \int_0^p v \, d\ln p \quad \ldots\ldots\ldots\ldots \quad (7)$$

Graphically, this integration corresponds to determining the area under a plot of v versus lnp. A difficulty, however, is involved with the uncertainty of estimating the area between zero pressure and the lowest measureable point. If the isotherm data are available to sufficiently low pressures, the ratio p/v may become constant, i.e. a linear or Henry's law is valid. Then eqn.(7) may be written in the form:

$$d\pi = \frac{RT}{v_0} \int_{(p/v) \text{ as } v \to o}^{(p_1/v_1)} v \, d\ln(p/v) + \frac{RTv_1}{v_0 A} \quad \ldots\ldots\ldots\ldots\ldots \quad (8)$$

If the entire region is linear, then p/v is constant and the above integral vanishes. Since the area, σ, per mole is given by $\frac{v_0 A}{v}$,

equation (8) reduces to the two-dimensional ideal gas law, $\pi\sigma = RT$. For adsorption data above the Henry's law region equation (7) may still be integrated between limits, giving:

$$\pi = \pi_1 + \frac{RT}{v_0 A} \int_{p_1}^{p_2} v \, d\ln p. \quad \ldots\ldots\ldots\ldots\ldots\ldots \quad (9)$$

Various discussions of the use of the Gibbs equation to obtain $\pi - \sigma$ values from adsorption data have been given by Innes and Rowley (54), Bangham (55) and Gregg (56). The latter has surveyed the various types of force area diagrams obtainable from adsorption isotherms in terms of phase changes (section 1.7) of the adsorbate.

A logical step to take next is to consider equations of state which contain a co-area term and an attractive force term, such as the two-dimensional Van der Waals equation, i.e.

$$\left(\pi + \frac{a_1 N^2}{A^2}\right) (A - Nb_1) = RT \quad \ldots\ldots\ldots\ldots\ldots\ldots \quad (10)$$

where the constants a_1 and b_1 are related to the three-dimensional constants for the same molecules in the gas phase. This predicts two-dimensional condensation phenomena just as does the three-dimensional analogue. The simplest isotherm corresponding to this type of equation is given (57) as:

$$\ln \frac{1 - \theta}{\theta} - \frac{\theta}{1 - \theta} + c\theta = -\ln kp \quad \ldots\ldots\ldots\ldots\ldots\ldots \quad (11)$$

where c is a function of a_1, b_1 and RT.

The various other types of two-dimensional Van der Waals equations generally lead to rather more complex isotherm equations. For example,

the virial type equation:

$$\pi = RT + \alpha\pi - \beta\pi^2 \quad \ldots\ldots\ldots\ldots\ldots\ldots \quad (12)$$

corresponds to the isotherm:

$$-\frac{\phi^2}{2\omega} + \frac{1}{2\omega}(\phi + 1)\left[(\phi - 1)^2 + 2\omega\right]^{\frac{1}{2}} - \ln\left\{(\phi - 1) + \left[(\phi - 1)^2 + 2\omega\right]^{\frac{1}{2}}\right\} = \ln kp \ldots \quad (13)$$

where $\phi = \frac{1}{\theta}$, and ω, the attractive interaction parameter $= \frac{2\beta RT}{\alpha^2}$.

An adsorption isotherm based on a two-dimensional equation of state which has aroused considerable interest was that suggested by Harkins and Jura (58). They proposed the equation

$$\pi = b - a\sigma \quad \ldots\ldots\ldots\ldots\ldots\ldots \quad (14)$$

and applied the Gibbs transformation to obtain,

$$\ln p/p_0 = B - A^1/v^2 \quad \ldots\ldots\ldots\ldots\ldots\ldots \quad (15)$$

where $A^1 = \frac{aA^2 v_0^2}{2RT}$. A great many Type II isotherms were shown to fit this equation, from the straight line plot of which the specific surface area can be calculated. The constant, a, is assumed to be related to the compressibility of the adsorbate and is independent of the nature of the solid. There is thus a close correspondence between the Harkins-Jura and B.E.T. equations, especially in the case of isotherms for which the B.E.T. constant, C, is 50 or higher (59). However, there is one point on which the two theories seem irreconcilable. The B.E.T. theory requires that, above a certain relative pressure, about $C^{-\frac{1}{2}}$ (57), the film is on the average, a multilayer, and that its thickness approaches infinity at saturation.

The Harkins-Jura treatment considers the adsorbate film to be monomolecular, or at least of constant thickness, and, moreover, fails to indicate that the saturation pressure should be of special significance.

1.4. Thermodynamics of Adsorption

1.4.1. Heat of adsorption

Two approaches have been used to derive the thermodynamic functions for the adsorption process. The first of these, standard solution thermodynamics, treats the adsorbate and adsorbent in association as a two component system, and leads to partial molar quantities. The second method, adsorption thermodynamics, considers the adsorbate as a one component phase in a potential field of the solid and leads directly to molar quantities. There are no differences in the results of the two methods but the former is easier to apply. Hill (60) has reviewed the essential points: these are as follows.

Consider a two component condensed phase of adsorbent A and adsorbed gas '1' in equilibrium with gas. The condensed phase has volume V, energy E, entropy S etc., and contains n_A and n_1 moles of the two types. E is completely determined by S, V, n_A and n_1. Then by the standard methods of solution thermodynamics it can be shown that:

$$dE = TdS - pdV + \mu_1 dn_1 + \mu_A dn_A$$

$$dG = -SdT + Vdp + \mu_1 dn_1 + \mu_A dn_A$$

$$d\mu_1 = -\bar{s}_1 dT + \bar{v}_1 dp + \left(\frac{\partial \mu_1}{\partial \Gamma}\right)_{T,p} d\Gamma$$

where,

$$\Gamma = \frac{n_1}{n_A} \; ; \quad \bar{s}_1 = \left(\frac{\partial S}{\partial n_1}\right)_{n_A,p,T}$$

and $$\left(\frac{\partial \ln p}{\partial T}\right)_{\Gamma} = \frac{s_G - \bar{s}_1}{RT} = \frac{H_G - \bar{H}_1}{RT^2} = \frac{q_{st}}{RT^2} \quad \ldots\ldots\ldots\ldots \quad (16)$$

This defines the isosteric heat of adsorption, usually denoted ΔH, which is a differential quantity.

ΔH is obtained from the slope of the plot of ln p versus $\frac{1}{T}$ at constant Γ. For calorimetric measurements with no external work (pdV) term the differential heat is given by,

$$q_d = \Delta H - RT \quad \ldots\ldots\ldots\ldots\ldots\ldots\ldots \quad (17)$$

However, RT does not usually amount to more than 5 to 10 per cent of the total heat of adsorption, and in some cases is not much more than the experimental error (6).

The measurement of the isosteric heat of adsorption plays an essential part in the interpretation of adsorption data. The magnitude of ΔH will usually indicate whether the attachment to the surface is of a physical nature or whether chemisorption has occurred. Also, investigations of the variation of ΔH with coverage can lead to a knowledge of the heterogeneity of adsorbents and the interactions between adsorbed molecules.

1.4.2. Entropy of adsorption

A knowledge of the entropy of adsorption is important from the point of view of the mobility and physical state of the adsorbate. The molar differential entropy, which is readily obtainable from eqn.(16), is given by:

$$s_1 = \left(\frac{\partial S}{\partial n_1}\right)_{n_A,p,T} \simeq \left(\frac{\partial S}{\partial n_1}\right)_{n_A,T} \quad \ldots\ldots\ldots\ldots\ldots \quad (18)$$

However, as is emphasised by Hill (60), it is the integral entropy, $S = n_1 s$, which is the quantity of direct statistical mechanical significance, being related, inter alia, to the number of possible quantum states of the system by the relation $s = k \ln W$, where W is the total number of indistinguishable configurations. The differential entropy is not relevant to discussions of order-disorder, randomness etc.

The various ways of obtaining integral entropies are summarised below.

(a) By finding the differential entropies down to very low coverages, extrapolating $\left(\frac{\partial S}{\partial n}\right)_{A,T}$ to $n_1 = 0$ and integrating. However, this is a very inaccurate method.

(b) From isotherm data at two different temperatures one can calculate the spreading pressure, $\pi = RT \int_0^p \Gamma \, d\ln p$ (T const.) ..... (19) using a much more accurate extrapolation to low coverage, and then employ the analogue of equation (16) at constant π.

(c) In the ideal case (Langmuir) of localised adsorption without interactions on a uniform surface, i.e. $\frac{\partial(\Delta H)}{\partial \theta} = 0$, the differential molar entropy is approximately equal to the integral molar entropy.

This can be seen by differentiating S = ns, i.e.

$$\left(\frac{\partial S}{\partial n}\right)_{T,p,n_A} \simeq \left(\frac{\partial S}{\partial n}\right)_{T,n_A} = s + n\left(\frac{\partial S}{\partial n}\right)_{T,p,n_A}$$

$$\text{or } \bar{s} \simeq s + n\left(\frac{\partial S}{\partial n}\right)_{T,n_A} \quad \ldots\ldots\ldots\ldots\ldots\ldots \quad (20)$$

and in the ideal Langmuir case, $\left(\frac{\partial S}{\partial n}\right)_{T,n_A} = 0$, so that $\bar{s} = s$. Here s refers to non-configurational entropy (section 1.4.3.).

Using the vapour in equilibrium with the adsorbate as the standard state, $\Delta G = 0$ and $\Delta S = S_s - S_G = \frac{-\Delta H}{T}$. The entropy S_G of the equilibrium gas phase is given by

$$S_G = S_G^o + \int_{T_o}^{T} \left(\frac{C_p}{T}\right) dT + R \ln(p/p_o) \quad \ldots\ldots\ldots\ldots\ldots \quad (21)$$

where S_G^o is the entropy at p_o and T_o. Thus absolute integral entropies of the adsorbate in the adsorbed state may be obtained from isosteric heats of adsorption and heat capacity data.

1.4.3. Non-configurational entropy

The entropy of the adsorbate is made up of two parts; the configurational term S_c which is a function of the number of ways the adsorbed molecules may be distributed over the surface, and the non-configurational term S_{nc} which is related to the partition functions for the various degrees of freedom of the adsorbate.

In the more commonly experienced cases of adsorption with lateral interactions on a heterogeneous surface the evaluation of S_c is extremely difficult, and in any case, as Hill (61) has pointed out, the division of entropy into configurational and non-configurational parts is quite arbitrary. However, for Langmuir adsorption,

$$\bar{S}_c = -R \ln \frac{\theta}{1-\theta} \quad \ldots\ldots\ldots\ldots\ldots \quad (22)$$

is an exact equation (62) and $S_{nc} = \bar{S}_{nc}$ can readily be determined.

A gas molecule containing n atoms has 3n degrees of freedom i.e. 3n modes of motion contributing to the entropy. For n = 3 there are 3 translational, 3 rotational and 3 internal vibrational terms. In the case considered it is unlikely that the internal vibrational term will be altered very much by the process of adsorption, so only the redistribution of the translational and rotational terms will be considered.

Kemball (63) has derived the expression

$$S = R \ln MTa + 65.8 \quad \ldots\ldots\ldots\ldots\ldots\ldots \quad (23)$$

for the translational entropy of a perfect two-dimensional gas of molecular weight M and with area, a, available per molecule. This provides a means of assessing the mobility of the adsorbed layer.

Now for localised adsorption where the adsorbate has little or no translational freedom,

$$S_{nc} = 3S_V + S_I + nS_R + (3 - n)S_L \quad \ldots\ldots\ldots\ldots \quad (24)$$

where

S_V = entropy associated with vibrations relative to the surface.

S_I = internal vibrational entropy.

S_R = entropy associated with unrestricted rotation about an axis normal to the surface,

S_L = librational or restricted rotational entropy terms about axes parallel to the surface.

S_V is given (63) by,

$$S = R\left[\frac{h}{kT}\left(\exp.\frac{h}{kT} - 1\right)^{-1} - \ln\left(1 - \exp\left(\frac{-h}{kT}\right)\right)\right] \quad \ldots\ldots\ldots\ldots \quad (25)$$

and S_R (64) by,

$$S = \tfrac{1}{2}R\left[\ln B + \ln T + 1\right] \quad \ldots\ldots\ldots\ldots\ldots\ldots \quad (26)$$

where $B = \dfrac{(8\pi^3 k.I_a)^{\frac{1}{2}}}{h}$ and I_a is the moment of inertia of the molecule.

S_L is given (45) by,

$$S = R\left[\ln A + 2\ln T - \ln\phi_m - \ln 2 + 2\right] \quad \ldots\ldots\ldots\ldots\ldots\ldots \quad (27)$$

for two restricted rotational degrees of freedom,

where $A = \dfrac{8\pi^2 k^2}{\sigma k^2}(I_b I_c)^{\frac{1}{2}}$

ϕ_m = restricting potential,

I_b and I_c are moments of inertia,

σ = symmetry number.

1.5. The Theoretical Basis of the Heat of Adsorption

At the equilibrium separation of the adsorbed atom or molecule from the adsorbent surface, the attractive and repulsive forces balance and the potential energy of the system is a minimum. The difference in energy of the adsorbate and adsorbent when completely separated, and when at equilibrium separation, is released as heat. The intermolecular energy terms involved are generally due to,

(a) Permanent electric moments)
(b) Polarisation effects) electrostatic energy

(c) Van der Waals dispersion forces

(d) Short range repulsive forces.

The energy of adsorption can be calculated by summation of the relevant interaction terms between the adsorbed molecule and all the atoms or ions of the adsorbent.

From this theoretical point of view the interaction of an inert gas atom and an alkali halide crystal is one of the best defined gas-solid adsorption systems. Lennard Jones and Dent (65) carried out calculations for the adsorption of neon on sodium fluoride and argon on KCl, making the assumption that the dispersion and repulsion energies acting between an ion of the crystal and the rare gas atom were the same as those determined from an analysis of virial coefficient data of the rare gas. It was found that, at the equilibrium distance directly above an ion, the electrostatic field was about 10 per cent of the van der Waals field, and that the position of minimum energy was actually above the centre of a lattice square where the electrostatic field is zero.

Lenel (66) calculated the van der Waals potential using the London equation, but evaluated the repulsion energy in a rather arbitrary way.

The most elaborate calculations so far have been made by Orr (67) for the systems argon on KCl and CsI, using the Kirkwood-Müller equation (68) for the dispersion energy, i.e.

$$U_{VDW} = \frac{\alpha_1 \alpha_2}{\frac{\alpha_1}{\chi_1} + \frac{\alpha_2}{\chi_2}} \cdot \frac{6mc^2}{R^6} \qquad \text{.....} \qquad (28)$$

where α = polarisability
χ = magnetic susceptibility
c = velocity of light
R = distance of separation
m = mass of the electron

and with complete summations of inverse 6th powers of distance over the whole crystal.

An exponential expression was used for the repulsion energy, the summation being for the nearest 14 to 16 ions. Integration over the remaining ions to infinity gave a negligible contribution.

Now in the case of water adsorbed on ionic crystals the calculation becomes considerably more complicated because, apart from the complex nature of the water molecule itself, the electrostatic terms due to ion-multipole and mutual polarisation energy have to be included in the Orr type summations. However, the problem can be much simplified in the case of the simple cubic crystals, such as KCl and AgBr, if it is assumed that the preferred adsorption site is above the cell centre where the electrostatic field is zero. The calculation of dispersion energy is similar to that for an inert gas, but the difficulty with using an exponential expression for the repulsion energy is in the evaluation of the disposable parameters. The best method is perhaps to consider the interacting species as having the same repulsion constants as the inert gases with which they are isoelectronic (69). Then the two constants for similar pairs may be related to the constant for an unlike pair by means of the equations (70),

$$A_{12}^{\frac{1}{n}} = \tfrac{1}{2}\left(A_{11}^{\frac{1}{n}} + A_{22}^{\frac{1}{n}}\right), \qquad \ldots\ldots\ldots\ldots\ldots\ldots \quad (29)$$

and $$U_R = \frac{A_{12}}{Z^n} \qquad \ldots\ldots\ldots\ldots\ldots\ldots \quad (30)$$

It would be expected that the interaction energy between a gas molecule and a plane surface of a crystal would depend on the distances and geometrical configurations characteristic of different crystal

faces. This has been treated theoretically by Lenel (66) and by Orr (67). Lenel calculated that the heat of adsorption of argon on caesium chloride was 3500 cal per mole for the 100 face of Cs ions, but only 2500 cal per mole for the 110 face. In this crystal the 100 face contains only one type of ion, the 110 face both types. Orr calculated that the heat of adsorption of argon on caesium iodide was 3170 cal per mole for the 100 face made up of Cs ions, and 2680 cal per mole for the same face composed of iodide ions. Generally it is not possible to investigate this experimentally with ionic crystals because ideal plane surfaces large enough to test adsorption theories are not available. Rhodin (71), however, found slightly different heats of physical adsorption on the three main crystal planes of copper; and the heat of adsorption on polycrystalline copper far exceeded that on the uniform planes. De Boer and Custers (72) and Barrer (73) have discussed that surface irregularities may profoundly alter the heat of adsorption.

The calculation of the surface field of ionic solids at distances appropriate to an adsorbed molecule is highly dependent on this distance, but no experimental method of measuring such has yet been developed. If an assumed distance is used, a field value of 4.3×10^7 v/cm (74) is found for argon on KCl; and, by measuring heats of wetting, Chessick (75) and co-workers have found the surface fields for CaF_2 and rutile to be 7.5×10^7 and 8.1×10^7 v/cm respectively. This gives some indication of the influence of the valency of the cation but the picture is rather complicated by the different anions and the diversity of crystal structure of these adsorbents.

1.6. Lateral Interactions between Adsorbed Molecules

Interactions between adsorbed molecules normally lead to an increased heat of adsorption for attraction, and a decrease for repulsion. Probably the simplest approximate approach to the problem is to assume that the adsorbate has sufficient mobility to obey a two-dimensional Van der Waals type equation of state (section 1.3.5.). A similar approach has been made by Lennard Jones and Devonshire (76) using a model based on the 'cell' theory of liquids. Both these theories, which arrive at the conclusion that the two-dimensional critical temperature, T_{2c}, is equal to half the three-dimensional critical temperature, T_{3c}, have been successful in explaining the behaviour of mobile adsorbates on uniform surfaces, but for localised adsorption the problem becomes considerably more complex.

Fowler and Guggenheim (77) have developed a quasi-chemical approximation based on the supposition that the $\frac{Bz}{2}$ pairs of nearest neighbour sites, where B is the number of surface sites and that each site has z nearest neighbour sites, are of three types: both sites occupied by adsorbed molecules; one occupied; and neither occupied. For a quasi-chemical equilibrium between the three different types of pairs, the equilibrium constant can be written as $4 \exp(\omega/kT)$, where 4 is the statistical factor and ω is the energy of interaction between adsorbed molecules on nearest neighbour sites. ($\omega > 0$ means repulsion). From this it is possible to find the equilibrium number of pairs of both occupied nearest neighbour sites as a function of temperature. This theory also

predicts the existence of a critical temperature, below which a first order phase change will be observed. For a plane square surface lattice of sites, T_{2c} is equal to $\frac{\omega}{1.386k}$.

The quasi-chemical approximation has been generalised by Hill (78), Yang (79) and Li (80) to include higher neighbour interactions over larger groups of sites than pairs. For a square array of sites involving different types of occupation by adsorbed molecules, the critical temperature is given by:

$$-\frac{\omega}{kT_{2c}} = 1.444\left[1 - 1.342(\omega^1/\omega) + 2.252(\omega^1/\omega)^2 - \ldots\right] \quad (31)$$

where ω^1 is the second neighbour interaction energy for the diagonal of a square. By extending the treatment to include third and still higher neighbour interactions, it should be possible to arrive at an exact solution, but in practice this is apparently too complex and has not yet been accomplished. The present solutions are still only approximate, and for this reason the present treatment of water adsorbed on ionic surfaces, where higher neighbour terms are expected to be particularly important, is restricted to a simple semi-quantitative approach.

1.7. Phase Changes of the Adsorbate

From a wide variety of adsorption data it seems that there is no great difference between the adsorbate and a compressed liquid or gas. Polanyi and Welke (81) first showed the phenomena of condensation of the adsorbate from a two-dimensional gas to a two-dimensional liquid in relation to their experiments on the adsorption of sulphur

dioxide on charcoal. They attributed a rising heat of adsorption to the heat given out in the condensation process. The condensation began when the adsorbate covered less than one per cent of the surface and the pressure was about 0.2 mm. The theory was later developed by Semenoff (82) and shown to explain the formation of liquid clusters or islands on the surface, suggested by Goldmann and Polanyi (83). There is also some evidence that at low enough temperatures the adsorbate behaves like a two-dimensional solid. Thus Jones and Gortner (84) measured by means of a dilatometer the freezing point of water adsorbed on silica gel. It was shown that the capillary adsorbed water froze at a continuously decreasing temperature, and at -48°C the adsorbate still contained 33 per cent of unfrozen water. Patrick and Kemper (85) came to a similar conclusion on the basis of measurements of the specific heat of water adsorbed on silica gel.

Following earlier work by Bangham (86), Gregg (56) showed that there was a resemblance between adsorbed films on solids and 'trough films' of insoluble substances on water. There was evidence for gaseous, liquid-expanded, intermediate, and liquid-condensed films at the gas-solid interface. These transformations were frequently much less sharp and correspondingly more difficult to detect than with the trough films. Harkins and Jura (87) later confirmed this resemblance using n-heptane adsorbed on reduced silver powder, Fe_2O_3 and graphite. Gregg and Maggs (88) used the two-dimensional compressibility of the film as a means of detecting phase transitions.

The compressibility, β, is given by

$$\beta = - \frac{S}{RTx} \cdot \frac{d\ln x}{d\ln p} \qquad \ldots\ldots\ldots\ldots\ldots\ldots\ldots \quad (32)$$

where S = surface area per g.

x = moles adsorbed per g.

and, writing $\beta^1 = \frac{\beta RT}{S} = - \frac{1}{x} \frac{d\ln x}{d\ln p}$ provides a means of detecting the phase transition by plotting β^1 against πS or, more simply, against $\ln p$.

The phenomenon of two-dimensional condensation is sometimes shown by marked discontinuities in the isotherms. Ross and Winkler (89) have discussed this for the system ethane adsorbed at 90°K on sublimed NaCl and KCl and commercial calcium fluoride. These authors stress that an important requirement for the condensation is that the adsorbent should have a large proportion of a single, unique and uniform surface ('homotattic' surface), in addition to the necessary condition that the temperature is below the two-dimensional critical temperature. Similar discontinuities in the isotherms have been observed by Edelhoch and Taylor (90) for argon and oxygen adsorbed on CaF_2. More recently, Fisher and McMillan (91) obtained reproducible two-dimensional condensations of krypton and methane, but not nitrogen, on sodium bromide. Surfaces sufficiently uniform to exhibit reproducible transitions were prepared by sintering the surface of the dehydrated hydrate on prolonged heat treatment. This reduced the surface area and sharpened the transition. A theory of localised adsorption was developed to explain this, and the

derived values of the energy of adsorption, lateral interaction energy and frequency of lateral vibration in the filled monolayer showed reasonable agreement with those calculated from independent atomic and ionic parameters.

Hodgson and McIntosh (92) have detected a phase change of water adsorbed on Vycor glass at -22°C by a technique involving dimensional changes. It was suggested that the transition was probably due to water contained in the pores. Phase changes of water adsorbed on glass, porcelain, selenium films and germanium have also been detected (93) by variations in the surface electrical conduction of the solid. No explanation of the type of change found was given for these systems.

The phase change of water adsorbed on silver iodide, but not silver chloride, shown by an increase in the isosteric heat of adsorption at the lower temperature has been referred to in section 1.2. Since no isotherms were determined between 0°C and -20°C it is not possible to tell whether the change was sharp or exactly at which temperature it occurred. It was noted, however, that the change became less marked as the coverage increased.

1.8. The Rate of Physical Adsorption

1.8.1. General

According to Langmuir (36), the adsorption process consists of three states: the motion of the molecules to the surface, the sojourn of the molecules on the surface, and the evaporation of the

molecules away from the surface to the gas phase. It is now known that the second stage also involves mobility: this movement may be along the surface, if it is a free surface, or into cracks or fissures or into the capillaries of porous solids.

Generally, the molecule in physical adsorption is not held by strong forces, and migration may take place readily even at low temperatures. However, since the heat of adsorption over different points of the crystal lattice is different (section 1.5), the migrating adsorbate molecule has to move over the surface from one potential minimum to another and has to traverse places of higher potential. The process therefore requires an activation energy. This is usually smaller than the heat of adsorption, unless the adsorbing centres are quite far apart in which case it can be almost as large as the heat of adsorption. When the thermal energy, RT, is approximately equal to the energy of activation the adsorbate molecule moves freely over the surface.

Tiselius (94) investigated the surface migration of adsorbed water and ammonia over zeolites. The adsorption of these strong permanent dipole molecules by such crystals gives a high heat of adsorption of 14-16 kcal per mole, so that a considerable activation energy would be expected for the slow surface diffusion. Tiselius obtained activation energies ranging from 40 per cent to 90 per cent of the heat of adsorption, depending largely on the crystal face.

In contrast, non-polar molecules adsorbed by Van der Waals forces have activation energies of about 400 cal per mole (95).

1.8.2. Rate equations

The theory of adsorption rates was first investigated by McBain (96), who regarded the rate determining step in the adsorption of hydrogen on charcoal as a process of solid solution, and, applying Fick's diffusion law, obtained:

$$v = A\left[\frac{\pi^2}{8} - \exp(-k^1 t)\right] \quad \ldots\ldots\ldots\ldots\ldots\ldots \quad (33)$$

where v is the volume dissolved at time t, and A and k^1 are constants.

In contrast, Langmuir (36) proposed that the experimentally measured rate of adsorption on a free surface was the difference between the rate at which molecules condense on the surface and the rate at which they leave the surface. From this it can be shown that

$$v = v_e\left[1 - \exp(-kt)\right] \quad \ldots\ldots\ldots\ldots\ldots\ldots \quad (34)$$

or

$$\log_e \frac{v_e}{v_e - v} = kt \quad \ldots\ldots\ldots\ldots\ldots\ldots \quad (35)$$

where v_e is the volume adsorbed at equilibrium, and k is a constant depending on the pressure. If the rate of adsorption is measured at constant volume and variable pressure, v_e will not be constant but will represent the equilibrium adsorption corresponding to the instantaneous pressure at time t.

Although the Langmuir equation was shown to be obeyed by a variety of gases on different surfaces, it was pointed out by Damköhler (97) that these were not free surfaces in the Langmuir

sense, and assumed that the slow step in adsorption was the diffusion of molecules into the pores of the adsorbent. He derived the equation:

$$\vartheta = 1 - \frac{8}{\pi^2}\sum_{m=0}^{\infty} \frac{\exp(-\delta(2m+1)^2)}{(2m+1)^2} \quad \text{(at constant pressure)} \quad \ldots\ldots\ldots\ldots\ldots \quad (36)$$

where ϑ is the fraction of the equilibrium amount adsorbed at time t, and $\delta = \left(\frac{2\pi}{L}\right)^2 Dt$, D being the diffusion coefficient and L the length of the capillary.

There is a strong formal resemblance between this equation and those of McBain and Langmuir, and it is not surprising that various adsorption systems could be fitted by the Langmuir equation. However, the crucial test of an adsorption rate equation is that, in addition to fitting the experimental data, it should also be consistent with the observed activation energies.

Adsorption times ranging from a few seconds to many hours and even weeks have been reported. For very long runs, Bangham and Sever (98) used the equation:

$$\log_e \frac{v_e}{v_e - v} = kt^n \quad \ldots\ldots\ldots\ldots\ldots\ldots\ldots \quad (37)$$

for the adsorption of polar molecules on glass. It may be noted that for n = 1, eqn.(37) becomes formally identical with Langmuir's equation, and that in the early stages of the process the normal laws of diffusion require that n = 0.5.

Isakawi and Kanamori (99) showed that the adsorption of light and heavy water vapour on MgO at 15°C to 30°C also obeyed eqn. (37), with n = 0.65 and k = 0.075 at 30°C. Half the equilibrium adsorption was reached in 10 to 30 mins. and it was concluded that the rate was mostly dependent on diffusion through the capillary pores. No activation energies were reported. However, recent studies (13) of the adsorption of water vapour on lead iodide showed that equilibrium was not reached even after several weeks.

Keii (100) has discussed the theoretical basis of empirical rate equations in terms of adsorption on a heterogeneous surface, for which it is possible to deduce the form of the isotherm from the rate equation. Thus, if E is the energy of adsorption and E^* the energy of activation, and if the distribution function $f^*(E^*)$ of a surface has an exponential form, $A^* \exp(\beta E^*)$, the form of f(E) of the surface should also be an exponential one, i.e. $A \exp(-\alpha\beta E)$. The former distribution leads to Bangham's rate equation, $C^* t^{\beta RT}$, while the latter leads to a Freundlich isotherm, $Cp^{\alpha\beta RT}$.

1.9. The Structure of Water

The infra-red spectrum of water vapour indicates that the water molecule has three different moments of inertia: it follows that the molecule is triangular. Both OH bonds are identical, and Herzberg (101) has calculated that the equilibrium OH internuclear separation is 0.958 Å, while the equilibrium oxygen bond angle, Θ, is 104° 27'.

The essential features of the electron distribution may be illustrated by reference to the work of Burnelle and Coulson (102). The bonding orbitals are sp^3 hybrids, implying that the electron distribution has approximately the symmetry of a tetrahedron. However, the bond orbitals and OH directions do not coincide, and each bond has dipole moments both along and at right angles to its direction. An important conclusion is the large contribution, μ_L, to the total molecular dipole moment, μ, that arises from the lone pair electrons. For $\Theta = 105^0$, the calculated values of μ and μ_L are 1.52×10^{-18} e.s.u. and 1.69×10^{-18} e.s.u. respectively, the lone pair contribution being greater than μ itself. Therefore the greater part of the dipole moment of water resides in the lone pairs. The experimentally determined value of μ is 1.83×10^{-18} e.s. .. (69).

The water molecule also has quadruple moments, the values of which are not known, but their existence makes it difficult to set up a satisfactory point charge model of the molecule (103). However, bearing this in mind, it is possible to arrive at models of the form shown in Fig.1. When considering water-adsorbent interactions these models must, a) explain the observed dipole moment, b) give an account of orientation effects, and c) to be useful, permit interaction energy calculations to be reasonably simple. These conditions are best met by resolving the models shown to the form of a linear dipole in which the dipole vector is directed along the bisector of the H-O-H angle and the charge separation is

Fig.1. Point-charge Models of the Water Molecule.

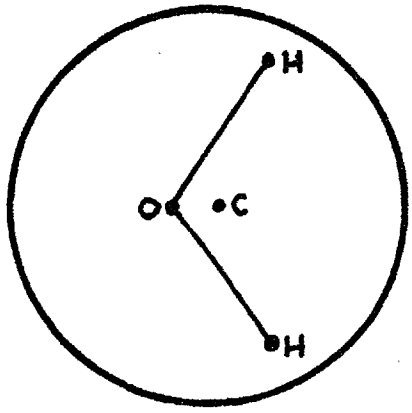

(a) Bernal and Fowler (1933)

at H : + 0.49e
at C : - 0.98e
OC = 0.15 Å

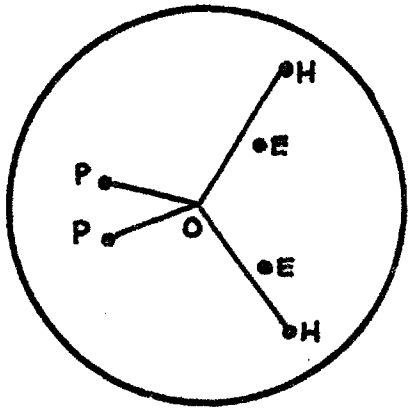

(b) Burnelle and Coulson (1957)

Positive charges at H and O, negative at E and P.
Tetrahedral angles.

at H : + e
at E : -2e
at O : +6e
at P : -2e

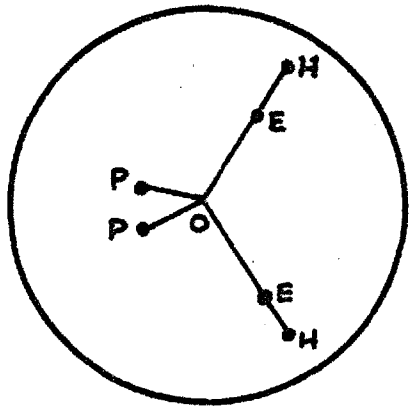

(c) Schneider (1955)

Tetrahedral angles.

at H : +e
at E : -2e
at O : +6e
at P : -2e

OH = .97 Å
OE = .609 Å
OP = .29 Å

taken to be the projection of the OH bond length on this bisector. The linear form used in this work comprises charges of 1.567×10^{-10} e.s.u. separated by a distance of 1.2 Å.

From the point of view of adsorption, water has the strongest dipole, although the absolute values of the dipole mements of many other molecules are greater. However, water has the largest value per unit surface, assuming that the area occupied by the molecule on the surface corresponds to liquid-like packing. Thus, the adsorption of water on ionic adsorbents occupies a rather unique place in physical adsorption.

The structure of the condensed phase of water has attracted considerable attention for many years. Ice is certainly known to exist in several different forms (104), depending on the temperature and pressure, all of which are based on the diamond-like model in which each molecule is co-ordinated tetrahedrally to four others, the arrangement extending throughout the whole crystal. X-ray data show that the O----O distance is 2.76 Å. In liquid water, the structure is not so certain: Bernal and Fowler (105) proposed that the regular tetrahedral arrangement extended over comparatively small groups of molecules, and for a given group persisted only for a short time. However, infra-red studies (106) show evidence of the existence of an octahedral structure, with an O---O distance of 3.1 Å. This represents the average molecular arrangement at room temperature. Probably the tetrahedral structure contributes to some extent to the overall arrangement, especially near the melting point and in the supercooled state.

2. Experimental

2.1. Apparatus

2.1.1. General description

The vacuum adsorption apparatus is shown in Fig.2a. The pumping section consisted of a single stage mercury diffusion pump backed by a Speedivac rotary oil pump. This was capable of obtaining a vacuum of 10^{-6} mm mercury. Mercury cut offs were incorporated in the apparatus where possible, but in the water vapour section stop-cocks and joints lubricated with silicone high-vacuum grease were used to exclude mercury vapour. The apparatus was largely made up of separate krypton and water vapour storage sections which could both be connected via the dosing system to the adsorption cell and thermistor assembly. The various parts are described in detail below.

2.1.2. The thermistor gauge

The principle of the thermistor pressure gauge is the same as that of the Pirani gauge, but with the important difference that the semi-conducting material of the thermistor bead shows an exponential variation of resistance with temperature, and therefore higher sensitivity. Thermistors also have the advantage of being very small, and hence of low heat capacity, and are extremely robust: they can be readily fitted into a very small adsorption cell. The thermistors used in this work were specially matched pairs supplied by Standard Telephones and Cables Ltd., and had the following characteristics at 20°C and 10^{-6} mm mercury:

Resistance at zero power;	50,000 ohms
Voltage at 0.5 mA;	2 volts
Voltage at 30 mA;	1 volt

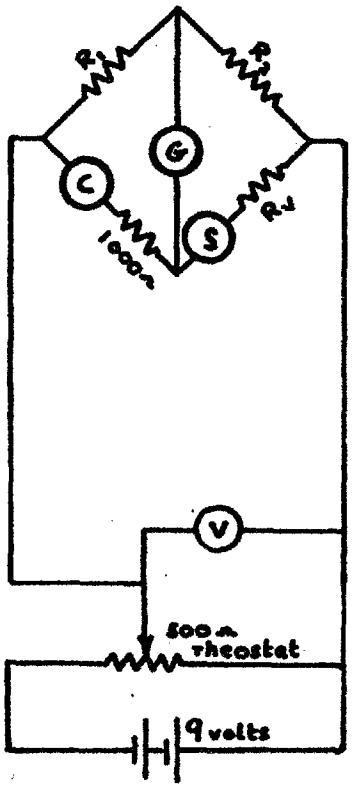

Fig. 2c.

Fig. 2b.

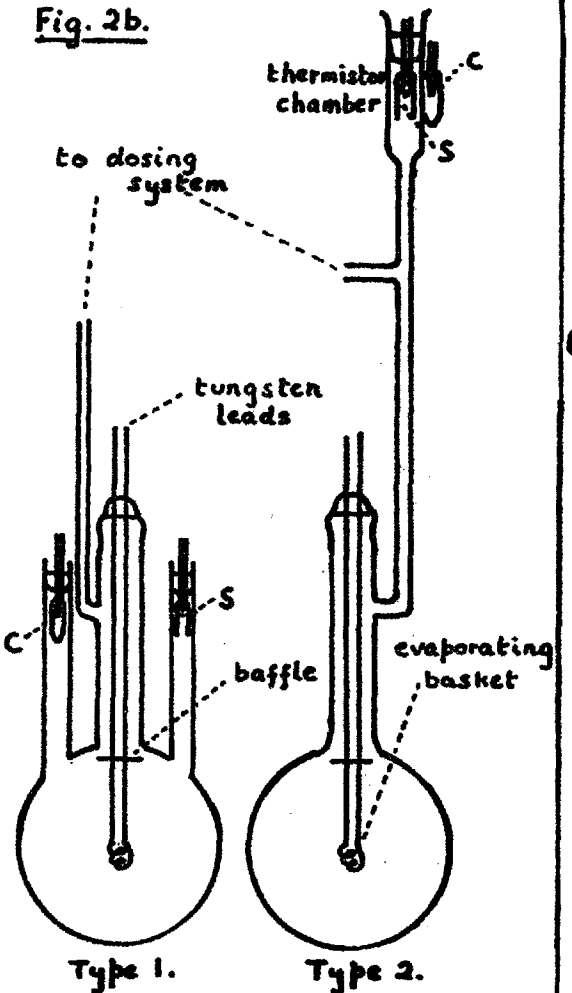

S = sensing thermistor
C = compensating thermistor

Fig. 2a

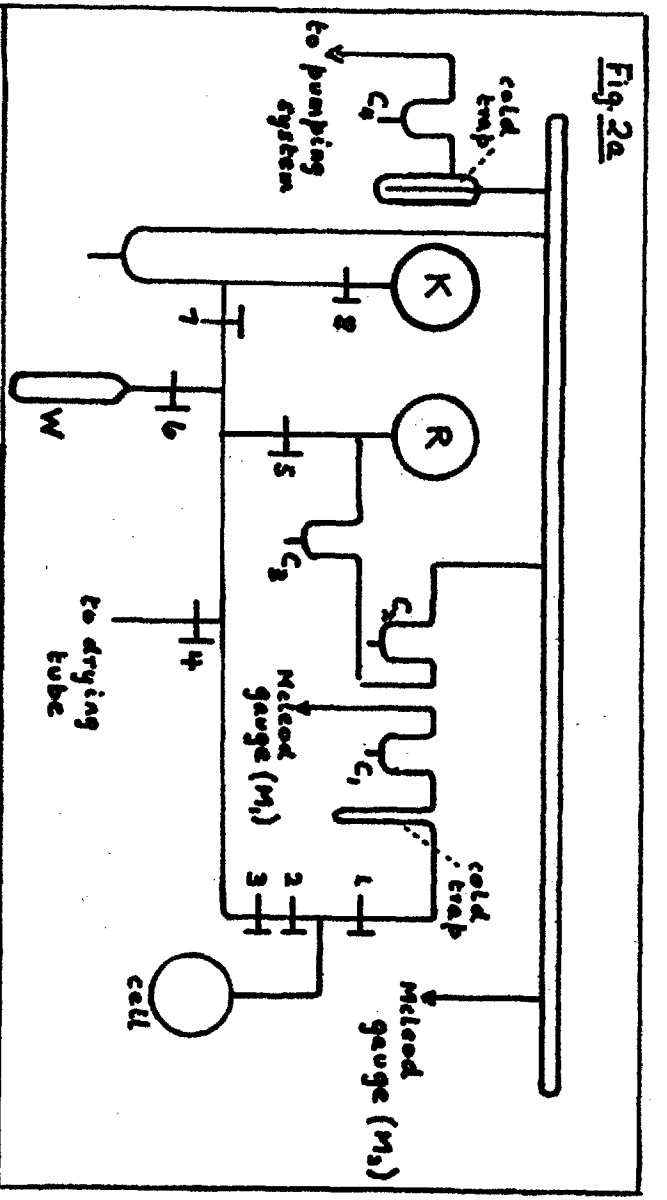

The thermistors were supplied with two platinum leads; these were spot welded $\frac{1}{4}$ inch from the bead junctures to tinned copper leads which could be pinch-sealed through a B.14 cone to the cell.

The control circuit shown in Fig.2c was a Wheatstone bridge network, powered by two 4.5 volt heavy duty batteries, with the exposed or sensing thermistor balanced against the matched compensating thermistor sealed inside an evacuated case. Admission of gas to the cell enhanced heat dissipation, hence lowered the temperature and raised the resistance of the thermistor, and a bridge imbalance resulted. By decreasing the variable resistance, R_v, the balance could be restored. The voltage across the bridge was set at 8 volts by means of the 500 ohm rheostat and the voltmeter (V), a type 8 avometer capable of being read to 0.02 volts. 8 volts was chosen to give a current through the thermistor, in vacuo, of 2.0 mA when the decade box ratio arms R_1, R_2 and R_v were 3000, 3470 and 1240 ohms. Two 1000 ohm decade boxes reading to 0.1 ohm were used for R_v, and an additional 1000 ohm decade box was added to the compensating thermistor arm of the bridge to ensure that the thermistor could not be damaged by currents heavier than 2.0 mA. The resistance of the Scalamp galvonometer (G) was 900 ohm.

The calibration curves for krypton and water vapour are shown in Fig.3. In the low-pressure region the gauge was about four times more sensitive to water vapour than krypton, as would be expected from the difference in thermal conductivity. Thus, below 0.02 mm mercury the sensitivity was 4.5 ohm/micron for water vapour and 1.1 ohm/micron for krypton. Since the galvonometer gave a deflection of

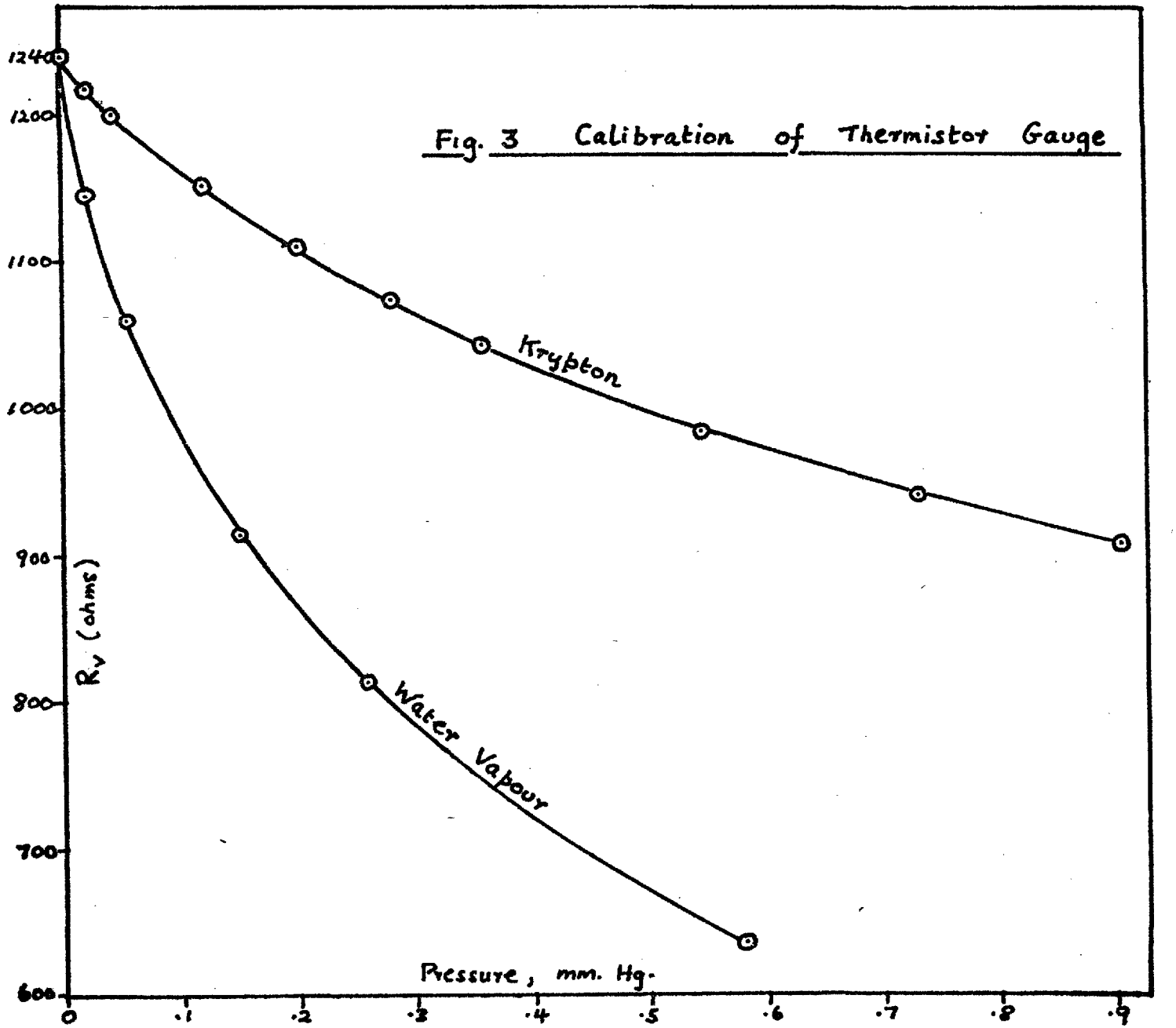
Fig. 3 Calibration of Thermistor Gauge
1240
1200
1100
1000
900
800
700
600
R_V (ohms)
Krypton
Water Vapour
Pressure, mm. Hg.
0
.1
.2
.3
.4
.5
.6
.7
.8
.9

about 4 mm/0.1 ohm in the highest sensitivity range, the thermistor was capable of measuring changes in water vapour pressure of about 5×10^{-5} mm, and detecting changes less than this. Both curves showed decreasing sensitivity with increasing pressure, and, in the region of 0.5 mm, the sensitivities to water vapour and krypton were 0.375 and 0.29 ohm/micron respectively.

2.1.3. The adsorption cell

The two types of adsorption cell used are shown in Fig.2b. In type 1 both thermistors were sealed by means of B.14 joints into side arms connected to the 55 mm diameter cell at the centre of which was located the molybdenum wire evaporating basket. The basket, made by winding on a conical former, was spot welded to nickel clips attached to two 1 mm tungsten rods which were led through a pinch seal to a variac and transformer. At the entrance to the spherical part of the cell a glass baffle plate was sealed to the tungsten rods to prevent film deposition inside the central arm.

Cell type 2, with which most of the adsorption experiments were carried out, was exactly the same as type 1, but with the two side arms replaced by a thinner (10 mm) single side arm leading to the thermistor chamber and the dosing system. The thermistor chamber enclosing the sensing thermistor, with the compensating thermistor secured to the side, was situated 18 inches above the cold bath level to eliminate the heat transfer effects experienced with cell type 1. During experiments with photo-sensitive adsorbents, the whole of the cell and thermostat assembly, described in section 2.1.4., was painted

black and covered with black cloth;and, in addition, the cell bulb was coated with aluminium foil, since heating and cooling of this part invariably caused some of the paint to flake off.

2.1.4. The thermostat system

Because the thermistor gauge proved to be very sensitive to fluctuations in room temperature, to the extent of about 1 ohm change in R_v per ^{o}C at 10^{-3} mm, it was necessary to thermostat the whole of the cell side arm including the thermistor chamber and the tube leading to the dosing system. This was done by means of tightly coiled rubber tubing (1 cm) wound round several layers of aluminium foil and through which water controlled at $35 \pm 0.2^{o}C$ was pumped from a reservoir via a Stuart Turner circulating pump. The purpose of the aluminium foil was to promote efficient heat transfer from the rubber tube to the glass, and to increase the diameter of the side arm so that the rubber coil could be wound tightly without folding. The temperature of the water in the reservoir was controlled by means of an immersed heating bulb and a Sunvic controller and relay.

2.1.5. The gas storage and dosing system

In Fig.2a, the bulbs marked K and W represent the krypton and water storage reservoirs from which measured pressures of the adsorbates could be introduced into the dosing volume (1.73 ml) enclosed by taps 2 and 3. The pressure of the spectrally pure krypton, supplied by British Oxygen Co. Ltd., was measured either with the mercury manometer or the McLeod gauge (M_1) calibrated to read pressures up to 5 mm mercury. The reservoir R was used to control the krypton supply and as a secondary storage chamber. The water storage reservoir (W)

contained glass wool soaked in distilled water, so giving a large surface area from which known (107) saturation vapour pressures could be established in the dosing volume by immersing the water reservoir in a constant low-temperature bath. Tap 4 led to a magnesium perchlorate drying tube through which dry air or nitrogen could be let into the apparatus, and Tap 1 and the cut offs, 1, 2 and 3 enabled the various sections to be pumped down separately. The two cold traps were cooled in liquid nitrogen and a separate McLeod gauge (M_2) was added to the main vacuum line.

2.2. Experimental procedure

2.2.1. Preparation of adsorbents

2.2.1.1. Vacuum deposition of films : KCl and AgCl

Films of KCl were deposited on the walls of the cell, under a vacuum of 10^{-5} to 10^{-6} mm, by passing a current of 3 amps through the evaporating basket containing a compressed pellet of KCl (A.R. 0.3 to 0.5 g) previously prepared in an ordinary pellet press. No cooling of the cell was required but in some cases it was necessary to rotate the evaporating basket, by turning the ground glass joint carrying the tungsten rods, in order to produce uniform films. The whole of the KCl pellet usually evaporated in about 30 minutes. However, attempts to apply the same method with silver chloride were unsuccessful; and even with slow and moderate heating of the pellet the film was discoloured. This was one reason why most of the other adsorbents, discussed below, were used in powdered form.

2.2.1.2. Silver halides

Finely divided AgCl (10 g), AgBr (20 g) and AgI (8 g) were precipitated in the cold by the slow addition of a slight excess of A.R. $AgNO_3$ solution to A.R. potassium halide solution. After filtration the precipitates were washed several times with distilled water before being transferred directly to the adsorption cell, where they were dried by pumping under vacuum for 48 hours prior to the normal outgassing procedure (section 2.2.2.). The whole operation was conducted in photo-insensitive red light.

2.2.1.3. Lead halides and calcium fluoride

Lead iodide (15 g) was precipitated in the cold by the addition of a slight excess of A.R. lead acetate solution to A.R. potassium iodide solution, filtered off, washed several times with distilled water and then dried in an oven at 100°C before being crushed to a powder and transferred to the cell. In the case of lead fluoride (6 g) a very finely divided precipitate was precipitated in the same way as the iodide, but using A.R. sodium fluoride, and, after filtration and washing, was transferred to the cell as a thick suspension in water. On evaporation of the water at 100°C, under vacuo, a thin film of lead fluoride was deposited on the walls of the cell. The calcium fluoride (1 g) used was supplied in laboratory fine chemical form by Hopkins and Williams Ltd. Before being transferred to the cell, the sample was ignited in a crucible at 600°C for 15 mins.

2.2.2. Outgassing procedure

A prime consideration in outgassing was the avoidance of temperatures which might cause excessive sintering of the adsorbent surface. The standard procedure was to heat slowly under vacuo to 110°C over a period of several hours and then maintain the salt at this temperature for about 18 hours to give an outgassing rate, at room temperature, of 10^{-4} mm per hour.

2.2.3. Photolysis

The photochemical decomposition of the silver bromide was carried out using a 150 watt tungsten lamp situated 12 inches from the side of the cell for first, two hours, and then for a further four hours. During the irradiation periods, the sample was stirred constantly with a spatula while a stream of dried nitrogen was passed through the cell to prevent contamination from the atmosphere.

2.2.4. Preparation of low temperature baths

Various organic solvents of laboratory reagent quality were used for producing low temperatures, in the range -10.5°C to -45°C, by adding liquid nitrogen to the solvent until a viscous mixture was obtained. The solvents were, diethylene glycol (-10.5°C); carbon tetrachloride (-23 to -25°C); bromobenzene (-31°C); ethylene chloride (-36°C) and chlorobenzene (-45°C). These temperatures were repeatedly checked using mercury in glass and alcohol in glass thermometers.

2.2.5. Calibration

2.2.5.1. Volume

The dosing volume enclosed by taps 2 and 3 was accurately calibrated by the method of weighing a bead of mercury. This volume was then used for expanding known pressures of krypton into other sections of the apparatus, where measurement of the resulting pressure with the thermistor and McLeod gauges allowed the various volumes to be calculated. The volume of the cell up to the cold bath immersion level was measured by filling with water.

2.2.5.2. Pressure

The krypton calibration of the thermistor gauge was carried out, when the cell was immersed in liquid nitrogen, by sharing known pressures of krypton contained in the dosing volume with the cell. For water vapour, the thermistor was calibrated for points corresponding to the saturation pressures of water vapour at the various low temperatures referred to in section 2.2.4. This was done by immersing the cell in each cold bath, including ice, before repeatedly sharing doses of water vapour with the cell until the thermistor gauge showed no further change in pressure.

Thermal transpiration corrections for water vapour were not made in view of the large diameter (20 mm) of the central tube, and the comparatively small temperature gradient (65°K). With krypton, the much higher temperature gradient (230°K) would mean a large correction, but even this is small, as is illustrated by the results of Table I calculated from the data of Bennett and Tompkins (108).

Table I. Thermal transpiration corrections for krypton

p_1 = pressure at 78°K, mm Hg
p_2 = pressure at 308°K, mm Hg
diameter of tube = 20 mm

p_2	p_1/p_2
.01	.94
.02	.978
.03	.989
.04	.993
.055	.996
.075	.998

The krypton B.E.T. surface area measurements are concerned with relative pressures above 0.02 mm, i.e. p = 0.05 mm, where the p_1/p_2 ratio is close to unity.

2.2.6. Adsorption measurements

The krypton adsorption isotherms were determined by admitting doses of about 20 mm pressure into the cell immersed in liquid nitrogen. The dose pressures were measured with the mercury manometer, using a cathetometer that could be read to 0.02 mm.

The water adsorption measurements were carried out using dose pressures of 4.58 mm obtained by maintaining the water reservoir at 0°C with taps 6 and 3 open and 7, 5, 4 and 2 closed. By admitting the doses at various stages into the empty cell it was shown that the minimum period for the water vapour in the dosing volume at room temperature to reach equilibrium with the ice in the reservoir was

about 45 mins. Prior to each run, the water reservoir was cooled in liquid nitrogen and pumped down for several minutes before closing tap 6 and warming the reservoir to room temperature. This process was repeated several times before allowing an equilibration period of one hour for the pressure in the dosing volume to reach 4.58 mm. The isotherms, and from these the isosteric heats of adsorption, were then determined either by the direct method or the temperature variation method. In the former, successive doses of water vapour were admitted to the cell maintained at constant temperature, the equilibrium pressures being recorded by the thermistor gauge at each stage. The same procedure was used for the second method but the temperature was varied for each dose by interchanging the various cold baths. The accuracy of the heat of adsorption determined by this methodis best indicated by the variation of the slopes of the straight lines which can be drawn through a set of experimental $\log p$ vs $\frac{1}{T}$ points at constant amount adsorbed. At low coverage this was about $\pm$ 0.25 kcal/mole, but at higher coverages the deviation was somewhat less.

3. Results and Discussion

3.1. Adsorption on Potassium Chloride Films

The experiments were divided into three series, each showing various aspects of the adsorptive properties of KCl. Four films of weight 0.3 g were studied; one each for series I and II, and two for series III. Cell type 1 was used for series I and the modified design (type 2) for II and III.

3.1.1. Series I: Comparison between krypton and water adsorption

The krypton isotherms and B.E.T. plots, before and after adsorption of water, at -23°C are shown in Fig. 4, together with the water isotherm and B.E.T. plot. Initially, the surface area of the film was 2.6 m^2 and this was reduced to 2.1 m^2 following the treatment with water vapour of relative pressure 0.09. The thickness of the KCl film was estimated to be about 0.035 mm i.e. about the maximum thickness before flaking from the cell wall occurs and at which the film, composed of loosely packed crystals with appreciable spaces between, apparently shows a strong, preferred 110 orientation (109).

The monolayer volume, v_m, derived from the water B.E.T. plot, was 0.23 ml, which, on the basis of the cross sectional area of 10.5 A^2 (110) for the water molecule, gave a surface area of 0.65 m^2, i.e. about one quarter of that obtained using krypton. This meant that the 'effective cross sectional area' of water was 42.4 A^2, a value considerably higher than the area of the lattice square of KCl = 9.86 A^2.

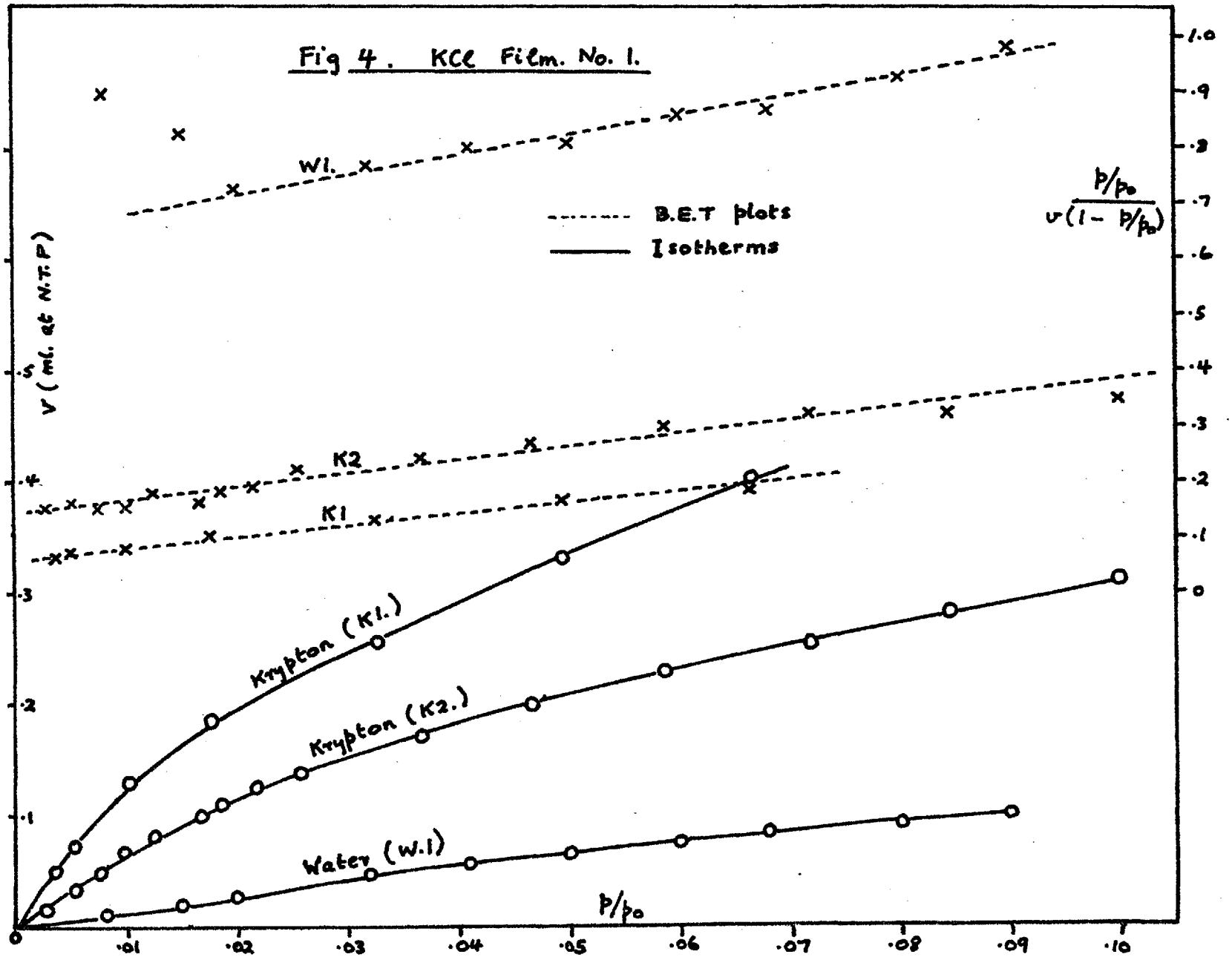
Fig 4. KCl Film. No. 1.
W1.
K2
K1
B.E.T plots
Isotherms
v (ml. at N.T.P)
p/p₀
v(1 − p/p₀)
Krypton (K1.)
Krypton (K2.)
Water (W.1)
p/p₀
·01
·02
·03
·04
·05
·06
·07
·08
·09
·10
·1
·2
·3
·4
·5
·6
·7
·8
·9
1·0

The value of p_0 for krypton = 2.5 mm was that measured by repeatedly dosing krypton into the cell at -196°C until no further change in equilibrium pressure occurred, and was found to be the same for all surface area determinations described later for the other adsorbents.

The B.E.T. constant, C, for water was 7.0, corresponding roughly to a heat of adsorption, E_1, in the first layer of 12.0 kcal per mole. To estimate this from C, the heat of liquefaction, E_L = 10.95 kcal per mole, was obtained by extrapolating Brunauer's data (6) down to -23°C.

3.1.2. Series II: Effect of sintering by the adsorbed water

One of the disadvantages of cell type 1 was the proximity of the thermistors to the cold bath. This caused drifting after a certain time, but the difficult was eliminated by using cell type 2. Exploratory experiments with film No.1 had showed that the film was quite stable for several cycles of heating to 100°C and cooling to -23°C, but on cooling in liquid nitrogen the film cracked and rapidly flaked off the glass. For this reason, no krypton adsorptions were carried out during this series. Instead, a series of water isotherms were determined at -23°C. The isotherms and B.E.T. plots at various stages during sintering are shown in Fig.5. Between each run the film was outgassed at 110°C for 16 hours. After two of these treatments with water vapour the film showed no further decrease in surface area, as illustrated by the close agreement between the isotherms of runs W4 and W5. The results are ammarised in Table 2 below.

Fig. 5 KCl Film No. 2 Adsorption of Water Vapour at −23°C

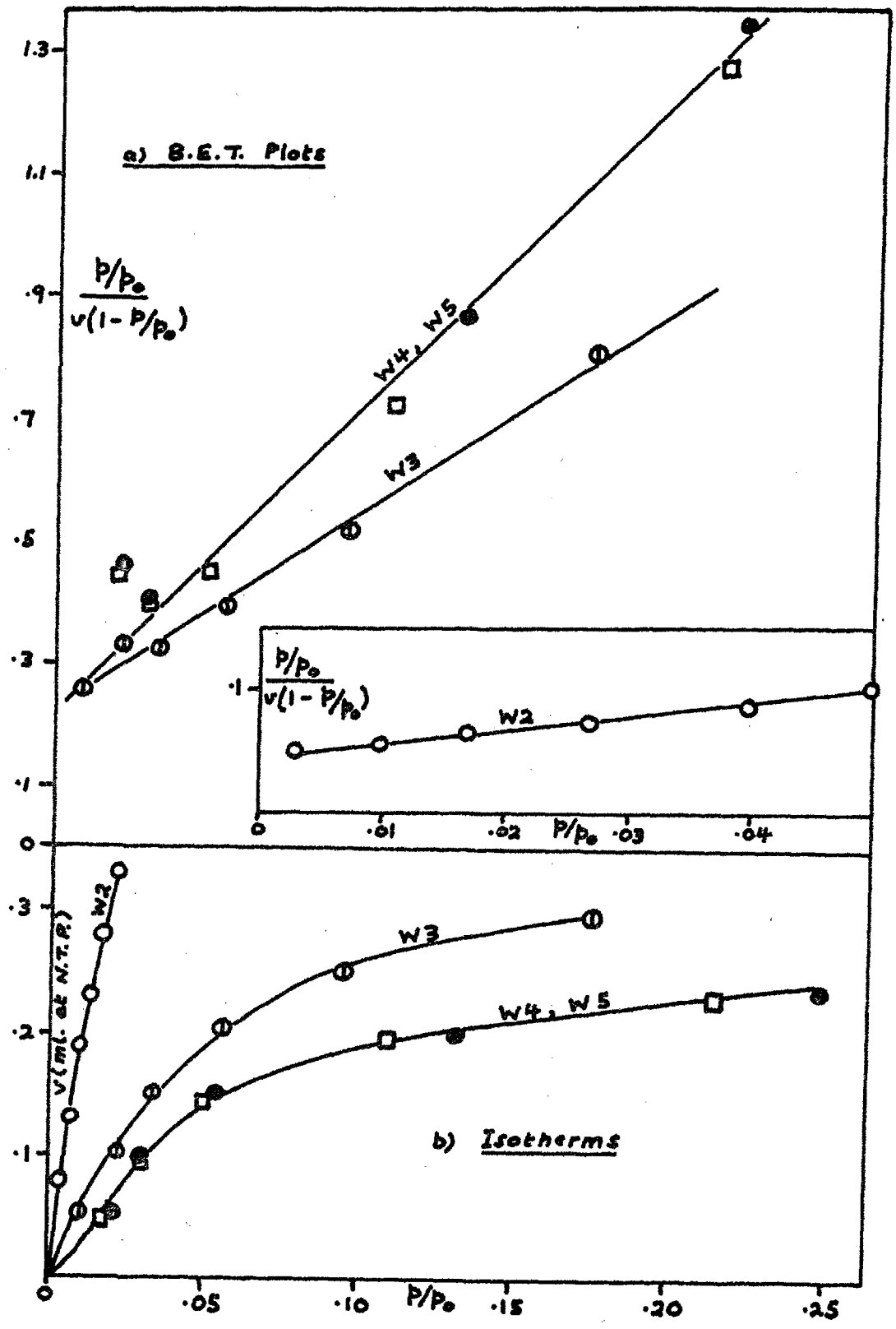

Table 2

Run No.	v_m (ml at N.T.P.)	Surface area (m^2)	C	E_1 (kcal per mole)
W2	0.97	2.6	22	12.45
W3	0.293	0.8	31	12.65
W4	0.195	0.54	51	12.95
W5	0.20	0.54	67	13.05

It is apparent that C, and hence E_1, increases slightly as the surface area decreases. Since C represents an average heat of adsorption for the whole range of the linear B.E.T. plot, it is difficult to interpret this small change except on the general grounds that a smaller surface area introduces a higher probability of lateral interactions between the adsorbed molecules.

3.1.3. Series III: The effect of temperature

3.1.3.1. Film No.3: Preliminary sintering

Owing to leakage troubles, this film was exposed several times to air at room temperature before determining the isotherms, shown together with the B.E.T. plots in Fig. 6. The first three isotherms at -23°C (W6, W7, W8) coincided fairly closely, but after a further run (W9), this time at -45°C, the surface area decreased with the next two runs at -23°C showing decreased adsorption. The results are shown in Table 3.

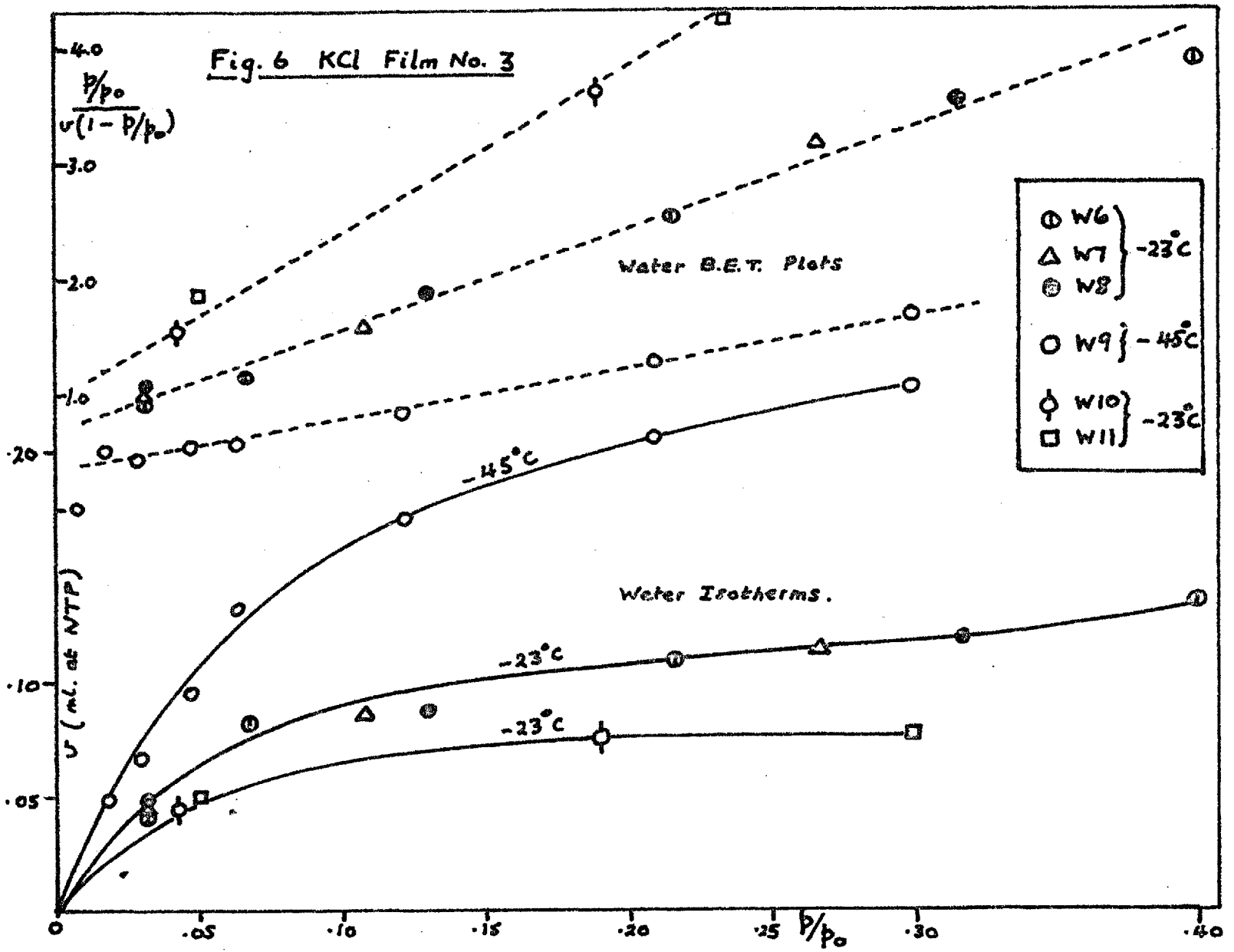
Fig. 6 KCl Film No. 3
4.0
p/p₀ / v(1 − p/p₀)
3.0
2.0
1.0
·20
·10
·05
v (mL. at NTP)
Water B.E.T. Plots
W6
W7
W8
-23°C
W9
-45°C
W10
W11
-23°C
-45°C
Water Isotherms.
-23°C
-23°C
0
·05
·10
·15
·20
·25
p/p₀
·30
·40

Table 3

Temp. °C	v_m (ml at N.T.P.)	Surface area (m^2)	C	E_1	E_2	Run No.
				kcal per mole		
-23	0.095	.27	21	12.47	10.95	W6 W7 W8
-45	0.21	.60	16	12.53	11.15	W9
-23	0.064	.18	23	12.52		W10 W11

A feature of these results was the substantially higher value of v_m at -45°C. (Normally v_m would be expected to vary only slightly with temperature; in fact, as a first approximation it may be assumed that v_m changes with temperature as $d^{2/3}$, where d is the density of the adsorbate.) This is probably related to the large difference between areas measured by krypton and water in series I, which implies that, at -23°C, a large proportion of the surface was still unoccupied at the water B.E.T. 'monolayer point'. At the lower temperature more water was adsorbed, and presumably some of this would be adsorbed on sites which were not occupied at -23°C. This would also explain why further sintering occurred at the lower temperature.

3.1.3.2. Film No.4: Isosteric heats of adsorption

In view of the above results the fourth film was preconditioned by exposing it to water vapour at the lowest temperature, i.e. -45°C, to be investigated for the purpose of determining isosteric heats

of adsorption, ΔH. Seven isotherms (Fig.7) were then determined in succession at this temperature, the last four of these by the temperature variation method. The film seemed to reach a constant surface area after run W13, but continuing the adsorption to a higher relative pressure than in any of the previous series resulted in the appearance of a 'step' (run W14). This might have been due to a smoothing-out effect giving a more uniform surface. At this stage the film showed signs of cracking. Two later runs (W15, W17) showed another decrease in area, and the last run (W18) was accompanied by a still further decrease. By this time the film had flaked off the glass completely. The breaking up of the film together with the changes in temperature during the last four runs probably caused the further sintering, but it is difficult to explain the anomalous position of the isotherm points of W16, which, although seeming to coincide with run W14, was actually carried out between W15 and W17.

The various isotherms and isosteric log plots for runs W15 to W18 are shown in Figs.8,9,10, and the resulting isosteric heats of adsorption are summarised in Table 4. At low adsorptions there was a marked increase in ΔH in going from the low to the high temperature range, and the effect became less marked as the adsorbed volume, v, increased. Because of the unusual nature of this result, W18 was carried out at two extra temperatures, $-10.5^{\circ}C$ and $-36^{\circ}C$; and in addition the temperature was varied both up and down to check the reversibility of the change in ΔH. The results

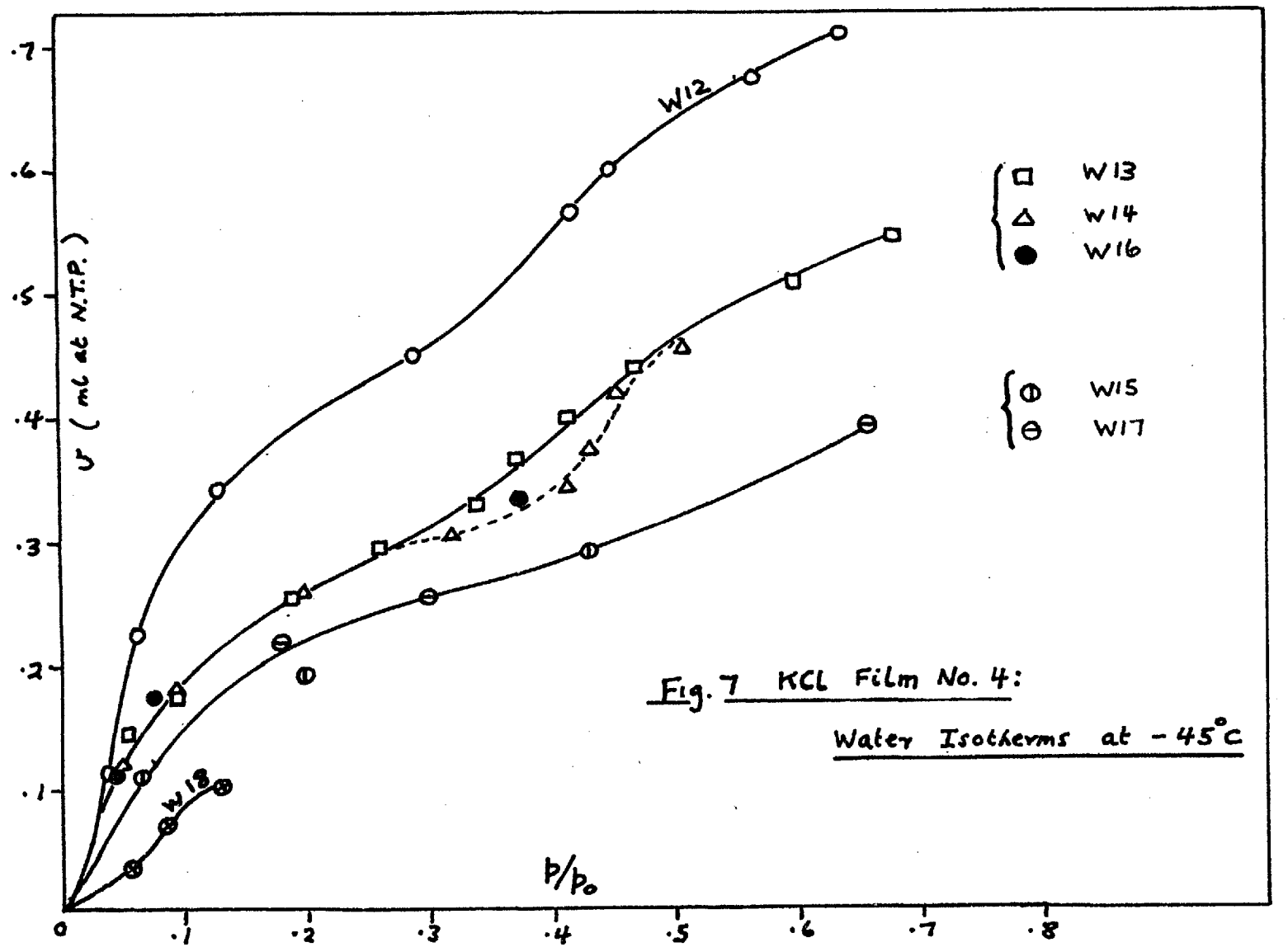

Fig. 7 KCl Film No. 4:

Water Isotherms at -45°C

Fig. 8 KCl Film No. 4. (Runs W15 and W17.)

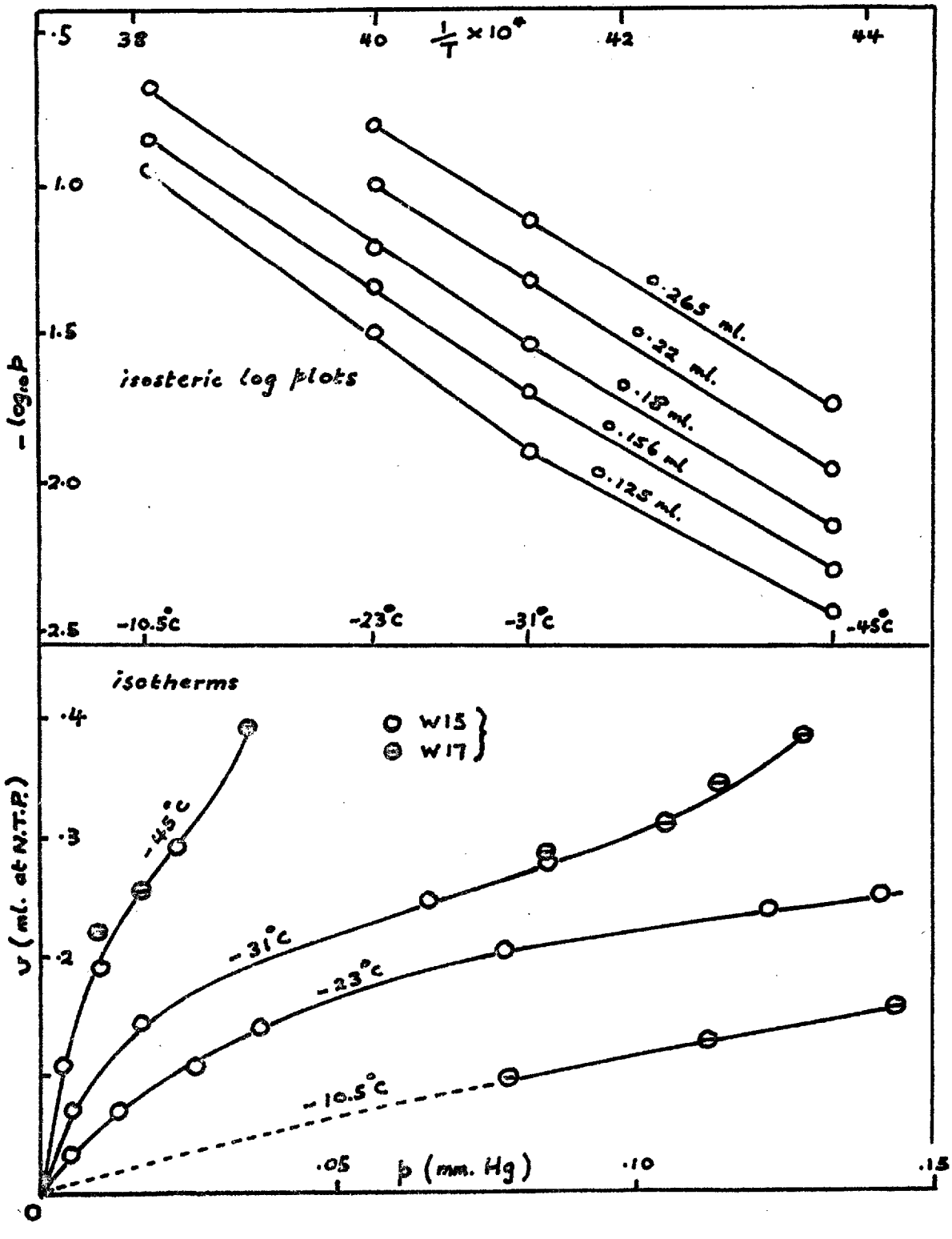

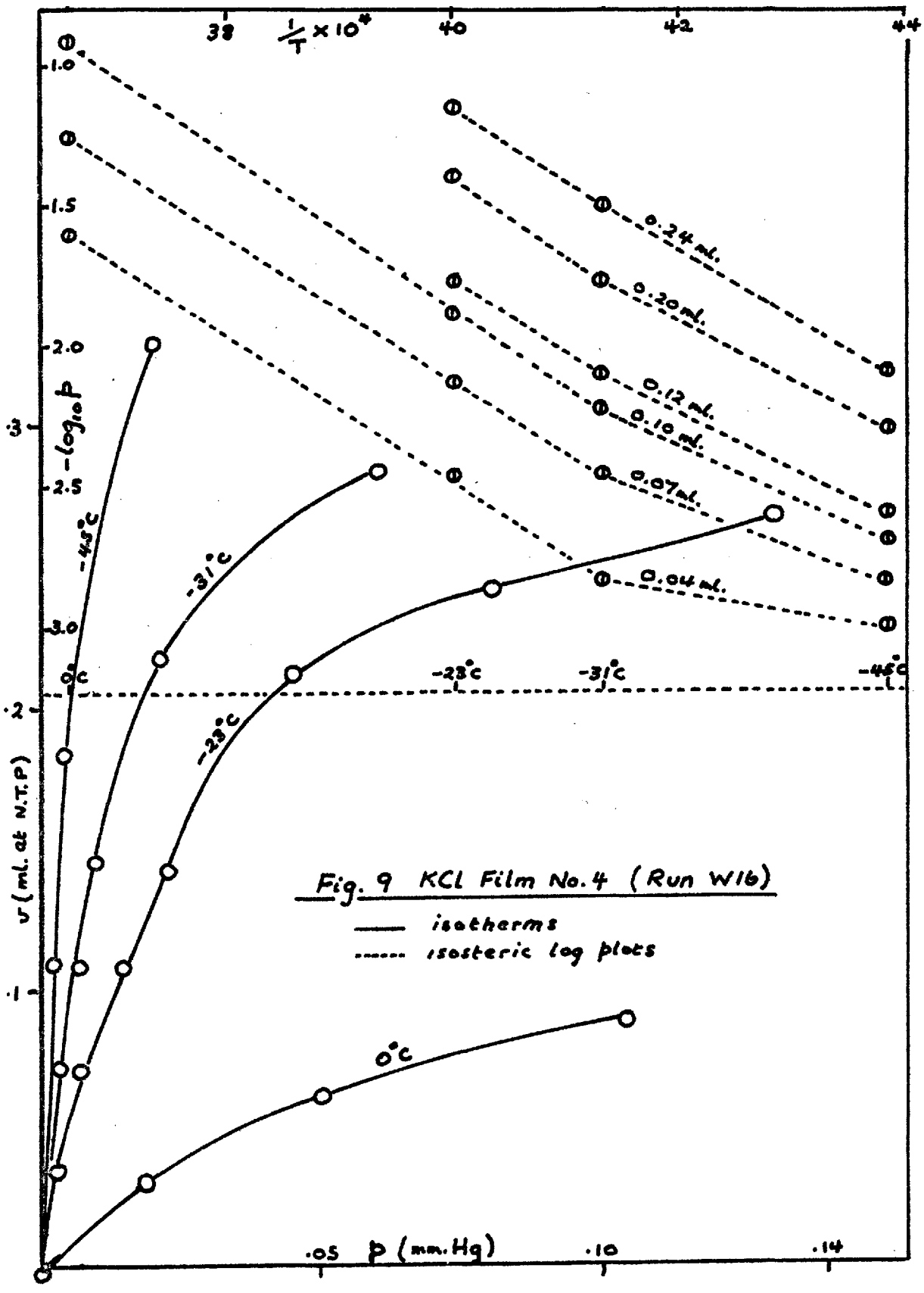

Fig. 9 KCl Film No. 4 (Run W16)

—— isotherms

..... isosteric log plots

Fig. 10 KCl Film No. 4 (Run W18)

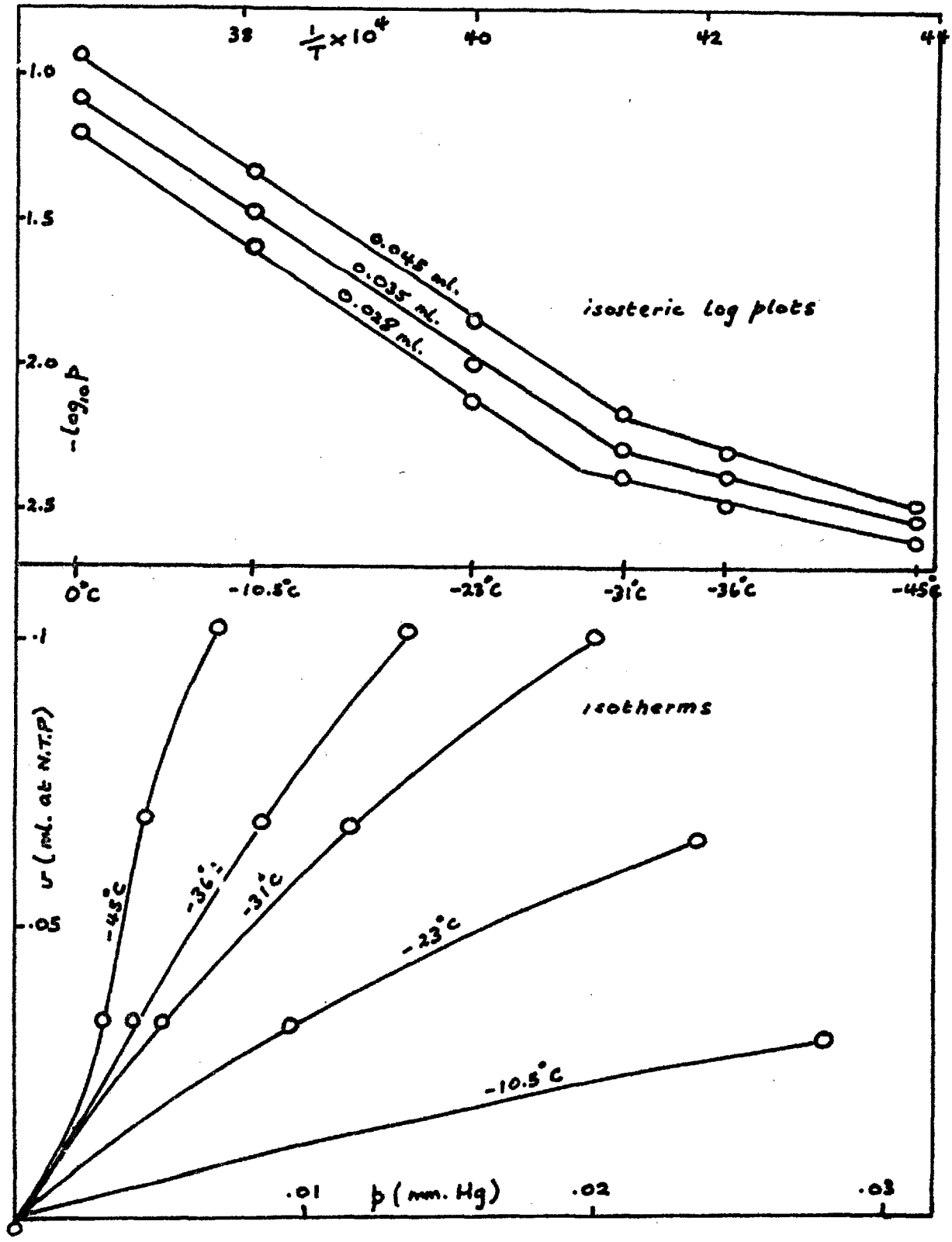

showed that the isotherm points were reproducible for both directions of temperature change.

Table 4

Run No.	v, (ml at N.T.P.)	ΔH (kcal per mole)	
		-23°C to -45°C	0°C to -23°C
W16	0.04	3.2	12.1
	0.07	7.0	11.8
	0.10	8.4	13.25
	0.12	9.1	11.6
	0.20	9.7	12.7
	0.24	10.9	12.7
		-25°C to -45°C	-25°C to 0°C
W18	0.01	3.04	12.35
	0.028	3.81	12.6
	0.035	4.28	12.7
	0.045	5.1	12.6
		-23°C to -45°C	-23°C - 0°C
W15 and W17	0.125	10.0	13.5
	0.156	11.0	12.0
	0.18	11.13	12.1
	0.22	11.5	11.5
	0.265	11.1	11.1

3.1.3.3. Adsorption on the glass

A separate run was carried out using the same procedure as for W18, but in the absence of KCl. The results showing the amount of

water adsorbed on the glass are given in Table 5, and the isosteric log plots are shown by dotted lines in Fig.11, together with the effect of correcting for this on one of the previous log plots for KCl. This confirmed that the sharp break in the log plots was due to adsorption on the KCl and not on the glass.

Table 5

Dose pressure = 4.58 mm Hg (Run W19)

Temp, ^{0}C	Pressure (mm Hg)		v, (ml at N.T.P.)	
	Dose 1	Dose 2	Dose 1	Dose 2
-10.8	.018	.039	.0061	.0116
-23	.0145	.0315	.0067	.0129
-31	.0125	.028	.0071	.0135
-36	.0115	.0245	.00725	.014
-45	.010	.0205	.0075	.015

The effect of adsorption on the glass on ΔH for KCl was negligible at temperatures below $-23^{0}C$, but above this it became appreciable. Thus in runs W15 and W17, at a pressure of 10^{-2} mm, the adsorption on the glass at $-45^{0}C$ was only $3\frac{1}{2}$ per cent of that on the salt, while at $-23^{0}C$ it was nearly 8 per cent and at $-10.5^{0}C$ over 10 per cent. The heat of adsorption on the glass was 3.3 kcal per mole which is significantly lower than the heats of adsorption on KCl in the temperature region above $-23^{0}C$, so, except in cases where the heat of adsorption on the salt is low, the competitive

Fig. 11 Adsorption of Water Vapour on the Glass

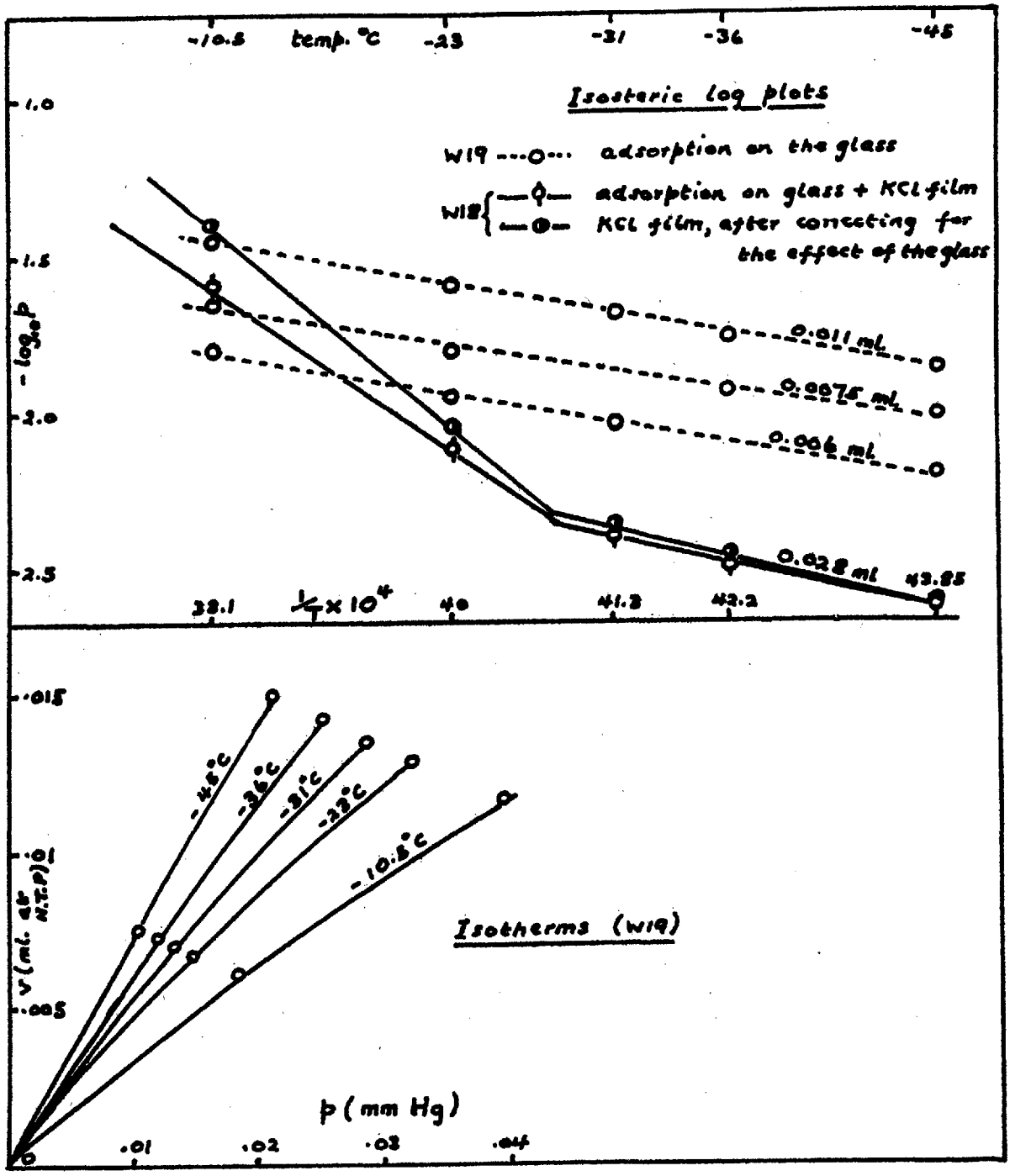

effect of the glass is probably much smaller than the above results indicate. However, much of the later work with other adsorbents was carried out at -23°C and below in order to reduce the effect as much as possible.

3.1.3.4. The variation of ΔH with coverage

The variation of the low-temperature heat of adsorption of water for the four runs is summarised in Fig.12. The heat of adsorption was about 3 kcal per mole on the bare surface, and increased markedly with increasing coverage up to about $\theta = 1$, above which it remained fairly constant at the heat of liquefaction. The coverage shown in Fig.12 was based on the monolayer volumes derived from the various water vapour B.E.T. plots at -23°C. According to the results of series I this would be about one quarter of the coverage for the surface area measured by adsorption of krypton. The marked increase in ΔH below $\theta = 1$ indicated strong lateral interactions between the adsorbed water molecules. This is discussed further in section 3.7.

3.1.4. Discussion

Normally, heats of physical adsorption are insensitive to temperature, although various examples are given (6) where the differential heat of adsorption either decreases or increases with increasing temperature. In the theoretical equations (section 1.5) for the heat of adsorption of a molecule on a uniform surface the temperature does not appear explicitly, but several of the terms depend on the temperature to some extent. The most important is perhaps the equilibrium distance, r^3, term which appears in

Fig. 12 Adsorption of Water on KCl : Variation of ΔH with Coverage

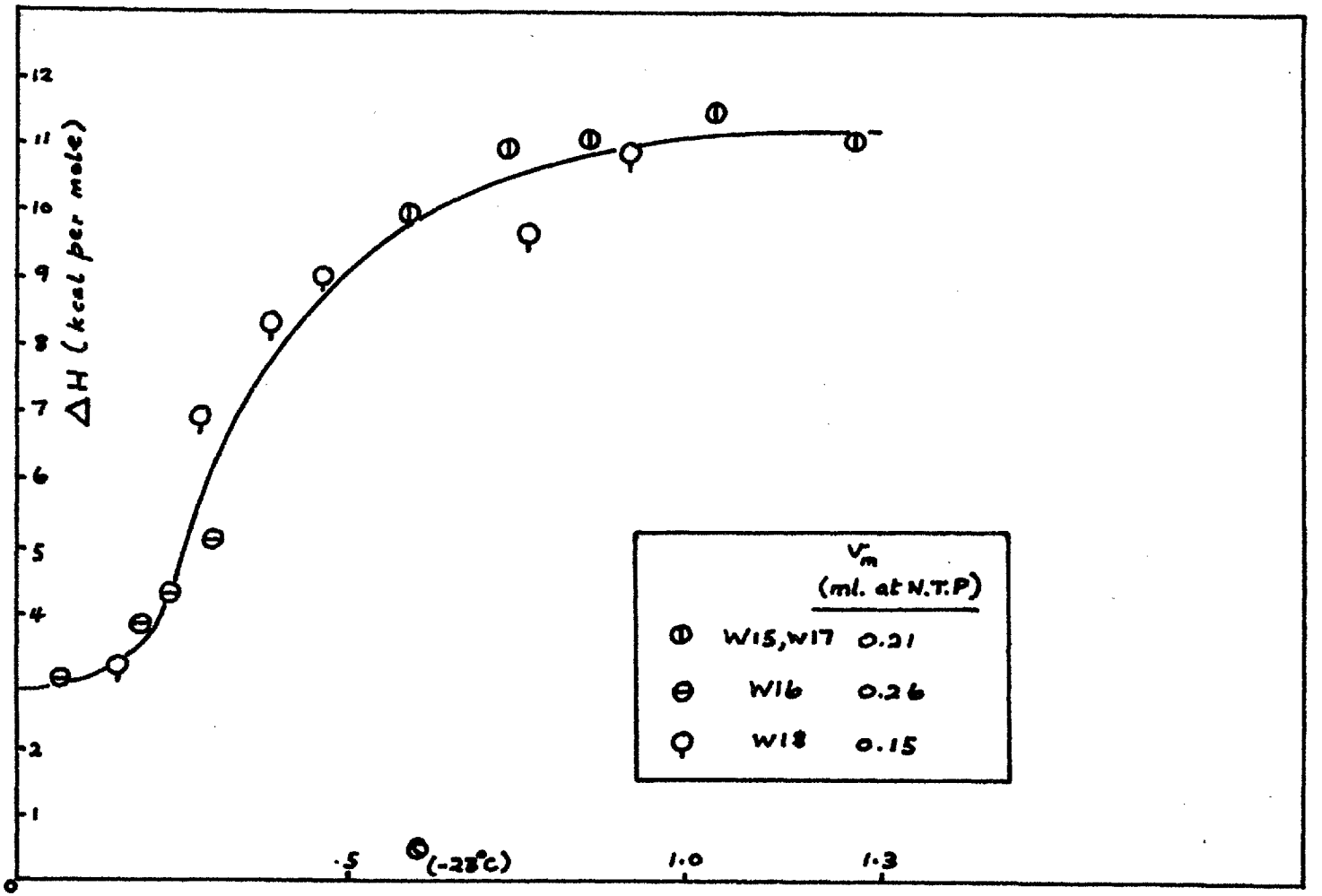

the denominator. Since r increases with increasing temperature, it would be expected that the heat of adsorption would decrease with increasing temperature. On the other hand, for polar molecules such as water the electrostatic contribution to the heat of adsorption is proportional to the dipole or quadrupole moment, and since there is evidence that the dipole length increases with increasing temperature, this would give the opposite effect. However, factors such as these are unlikely to explain the very large differences of about 9 kcal per mole observed with KCl. Furthermore, the change was sharp, and seemed to be limited to low coverage. This suggested that the same amount of adsorbate was not in a strictly comparable condition or state of aggregation in the two different temperature ranges. Alternatively, at the higher temperature, parts of the surface previously blocked may have become available for adsorption. However, it is difficult to reconcile this with the reversibility of the system, which, together with the sharpness of the change, suggests that a phase change of the adsorbate occurred. This change was shown to be abnormal by the decrease of entropy of adsorption with increasing temperature. The differential entropy changes (Table 6) were obtained from the equation,

$$\Delta H = \Delta G - T\Delta S$$

where $\Delta G = RT \cdot \ln (p/p_o)$.

Strictly, only integral entropies should be referred to for discussions in terms of physical models etc., but in this case there

were not enough low pressure results to be able to calculate these with any accuracy. However, it is reasonable to assume that, qualitatively, where such large changes with temperature as those of Table 6 are concerned, the direction of the change would be the same for the integral entropy.

Table 6

W18 Differential ΔS (cal/mole/°C)						
v (ml at N.T.P.)	0°C	-10.5°C	-23°C	-31°C	-36°C	-45°C
0.034	34.5	36.25	38.5	3.3	4.2	6.2
0.049	36.45	38.0	40.5	12.3	13.4	15.5
0.069		40.0	42.5	20.7	21.7	23.8
0.086		41.8	44.0	23.0	24.0	26.1
0.098				25.6	26.7	28.7

The phase change, discussed below, was presumed to arise from the solubility of the surface ions of the adsorbent; and, in fact, the effect was absent with insoluble adsorbents (section 3.2.1.).

Of the two sets of heats of adsorption, those at the lower temperatures (Fig.12) represent normal behaviour since they compare favourably with the theoretical values (section 3.6.1) The situation above -23°C, on the other hand, probably involves partial hydration of surface ions 'freed' at the higher temperature from isolated defect edges or corners. At these points the adsorbed layer forms three-dimensional clusters in a state of lower entropy than the normal low temperature case, and the heat

of adsorption is about the same as the heat of liquefaction. Since the defect sites at which this process occurs are expected to be less numerous than normal sites, the phase change becomes less marked as the coverage increases. The picture thus presented is in some ways analogous to that of water adsorbed on KBr (section 1.2) but in the latter case the threshold for the sudden change, i.e. the marked increase in adsorption and surface electrical conductance, was dependent on the coverage, not the temperature.

3.2. Adsorption on Silver Halides

3.2.1. Silver chloride

The isotherms (Fig.13) at four temperatures in the range 0°C to -45°C were determined with the primary aim of investigating possible phase changes of the type found with KCl. The resulting isosteric log plots, also shown in Fig.13, however, showed no sign of a break over the range investigated. This suggested that the phase change observed with KCl was a characteristic of the solubility of the adsorbent. The heats of adsorption on AgCl are shown in Table 7.

Table 7

v, (ml at N.T.P.)	.01	.0175	.028	.037	.045	.055
ΔH (kcal per mole)	5.5	7.4	8.7	9.2	8.8	9.3

3.2.2. Silver iodide

The adsorption of water vapour on AgI was confined to the temperature range -23°C to -45°C. Two separate runs, W24 and W25, were carried out, one covering the region of low adsorption and the

Fig. 13 Adsorption of Water on AgCl

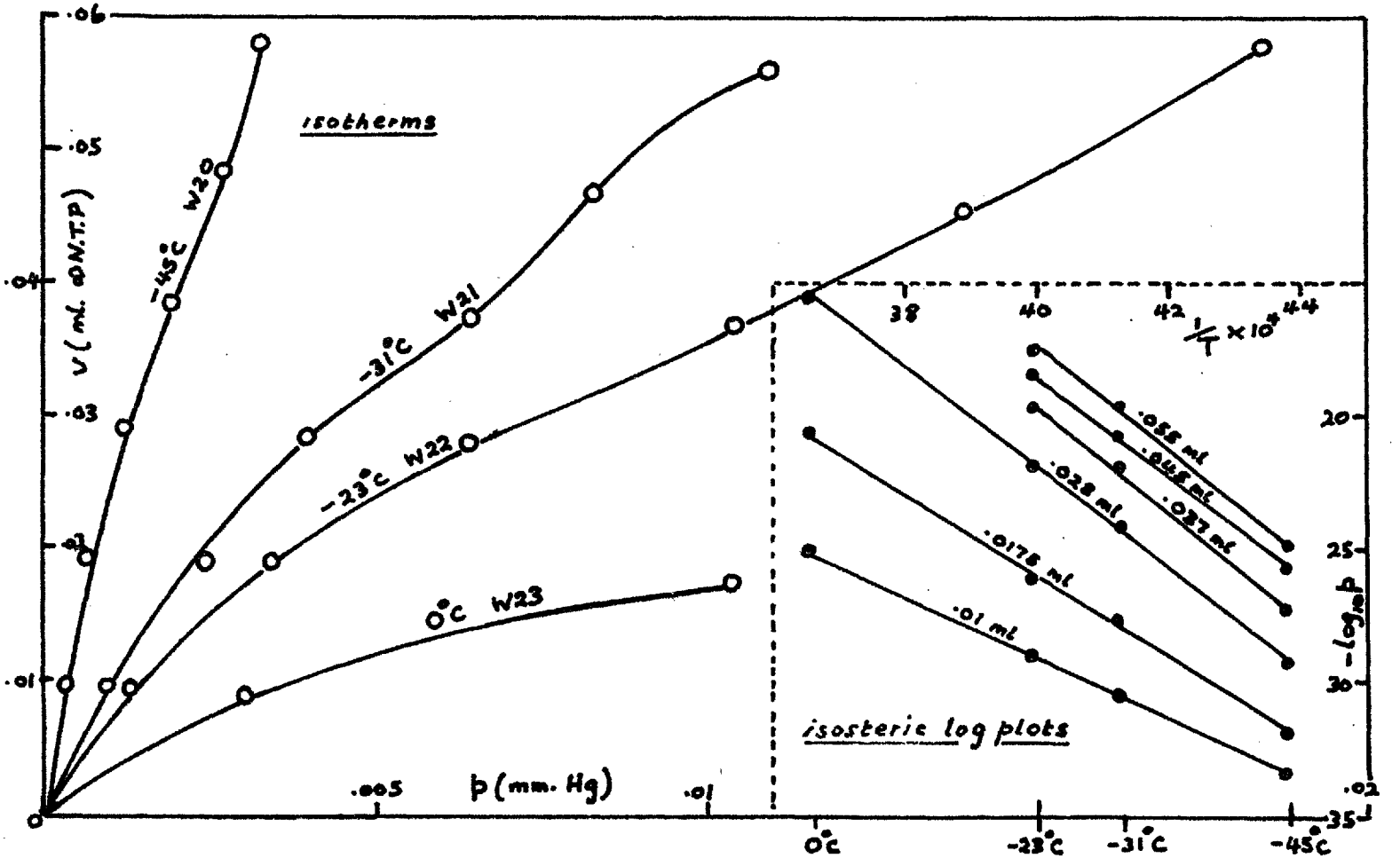

other continuing above this. The isotherms (Fig.14) showed close agreement between the two sets. The resulting heats of adsorption are given in Table 8.

Table 8

W24	v, (ml at N.T.P.)	.008	.013	.018	.023	.026	.030	.034
	ΔH (kcal per mole)	7.4	8.4	9.1	8.5	7.9	7.7	8.1

W25	v, (ml at N.T.P.)	.045	.0525	.06	.07
	ΔH (kcal per mole)	9.6	10.3	11.0	11.3

Two surface area determinations using krypton were also carried out on this adsorbent; one (K4) immediately following the other (K3) after desorbing the krypton by raising the cell to room temperature and outgassing for 15 mins. The isotherms and B.E.T. plots almost coincided (Fig.15) showing the ease with which krypton is removed at room temperature. The surface area was 0.4 m^2, whereas from the water adsorption (the -23°C water B.E.T. plot is also shown in Fig.15) the area was 0.27 m^2, i.e. not as much difference as with KCl.

3.2.3. Silver bromide

The adsorption of water vapour and of krypton was studied before and after two periods of photochemical decomposition. The krypton isotherms and B.E.T. plots are shown in Fig.16, and the water vapour isotherms in Figs. 17 and 18. The stages of decomposition

Fig. 14 AgI : Water Isotherms

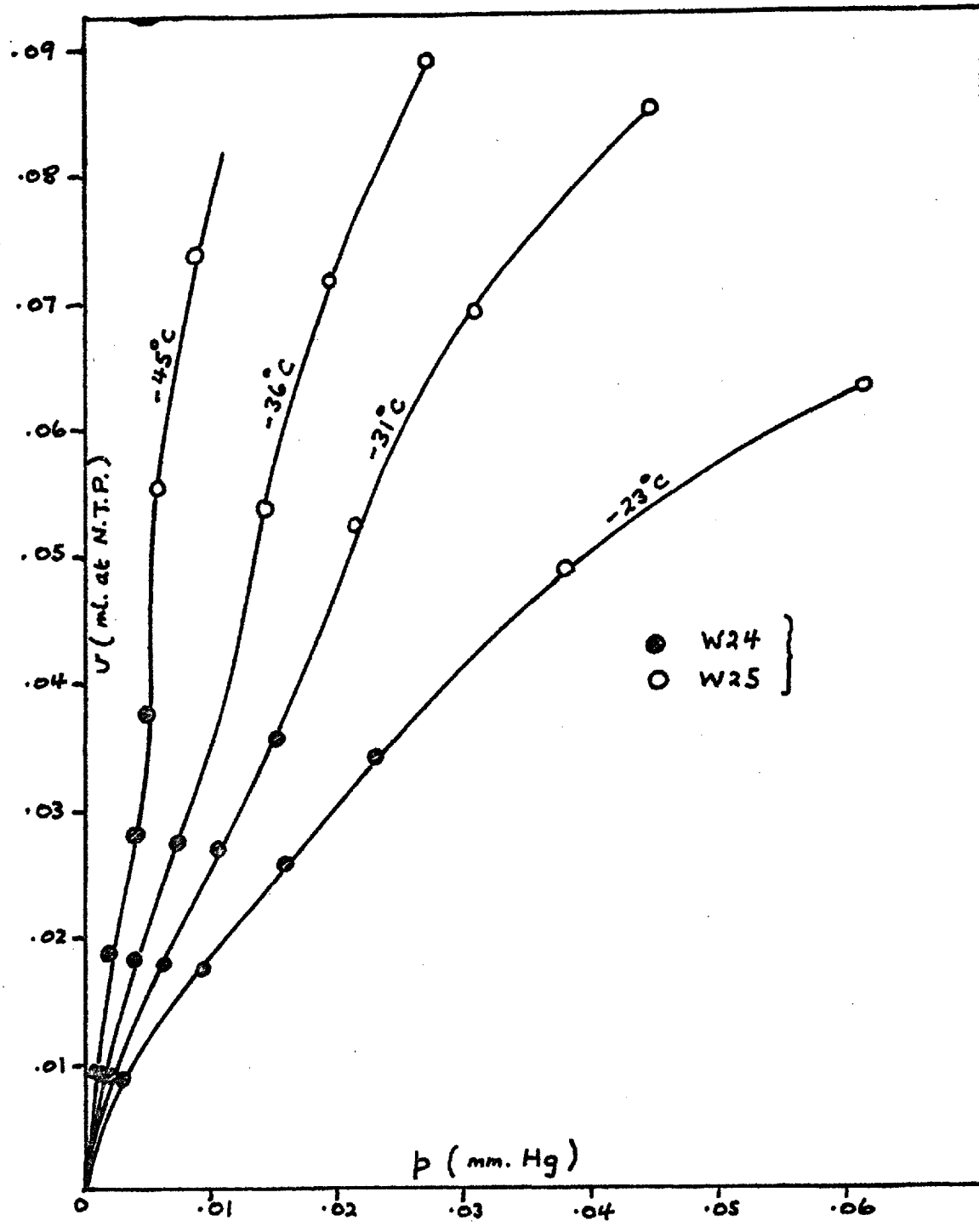

Fig. 15 Adsorption of Krypton on AgI

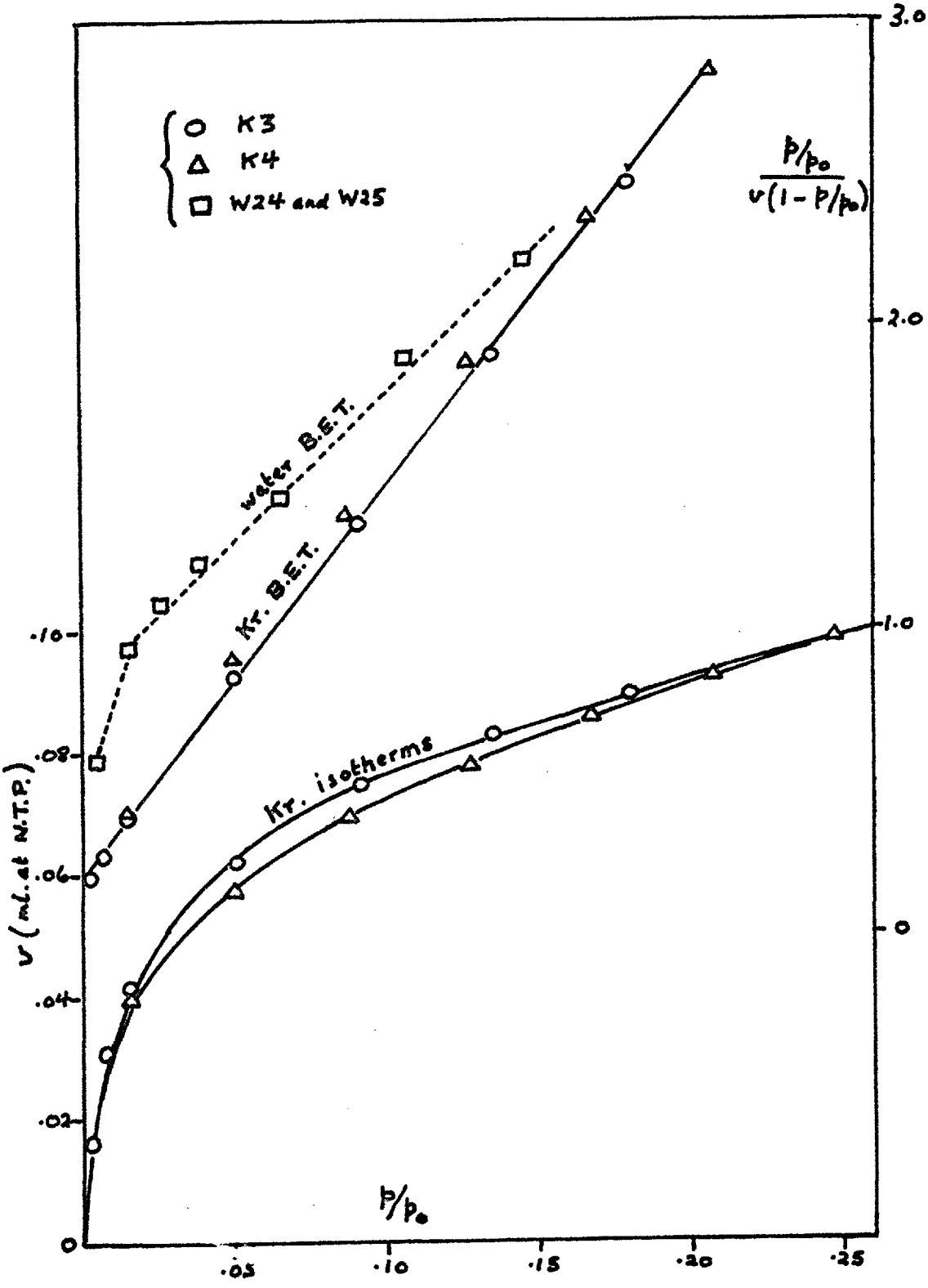

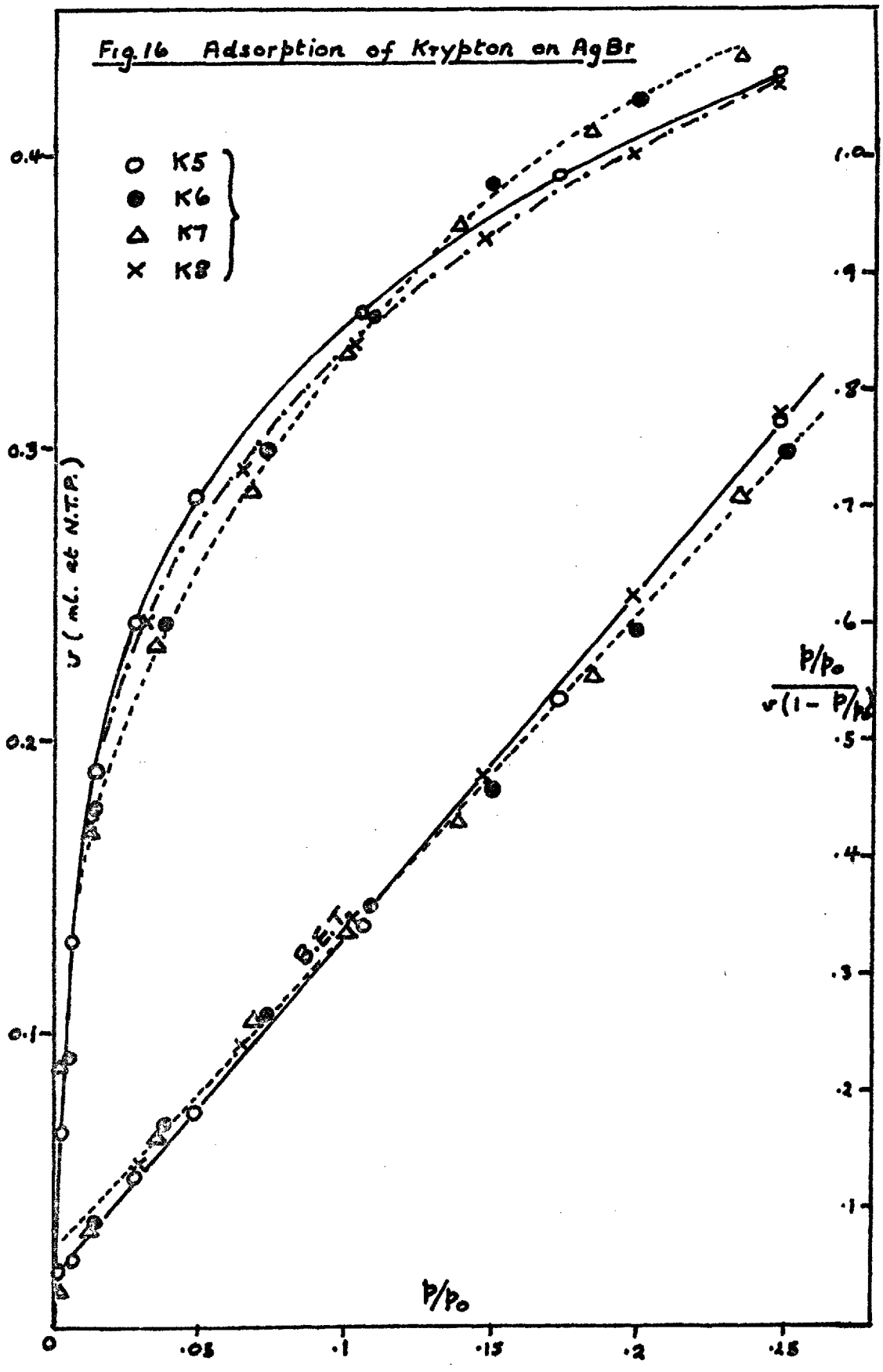
Fig. 16 Adsorption of Krypton on AgBr
K5
K6
K7
K8
v (ml. at N.T.P.)
p/p₀
v(1 − p/p₀)
B.E.T.
0.4
0.3
0.2
0.1
0
1.0
.9
.8
.7
.6
.5
.4
.3
.2
.1
.05
.15
.25

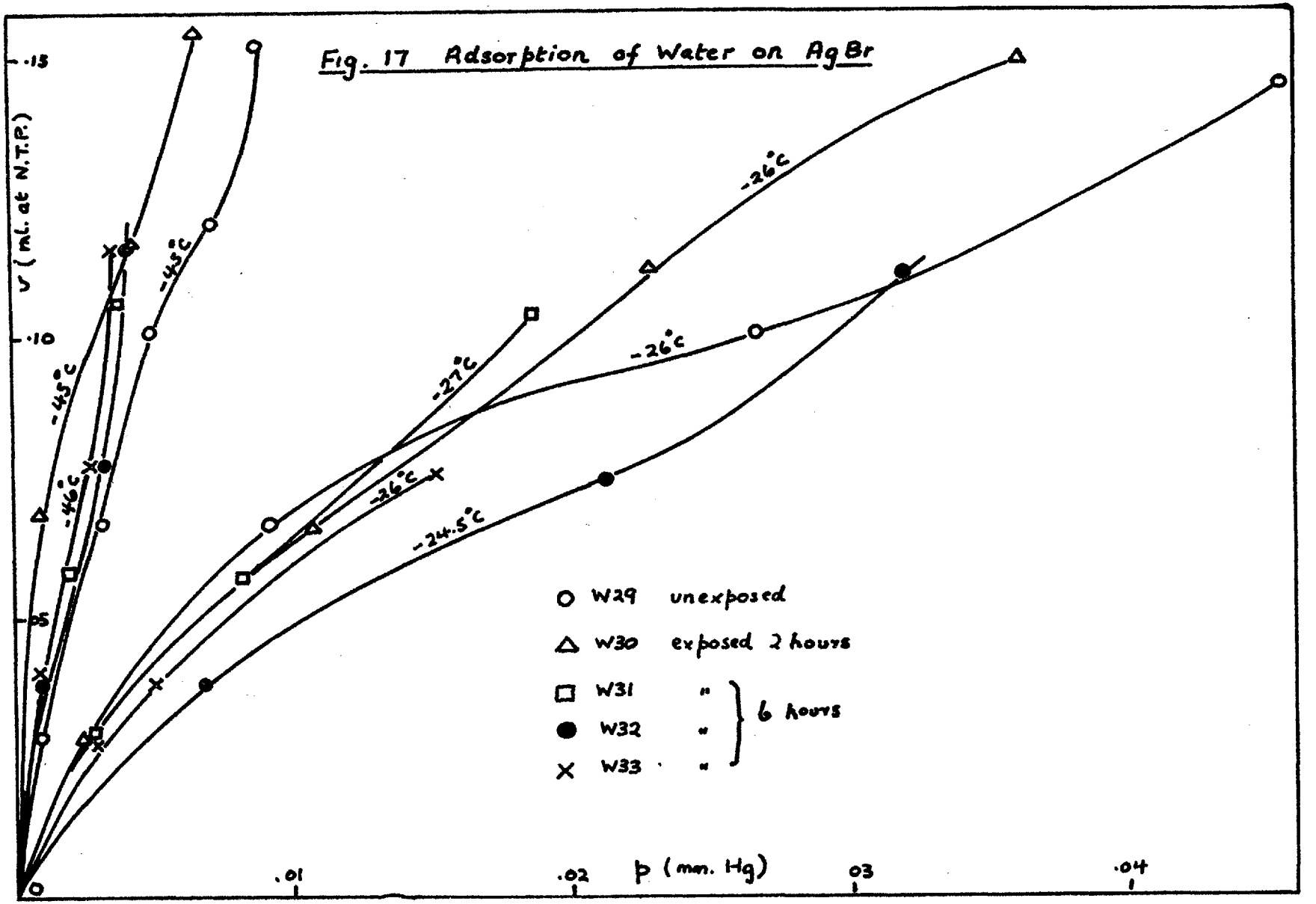
Fig. 17 Adsorption of Water on AgBr
v (ml. at N.T.P.)
.15
.10
.05
-45°C
-46°C
-45°C
-27°C
-26°C
-26°C
-26°C
-24.5°C
W29 unexposed
W30 exposed 2 hours
W31 "
W32 "
W33 "
6 hours
.01
.02
p (mm. Hg)
03
.04

Fig. 18 Adsorption of Water on AgBr

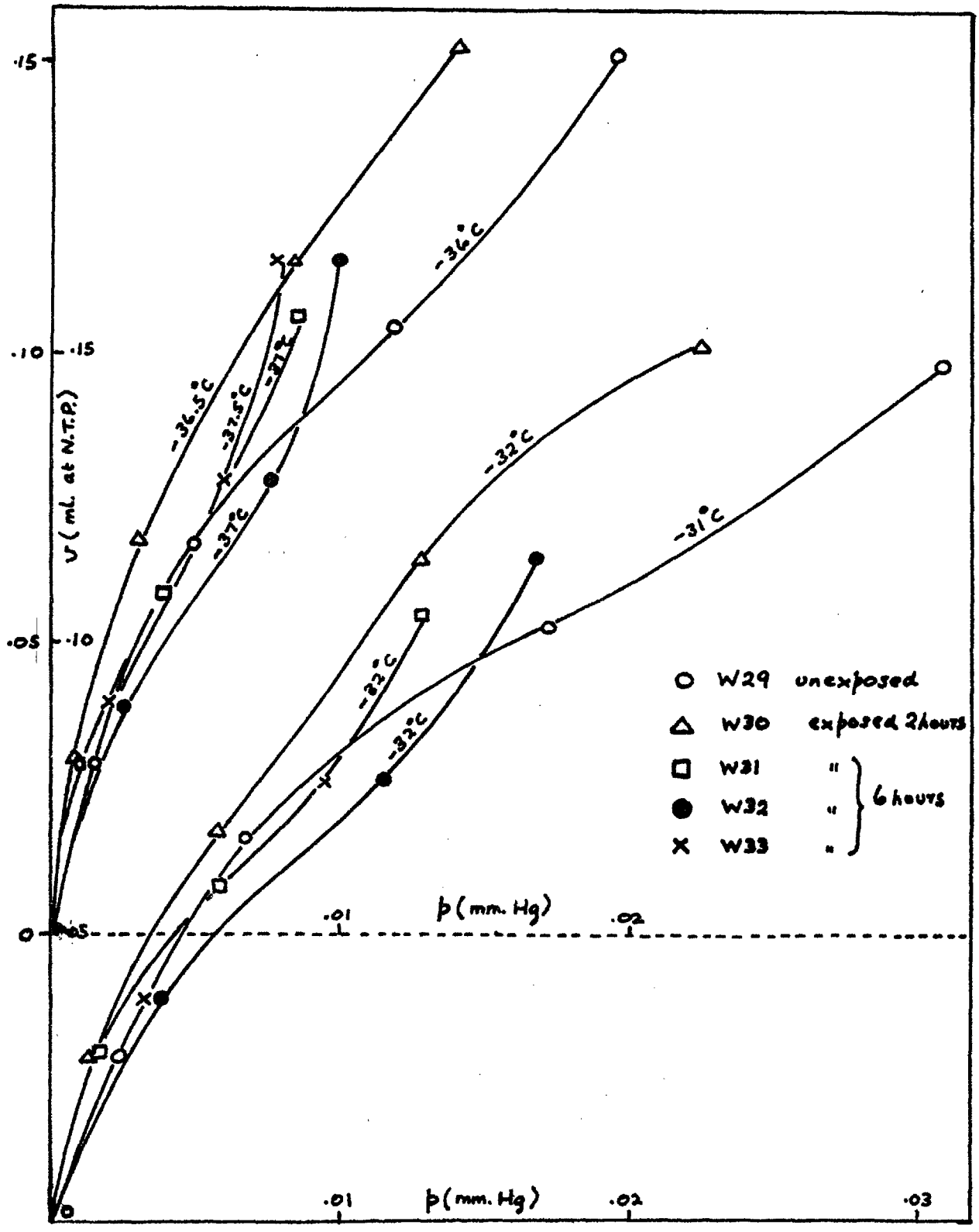

corresponded to first, 2 hours irradiation during which the sample became light-greyish green in colour (stage 1) and a further 4 hours when the colour darkened considerably (stage 2). For krypton adsorption, one run, K5, was carried out before exposure to light, then two runs, K6 and K7, after stage 1, and a final run, K8, after stage 2. The results are given in Table 9.

Table 9

	V_m (ml at N.T.P.)	Surface Area (m^2)	C	E_1 (kcal per mole)
K5	.335	1.75	86	2.95
K6) K7)	.355	1.9	47	2.85
K8	.335	1.75	60	2.90

The surface area of the unexposed sample was 1.75 m^2; and, after stage 1, this increased slightly to 1.9 m^2 and then returned to the original value after stage 2. At first sight these small changes might seem negligible, in spite of the exact agreement between the results of K6 and K7 and the high accuracy (section 1.3.4.) claimed for this method of surface area determination, but they are reflected by the results for water adsorption discussed below. In addition, these results correspond with X-ray evidence (111) that the lattice constant of silver bromide changes slightly on first exposing to radiation and then returns to near the original value after more prolonged exposure.

The water vapour isotherms were determined by the temperature variation method, during which the temperatures of the cold baths changed as a result of contamination from other baths, caused by the difficulty in removing the last traces of solvent from the crinkled aluminium foil surface round the cell. This was in part responsible for the differences in the various isotherms shown. The other reason was the change in the heats of adsorption summarised in Table 10. Altogether five runs were carried out, three of these following stage 2; and before the final run, W33, the sample was outgassed at 130°C instead of 100°C.

Table 10

unexposed		stage 1		stage 2					
W29		W30		W31		W32		W33	
v	ΔH	v	ΔH	v	ΔH	v	ΔH	v	ΔH
.028	6.9	.028	11.75	29	10.6	.039	9.5	.035	9.5
.05	6.0	.05	13.0	.04	10.1	.06	10.0	.055	9.8
.065	6.35	.068	13.0	.056	9.5	.075	10.0	.075	10.1
.085	7.6	.09	11.5	.08	9.5	.09	10.3	.09	10.2
.10	9.7	.115	9.7	.105	10.0			.115	10.0
.12	9.1	.15	9.3						
.145	9.2								

v : ml at N.T.P.
ΔH : kcal per mole

3.2.4. Discussion

3.2.4.1. The variation of ΔH with coverage

The variations of the heat of adsorption of water with coverage at the various stages of photochemical decomposition of AgBr are shown in Fig.19, together with the results for unexposed AgI; and in Fig.20 similar curves are plotted for all three unexposed silver halides. The coverage, θ, in Fig.20 refers to the surface area obtained from the water B.E.T. plot at -23°C. This was chosen arbitrarily for purposes of comparison, since no krypton adsorptions were carried out on silver chloride.

The isosteric heat of adsorption on unexposed AgBr first decreased slightly from about 7 to 6 kcal per mole, at low coverage, before rising fairly sharply, in the same way as KCl (Fig.12), to a maximum at 10 kcal per mole, and then decreasing finally to 9 kcal per mole. This decrease, although slight and based on only a few experimental points, was not apparent with KCl and is considered real because the same variation occurred for all three silver halides. With silver iodide, the maximum, point C, was more marked than the others and occurred at lower coverage. Moreover, the curve continued to rise presumably to a secondary maximum corresponding to the heat of liquefaction of water. On this basis, the curves for unexposed AgBr and AgCl were, no doubt, incomplete in the sense that they would also have continued to rise in the same way. Thus, the general form of curve for the silver halides could be represented by that shown for silver iodide. The initial decrease in ΔH with unexposed silver

Fig. 19 AgBr : Variation of ΔH with Coverage

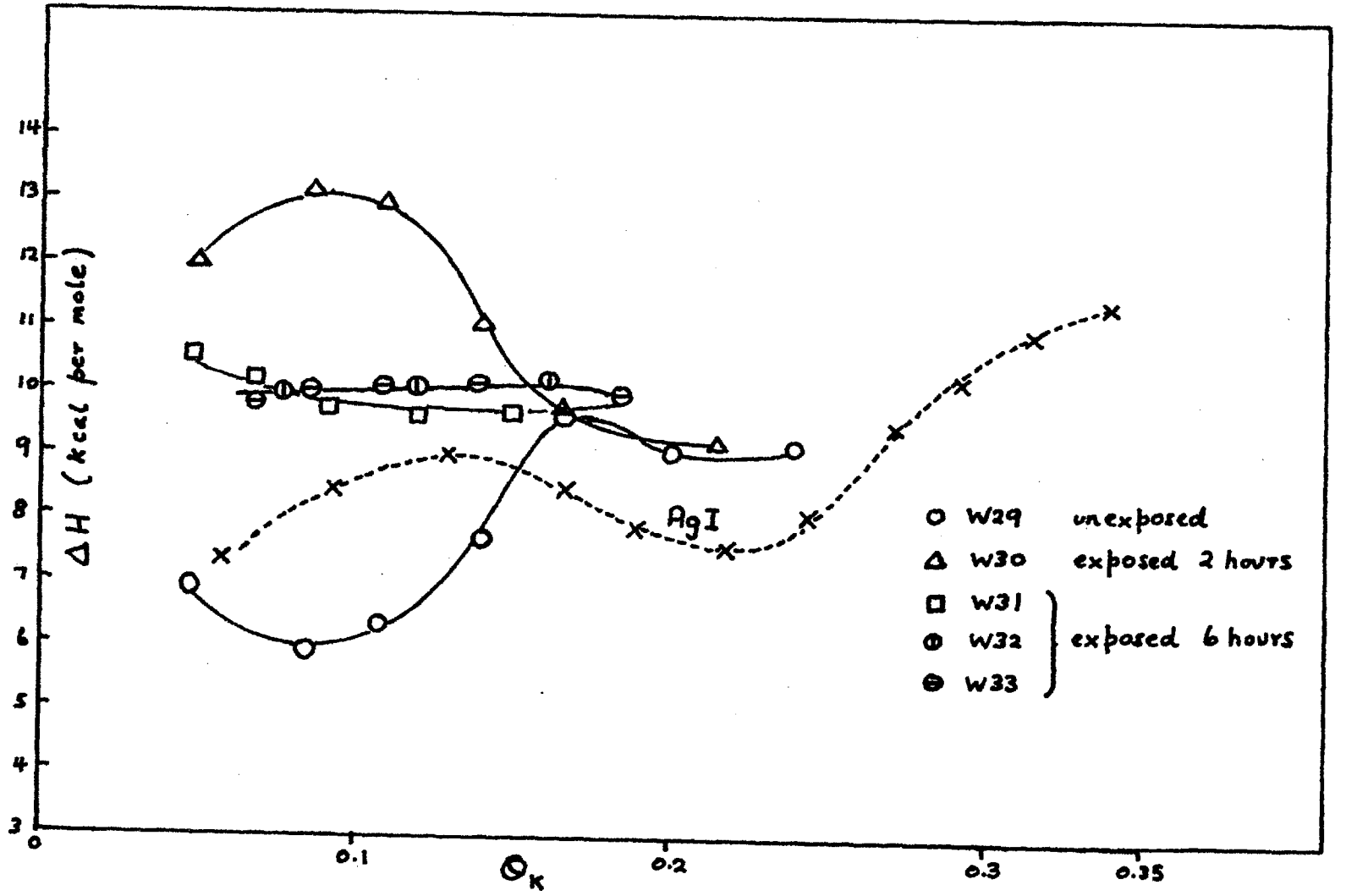

Fig. 20 Silver Halides: Variation of ΔH with Coverage.

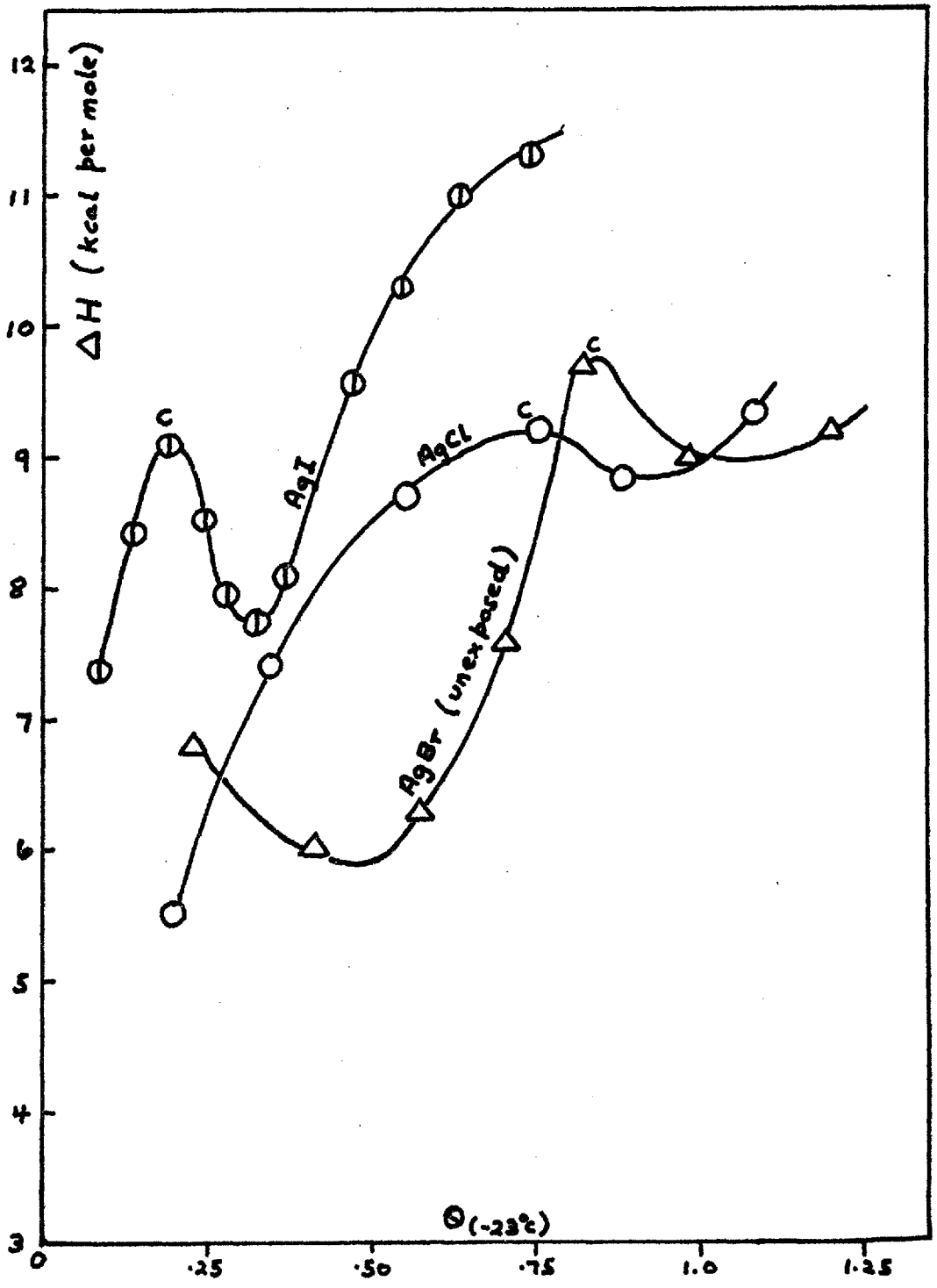

bromide was probably the result of surface heterogeneity (section 3.3.3.).

In Fig.20, the positions of the maxima were are about $\theta = 0.8$ for AgBr and AgCl, and 0.2 for AgI. However, in terms of the real coverage, θ_K measured by adsorption of krypton, these maxima occurred at a much lower coverage, and AgI was not as unique as Fig.20 suggests. The reason for this is discussed in section 3.3.3. In Fig.19 the maxima for AgI and AgBr were at $\theta_K = 0.13$ and 0.18 respectively.

After stage 1, the heats of adsorption on silver bromide showed a marked change characterised by elevation of the maximum to 13.0 kcal per mole and a decrease in the coverage at which the maximum occurred. Following the maximum, the heat of adsorption decreased to about 9.0 kcal per mole, and at this point the curve coincided with that of the unexposed sample. On further irradiation, the maximum was apparently eliminated and the heat of adsorption remained constant at 10.0 kcal per mole. There was no difference in the results between the sample outgassed at 130°C and those at 100°C. The various changes seemed to be related to the surface area changes shown in Table 9, although the heats of adsorption of water after stage 2 were more different from those after stage 1 than might be expected from these results.

3.2.4.2. <u>The effect of photochemical decomposition</u>

In order to understand the various changes discussed in the previous section it is necessary to examine the mechanism of

photochemical decomposition of silver bromide (112). The absorption of light by the crystal is apparently accompanied by the liberation of bromine and the formation of metallic silver at crystal imperfections. The primary stage is the emission from Br^- of a photoelectron, which combines with an interstitial Ag^+ ion and an Ag^+ ion at a kink site around the emergence of dislocations through the surface of the crystal. Stable latent image specks are produced by further combination with interstitial silver ions and conduction electrons to give first stable pairs and then groups of three silver atoms. These groups can adsorb a silver ion and become positively charged, neutrality being maintained by the production of a cation vacancy. In this state the silver atoms repel positive holes and can trap conduction electrons, a process which is immediately followed by the adsorption of a further silver ion: thus the silver nuclei grow. Positive holes are normally trapped at kink sites and then free bromine is desorbed from the crystal.

Presumably the state of affairs after stage 2 was that large silver aggregates containing cation vacancies at and near the surface were accompanied by anion vacancies created by loss of bromine. Now it wasshown in section 3.6.2. that preferential adsorption of water in the anion vacancies would give a much greater heat of adsorption than observed experimentally unless the vacancy were surrounded by silver atoms instead of ions. However, the above mechanism means that the silver centres repel positive holes, so it is more feasible that the adsorption took place at the cation vacancies, which were in effect

embedded in the silver aggregates. On this basis the observed experimental heats of adsorption compared favourably with theoretical values (section 3.6.2.). The presence of lateral interactions was evident from the interaction maximum.

At the second and final stage of the decomposition the surface probably consisted mainly of silver atom aggregates surrounding numerous cation lattice vacancies. There is, in this case, a much greater probability that the water would be adsorbed in other vacancies instead of around those already occupied as in stage 1: hence the disappearance of the interaction maximum. Since the surface layers would contain a greater number of silver atoms the influence of the electrostatic potential on the heat of adsorption is reduced, so that the stage 2 heats of adsorption were lower than those of stage 1.

3.3. Adsorption on Lead Halides : PbI_2 and PbF_2

3.3.1. Adsorption of water vapour and krypton

The isotherms for the adsorption of water vapour on lead iodide and lead fluoride are shown in Figs.21 and 22, together with the corresponding krypton isotherms and B.E.T. plots. The krypton results showed effects not observed during the previous work on KCl and the silver halides. Thus with PbI_2 there was a marked deviation from B.E.T. theory at relative pressures below 0.05, and for the fluoride there was a definite step in the isotherm beginning at p/p_0 = 0.12. The latter had the form of a Type 4 isotherm in the Brunauer classification (6), although the step was only slight, implying that some filling of the pores of the adsorbent occurred at a pressure

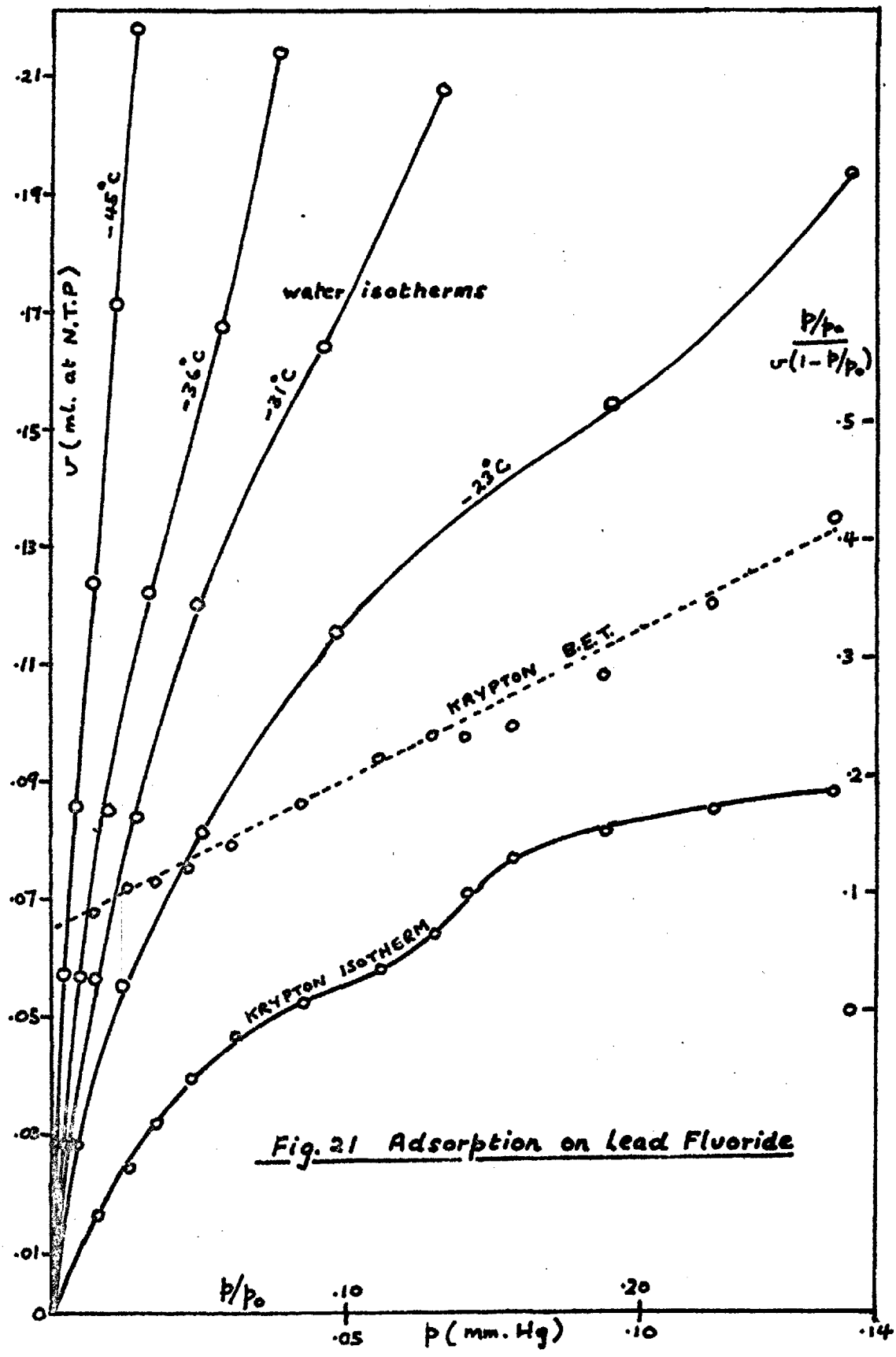

Fig. 21 Adsorption on Lead Fluoride

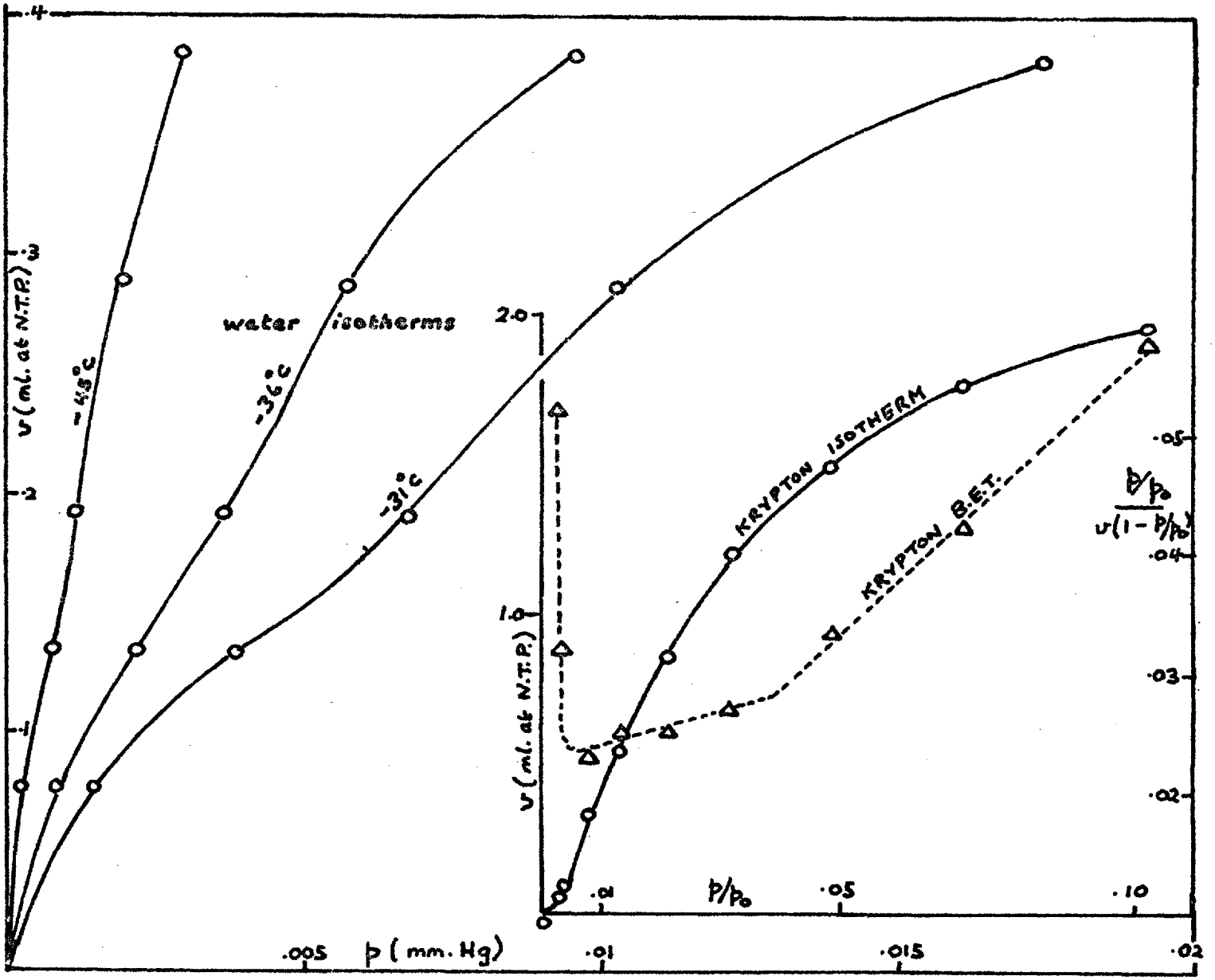

Fig. 22 Adsorption on lead Iodide

substantially lower than the saturation pressure. The low pressure deviation for PbI_2 agreed closely with the established lower limit for B.E.T. linearity with some adsorption systems, but in this case the whole B.E.T. plot could, feasibly, be divided into three parts; a) below $p/p_0 = 0.005$, where the slope is negative, i.e. the heat of adsorption is less than the heat of liquefaction; b) between $p/p_0 = 0.0075$ and 0.04, where C = 9; and c) above $p/p_0 = 0.05$ where C = 55. Thus the heat of adsorption of krypton increased with increasing coverage, in fact opposite to the effect discussed below, shown by the adsorption of water at low coverage. The surface areas of the two samples were 10.5 m^2 for PbI_2 and 3.4 m^2 for PbF_2.

The water isotherms for PbI_2 and PbF_2 were shaped in much the same way as those of the silver halides, being slightly undulating Type II forms. The resulting isosteric heats of adsorption are shown in Table 11.

Table 11

PbI_2		PbF_2	
v (ml at N.T.P.)	ΔH (kcal per mole)	v (ml at N.T.P.)	ΔH (kcal per mole)
.077	14.7	.015	9.2
.085	13.9	.03	10.1
.10	13.4	.055	10.0
.135	13.5	.08	9.9
.15	13.0	.12	10.65
.175	13.6	.16	12.2
.19	14.25	.195	12.6
.225	14.05		
.25	13.8		
.285	13.2		
.325	13.4		
.38	14.0		

3.3.2. The variation of ΔH with coverage

The isosteric heat curves for the adsorption of water on the lead halides are shown in Fig.23. Both curves are plotted against surface coverage θ_K, relating to surface areas measured by adsorption of krypton, and, in addition, the lead iodide curve is represented as a function of θ_1, shown by dotted lines. θ_1 refers to the coverage relating to the monolayer volume $(v_m)_1$ obtained from the first linear portion of the water B.E.T. plot. The significance of this can be seen from the -45°C water B.E.T. plot for PbI_2, illustrated together with similar plots for PbF_2 and the silver halides in Fig.24. Each of these shows a definite break into two straight line portions corresponding to adsorption on different parts of the surface. The various results are summarised in Table 12, in which $(v_m)_2$ is the monolayer volume corresponding to the second part of the B.E.T. plot.

The heat of adsorption of water on PbI_2 decreased initially from about 15.0 to 13.0 kcal per mole, before rising to 14.2 kcal per mole then falling and rising again to 14.0 kcal per mole. This occurred at very low real coverage, θ_K, but the position of the secondary maximum, C, coincided with $\theta_1 = 1.0$. Although there were insufficient experimental points to indicate heats of adsorption beyond point E it is expected that the curve would reach a third maximum.

In contrast, the lead fluoride curve was of the same form as the silver halide group. The θ_1 positions derived from both the -23°C and -45°C water B.E.T. plots are marked in Fig.23 by broken lines,

Fig. 23 Lead Halides : Variation of ΔH with Coverage

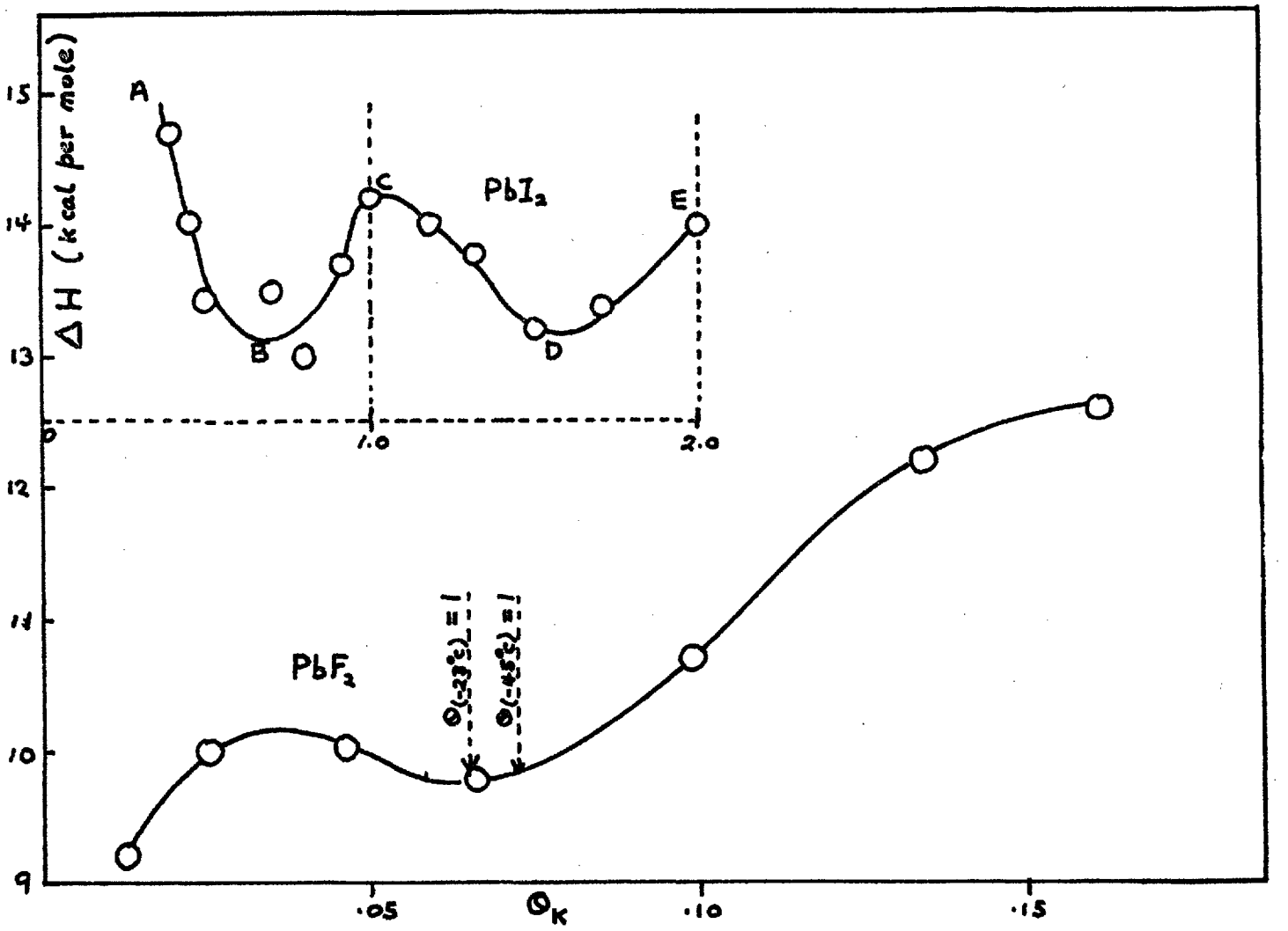

Fig. 24 Water B.E.T Plots : Lead and Silver Halides

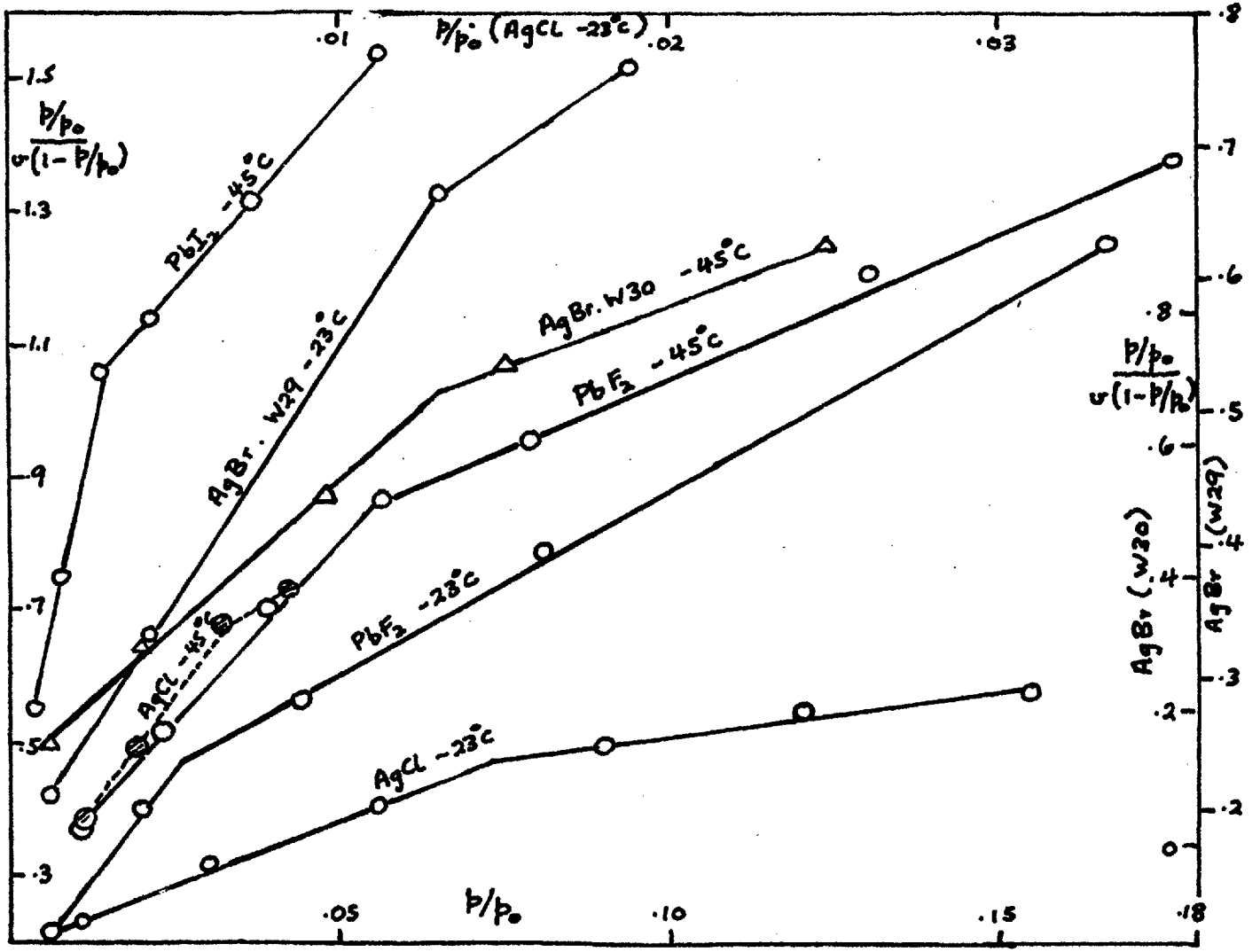

Table 12

	$(v_m)_1$		$(v_m)_2$		C_1		C_2	
	ml.at N.T.P.							
	-23°C	-45°C	-23°C	-45°C	-23°C	-45°C	-23°C	-45°C
AgCl	.05	.07	.155	.17	106	64	16	11
AgI	.03		.095		81		13	
AgBr (W29)	.12	.10	.24	.195	51	23	10	8
AgBr (W30)		.115		.245		80		9
PbI_2		.20		.85		155		13
PbF_2	.075	.09	.17	.205	120	45	18	8

and are seen to coincide with the position of the minimum, as observed previously with AgCl and AgBr.

3.3.3. Discussion

It was noted in section 3.2.4.1. that the apparently anomalous position of the silver iodide curve in Fig.20 was not reflected by its position with respect to the real coverage, θ_K. The reason for this can be seen from the division of the water B.E.T. plots into two linear portions. While the AgI coverage shown in Fig.20 was obtained from the water B.E.T. line (Fig.15) drawn through all points except the first, the AgCl and AgBr curves corresponded to θ_1 values. However, if the water monolayer volume for AgI was derived instead from a line drawn through the first few, low pressure points only, then the curve in Fig.20 was shifted to the right, and

the position of $\theta_1 = 1$ coincided exactly with the minimum. On this basis it was concluded that the isosteric heat curves for the three silver halides and for lead fluoride had a common shape with a minimum occurring at the arbitrarily defined $\theta_1 = 1$. A theoretical interpretation of this form of curve is given in section 3.7.

The lead iodide curve stood alone amongst this group of adsorbents in the sense that its shape did not conform to this general pattern, and also the magnitude of the heat of adsorption of water was higher than any of the others. This type of curve probably corresponds to adsorption with lateral interactions on small fractions of a heterogeneous surface, the secondary maximum in the curve occurring at monolayer coverage of the first fraction. Lead di-iodide crystallises with a layer lattice (113) structure in which ions of both types occupy the exposed faces, although there will be a smaller porportion of high adsorption potential faces containing either Pb^{++} or I^- ions. Presumably these were responsible for the heterogeneity. Orr (67) has shown that the occurrence of a maximum in the heat of adsorption on a uniform surface coincides with completion of the monolayer, but in this case it seems that the secondary maximum is due to the intersection of curves relating to two separate faces. Thus the decreasing portions (AB and CD) indicate the surface heterogeneity, while the increasing portions (BC and DE) were probably caused by multilayer adsorption centred around the sites of high adsorption potential. This was indicated by the integral entropy of adsorption (section 3.5.1.).

3.4. Adsorption on Calcium Fluoride

3.4.1. Adsorption of water vapour and krypton

The water isotherms for two runs, W40 and W41, are shown in Fig.25. Run W40 was carried out at one temperature, -36°C, and W41, after desorption at 100°C, was carried out by the temperature variation method embracing the range -23°C to -45°C. The dotted line extrapolations in Fig.25 represent the probable shapes of the W41 isotherms at low coverage. The significant feature of these results was the almost vertical discontinuity of the -36°C isotherm, and the stepwise shape of this and the others. The marked discontinuity indicated a two-dimensional condensation or phase change, the conditions for which have been summarised in section 1.7. It may be noted that these isotherms were very similar to those obtained by Ross and Winkler (89) for ethane adsorbed on CaF_2 at 90°K. CaF_2 is a cubic crystal that normally occurs with the 100 crystal faces, although it fractures along the octahedral of 111 planes (114). It would, therefore, be expected that two 'homotattic' surfaces are present, so that a marked two-dimensional condensation is not surprising. Furthermore, the 100 plane of CaF_2 contains ions of all one type (F^-) and uniformity of surface to a greater degree than for the heteroionic surfaces of KCl, AgI etc., is thus possible. This was borne out by the krypton isotherms and B.E.T. plots (Fig.26). The latter showed a clean break into two straight line portions corresponding to surface areas of 0.18 and 0.35 m^2 respectively. Also shown in Fig.26 is the -36°C water B.E.T. plot which, like the krypton B.E.T. plot and the various

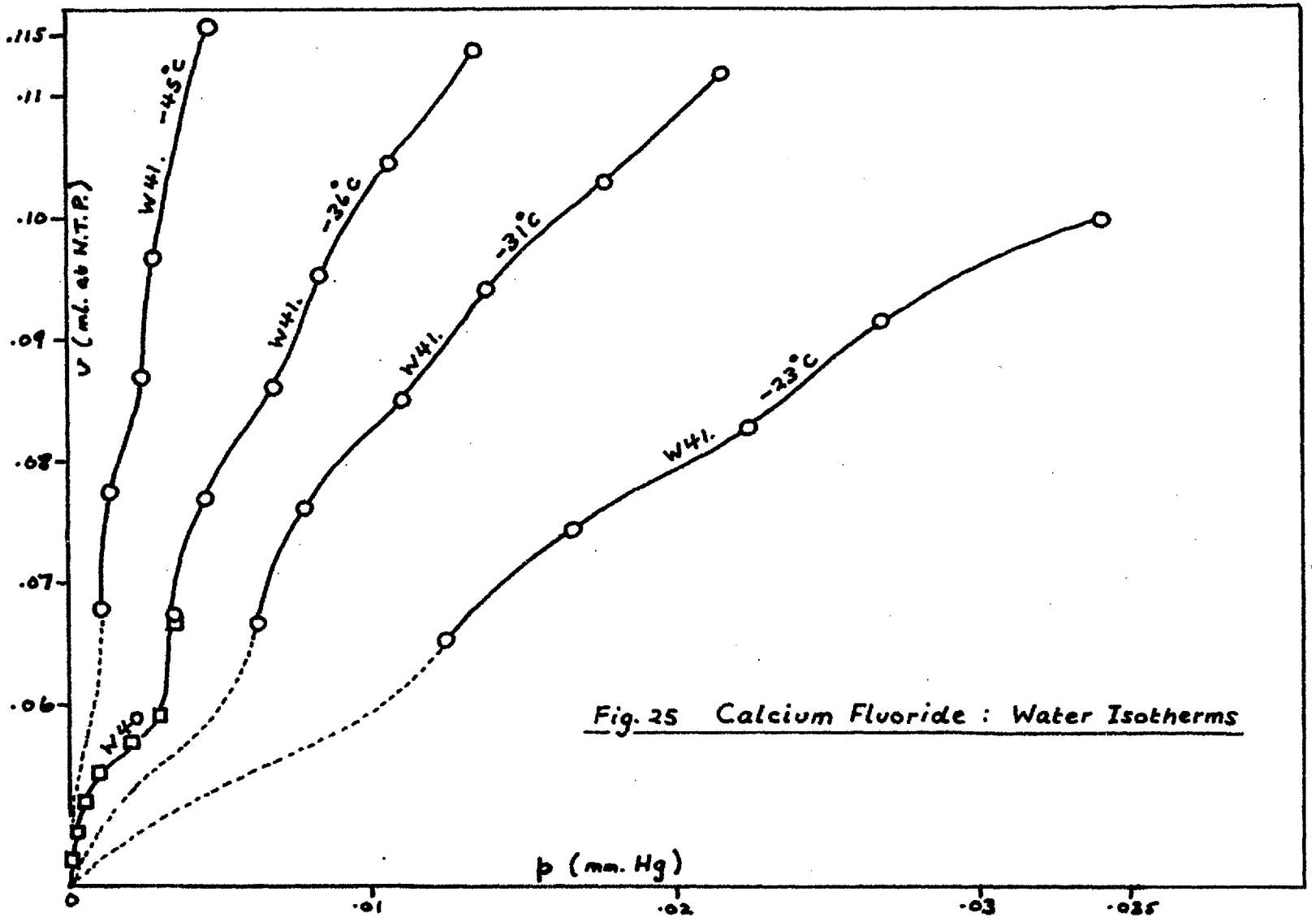

Fig. 25 Calcium Fluoride : Water Isotherms

Fig. 26 Calcium Fluoride

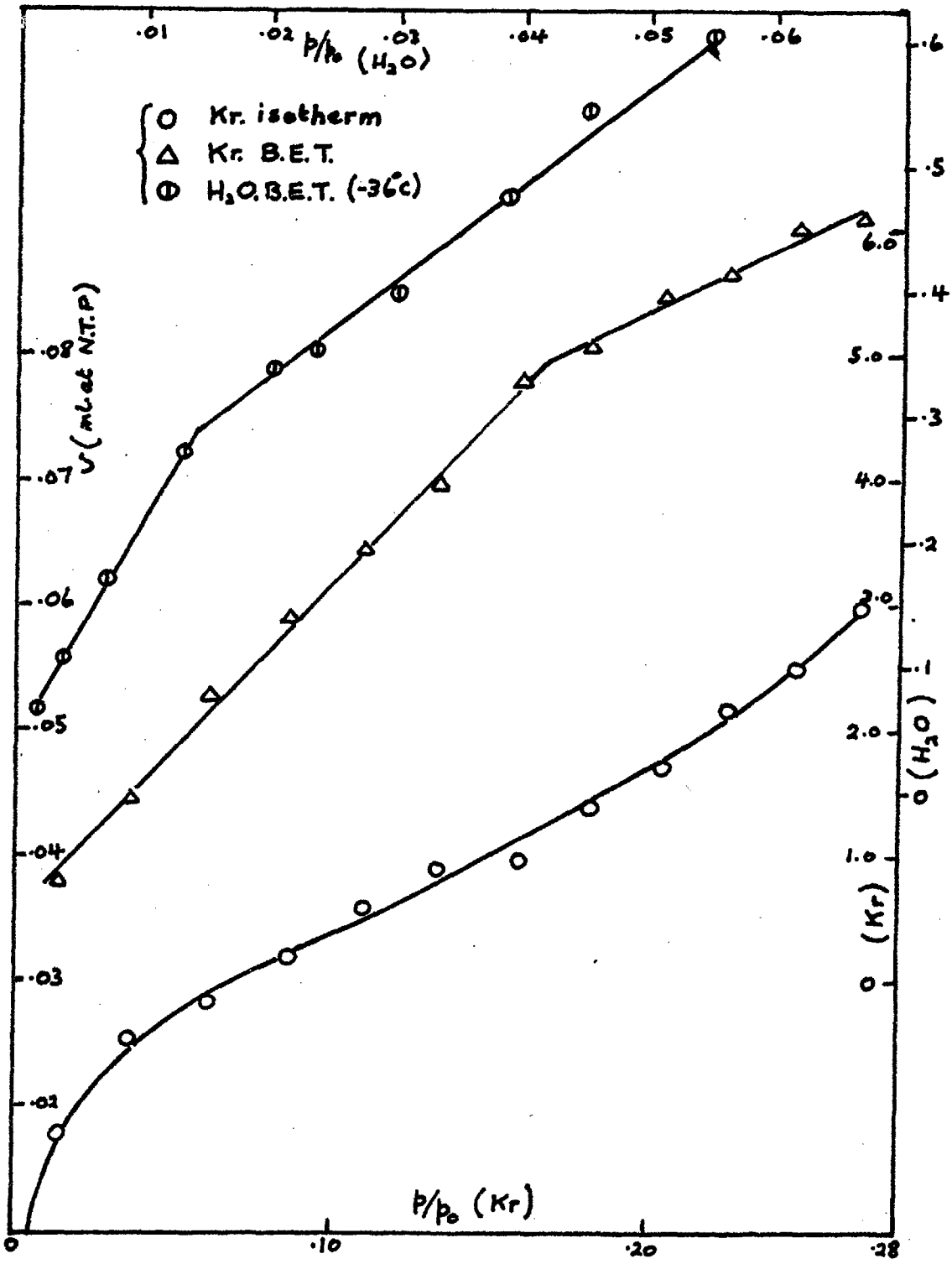

water B.E.T. plots for the other insoluble adsorbents, gave the same type of break, the surface areas in this case being 0.17 and 0.365 m^2. There was thus very close agreement between the surface areas of the two faces of CaF_2 determined by krypton and water adsorption. In this respect CaF_2 was unique amongst the various adsorbents, including KCl, since all the others gave much smaller areas when measured by the adsorption of water. This indicated that an entirely different mechanism was operating, and although the similarity between the water B.E.T. plot for CaF_2 and those in Fig.24 might suggest otherwise, this was probably due more to the effect of lateral interactions than the nature of the surface.

The compressibility function β' (section 1.7) was calculated from the slopes at various points on the curve of lnx versus lnp. The results, together with the isosteric heats of adsorption are given in Table 13 and shown as a function of v in Fig.27.

Table 13

v (ml at N.T.P.)	-lnx	-lnp	$-\beta^1$ ($mole^{-1}g$)	ΔH (kcal per mole)
.0095	3.635	9.905	21.7	
.014	3.26	9.20	13.9	
.0195	2.916	8.519	9.2	
.029	2.519	7.685	5.75	
.039	2.223	7.015	3.2	
.048	2.018	6.216	2.1	
.052	1.94	6.00	3.05	
.0575	1.835	5.81	5.6	
.067	1.677	5.656	3.9	12.8
.077	1.549	5.405	1.7	13.3
.085	1.429	4.992	1.65	12.2
.095	1.328	4.793	1.65	12.2
.105	1.237	4.548	1.2	12.7
.115	1.150	4.306	1.1	11.95

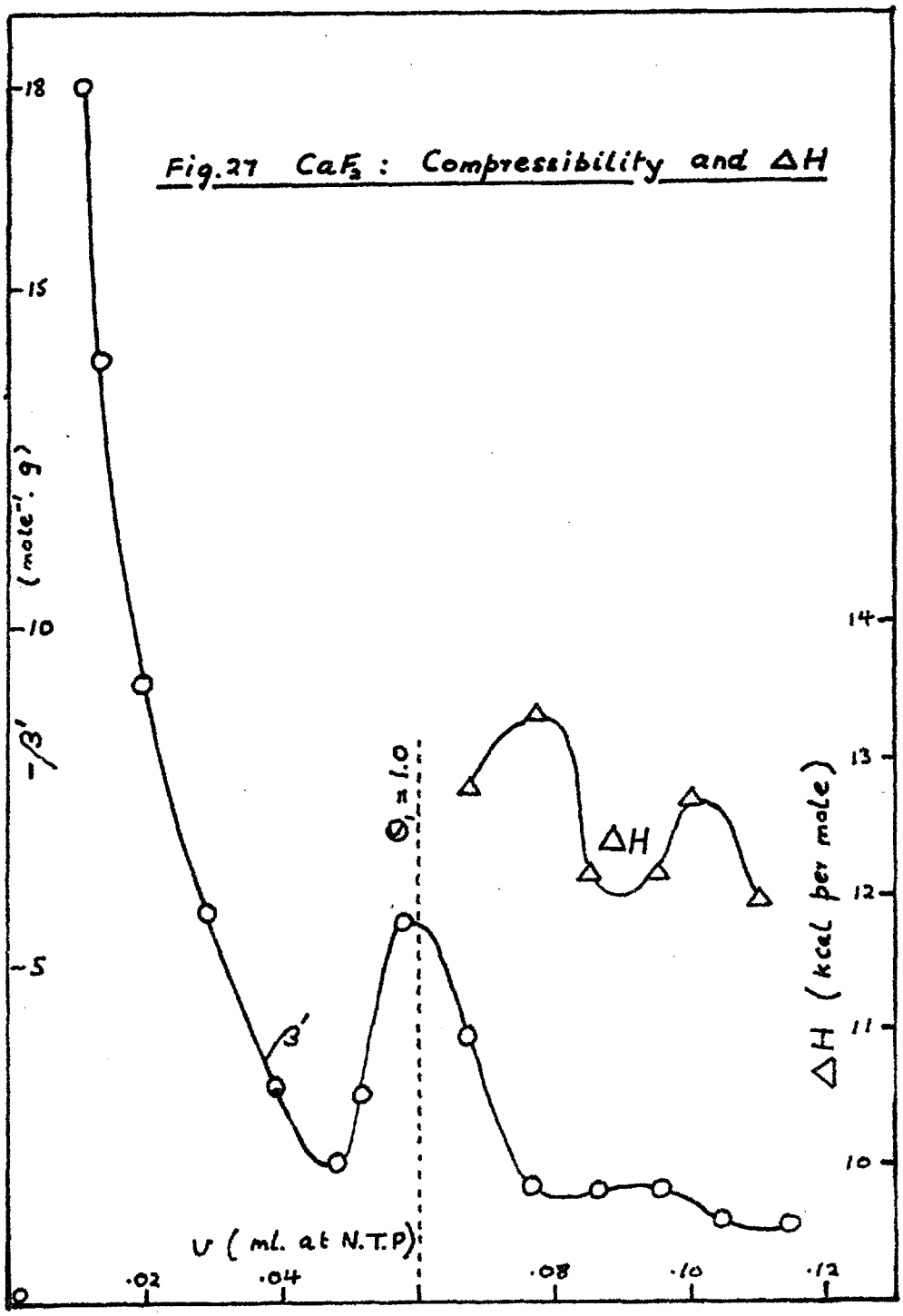
Fig.27 CaF_2 : Compressibility and ΔH
18
15
10
5
-β'
(mole⁻¹. g)
3'
θ₁ = 1.0
ΔH
14
13
12
11
10
ΔH (kcal per mole)
V (ml. at N.T.P)
.02
.04
.08
.10
.12

The secondary peak in the compressibility curve coincided almost exactly with the position of $\theta_1 = 1$. This meant that the two-dimensional condensation, shown by the sudden increase in the compressibility of the adsorbate, occurred when the monolayer for one of the homotattic faces was completed. According to the B.E.T. surface area measurements this surface was the smaller of the two, having an area about half that of the water.

The wavy shape of the isosteric heat curve reflected the stepwise nature of the isotherms in these regions, but there were not enough results to show any correspondence between the peaks of the curve and the positions of θ_1 or θ_2 ($v_m = 0.14$ ml) = 1.

3.4.2. Discussion

The adsorption of a water molecule on the 100 face of CaF_2 consisting only of fluoride ions presents the possibility of attachment by means of hydrogen-bond formation. This is illustrated by Fig.28 which shows a) a scale plan of the 100 fluoride face, and b) the position of a water molecule adsorbed by forming two hydrogen bonds across the diagonal of the cell square. This position is the most probable since there is very little distortion of the H - O - H bond angle. The oxygen-fluoride distance was taken as the mean of the hydrogen bond distances in HF and H_2O. On this model the water molecule is adsorbed above the centre of the cell square, and its effective cross sectional area is about 9.0 A^2, i.e., only slightly lower than the value of 10.5 A^2 generally accepted for use in surface area measurements. This probably accounts for

Fig.28 Scale drawing of CaF_2 crystal face (100) showing H_2O molecule adsorbed by H-bond formation

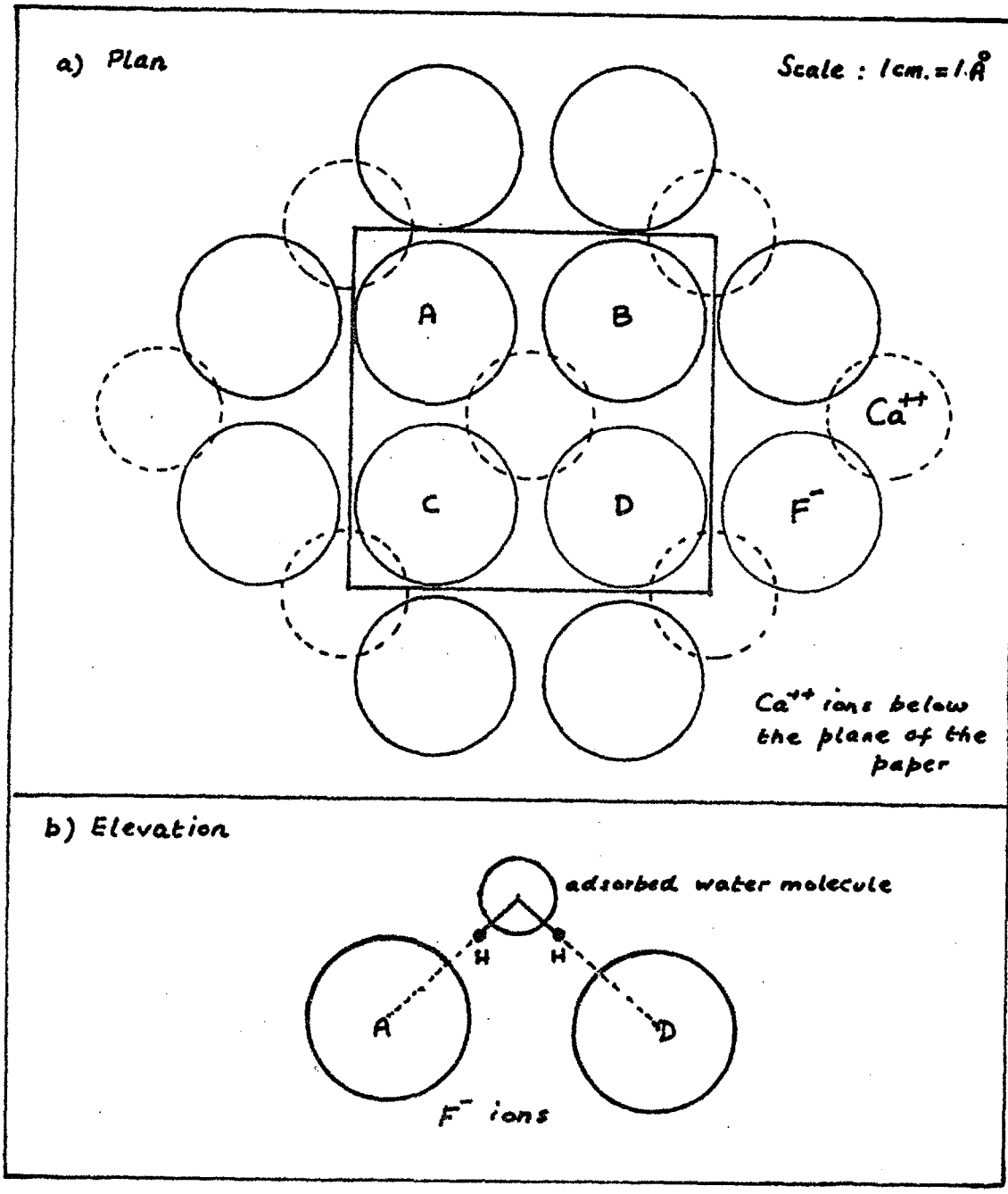

the good agreement between the surface areas of CaF_2 measured by krypton and water adsorption. Such a mode of attachment necessarily incurs alignment of the water multipoles in the same direction, so that any electrostatic dipole-dipole contribution to the lateral interaction potential (section 3.7.2.) would be a repulsion. The repulsion would be a maximum at the completion of the monolayer, as the molecules become more crowded together, but it is expected that before this stage is reached the adsorbed film would rearrange to a more condensed structure, eliminating the high repulsion energy.

3.5. Entropy of Adsorption

3.5.1. Integral entropy from spreading pressure

Equation (19) may be rewritten in the form,

$$\pi = KkT \int_0^x v \, d\ln x \qquad \ldots\ldots\ldots\ldots\ldots\ldots\ldots\ldots \quad (38)$$

where $x = p/p_c$, v = volume adsorbed per g at N.T.P., and the constant, K, $= \Gamma'/v$.

Curves of x versus $\frac{v}{x}$ were plotted at two different temperatures, T_1 and T_2, and the areas ($= \int_0^x v \, d\ln x$) under the curves then obtained by graphical integration. A linear extrapolation, $v = ax$, where a = constant, was used for the low pressure region. This corresponded to computation I of the methods of Emmett, Hill and Joyner (115). The entropy change, $S_s - S_{L^1}$, subscripts s and L^1 referring to the adsorbed and liquid states, was calculated for various values of π by means of the equation,

$$\frac{S_s - S_{L1}}{k}\ \pi = \text{const.} = \frac{\frac{1}{\bar{T}}\,(\Delta \ln x)}{\frac{1}{T_1} - \frac{1}{T_2}} + \ln \bar{x} \quad \ldots\ldots\ldots\ldots \quad (39)$$

where $\frac{1}{\bar{T}} = \frac{1}{2}\left(\frac{1}{T_1} + \frac{1}{T_2}\right)$,

$\Delta \ln x = \ln x_2 - \ln x_1$,

and $\ln \bar{x} = \frac{\ln x_1 + \ln x_2}{2}$

The results for AgI and PbI_2 are shown in Table 14. The entropy of the liquid was obtained by graphical integration of heat capacity data (116) for liquid water, i.e.

$$S_{L1} \text{ at temp. } T = 14.38 - \int_{T}^{T_0 = 273^{\circ}K} \frac{Cp}{T}\, dT$$

$$= 10.0 \text{ cal per mole per } {}^{\circ}C \text{ at } 235^{\circ}K$$
$$\text{and } 10.35 \text{ cal per mole per } {}^{\circ}C \text{ at } 238^{\circ}K$$

The absolute entropy, S_s, of the adsorbed phase is shown as a function of coverage, θ_K, in Fig.29. It will be recalled that these are total ($= S_c + S_{nc}$) values, and in the particular cases considered, i.e. AgI and PbI_2, it was uncertain to what extent the configurational term contributed to the total. The entropy values, therefore, could not be related to the various degrees of freedom of the adsorbate: it was only possible to examine the physical state and degree of mobility. For this it was assumed that the area, a, available per molecule, was equal to $\frac{l^2}{\theta_K}$, where l = lattice constant. Then by equation (23) the translational entropy of the 2-dimensional gas is given by: $16.5 - 4.56 \log_{10}\theta$ .... for AgI

$15.1 - 4.56 \log_{10}\theta$ .... for PbI_2

Fig. 29 Variation of Entropy of Adsorption with Coverage

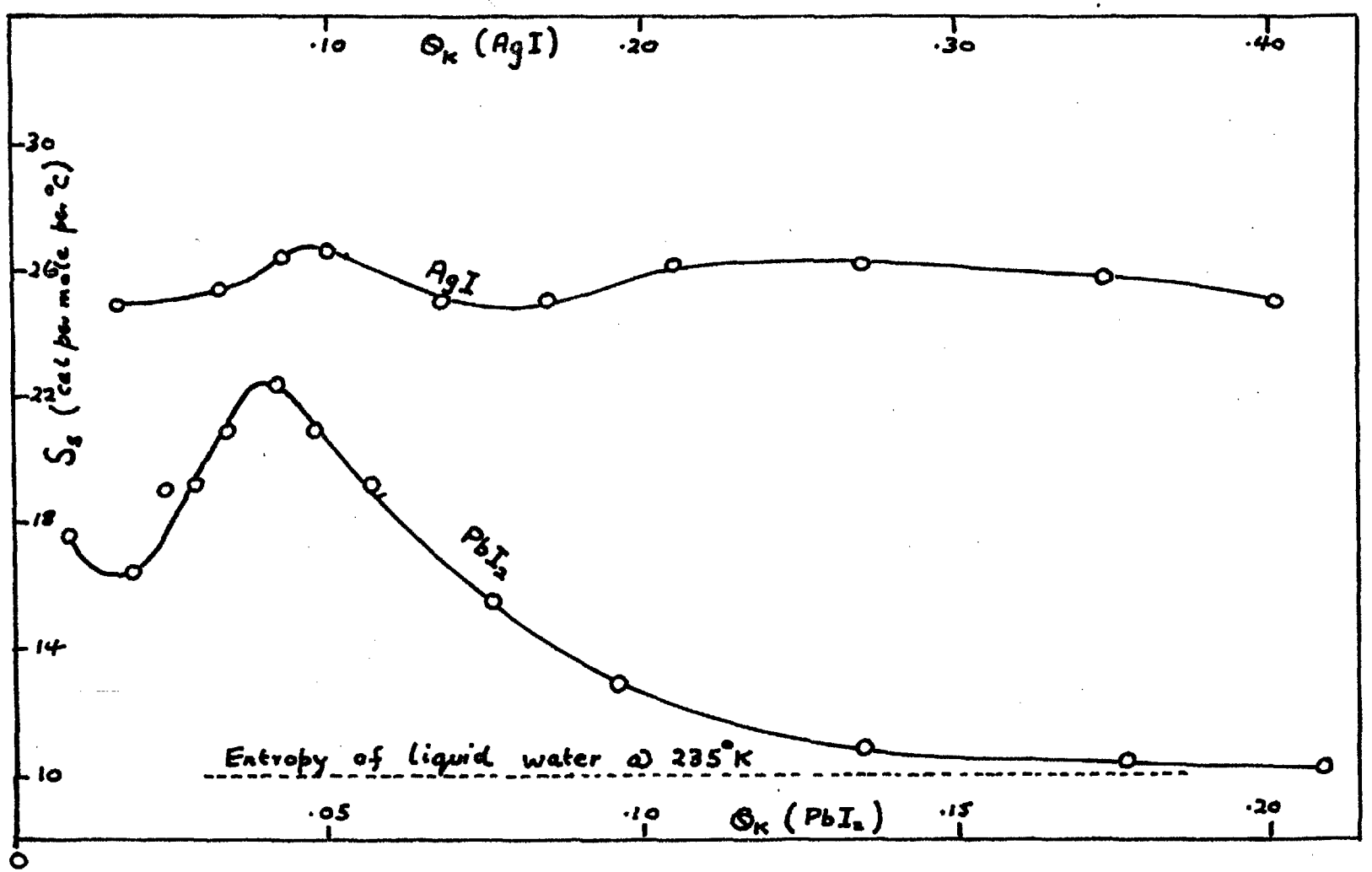

Table 14

θ_K		π (erg cm^{-2})		$x_1 \times 10^{-3}$		$x_2 \times 10^{-3}$		$S_s - S_{L^1}$ (cal per mole/°C)	
AgI	PbI_2	AgI	PbI_2	AgI -45°C	PbI_2 -45°C	AgI -23°C	PbI_2 -31°C	AgI	PbI_2
	.009		0.1		.3		.6		7.6
	.018		0.2		.65		1.2		6.4
	.0235		0.3		.95		1.85		9.0
	.029		0.4		1.3		2.5		9.2
	.034		0.5		1.63		3.25		10.9
	.042		0.7		2.35		4.8		12.4
	.0475		0.8		2.9		5.6		10.9
.033	.057	1.0	1.0	2.2	4.15	7.1	7.45	14.4	9.15
	.076		1.5		8.25		12.8		5.5
.066	.096	2.0	2.0	4.5	14.0	14.0	19.5	15.0	2.9
.085	.135	2.5	2.5	5.6	21.15	18.0	27.1	16.15	.84
.10	.18	3.0	3.0	6.9	28.35	21.8	35.3	16.2	.44
	.21		3.5		35.9		43.8		.21
.135		5.0		13.5		37.5		14.6	
.17		7.0		21.5		57.5		14.7	
.215		9.0		30.4		82.8		15.8	
.265		10.0		35.5		95.5		15.8	
.40		12.0		46.3		115.9		14.7	
.455		14.0		57.7		135.0		13.6	
.53		17.3		70.4		170.0		14.7	

For example, at $\theta_K = 0.01$, $(S_T)_{20}$ would be 25.6 cal per mole per °C for AgI and 24.2 cal per mole/°C for PbI_2. Thus the water adsorbed on AgI was in a state equivalent to that of a 2-dimensional gas, and remained much the same over the range investigated. In contrast

the entropy curve for PbI_2 gave a fairly sharp peak at $\theta \approx 0.04$ and then decreased monotonically to the entropy of the 3-dimensional liquid. This indicated second and higher layer adsorption, producing liquid aggregates at isolated sites on the surface.

3.5.2. Integral entropy for Langmuir adsorption on AgBr

The isosteric heats of adsorption of water for stage 2 photolysed AgBr (Fig.19) were fairly constant over the range investigated. In fact, as a first approximation, the adsorption could be regarded as Langmuir in character; therefore the method described in section 1.4.2. was applied. Table 15 shows the integral entropy results obtained.

Table 15

θ_K	S_g	ΔS	$\bar{S}$	$\bar{S}_c$	S_{nc}
	cal per mole/°C				
.032	71.7	43.85	27.8	6.9	20.9
.048	70.9	43.85	27.0	5.9	21.1
.068	69.9	43.85	25.0	5.2	19.8
.097	68.7	43.85	24.85	4.4	20.45
.115	68.15	43.85	24.3	4.0	20.3
.135	67.7	43.86	23.85	3.6	20.25
.160	67.5	43.85	23.6	3.2	20.4

S_g was calculated from equation (21) using the spectroscopic value (117) of 45.13 cal per mole per °C for S^o_g. The integral $\int_{T_o}^{T} \frac{Cp}{T} dT = 2.035$ for T_o - 298°K and T = 228°K was estimated graphically from the data of Guiague and Stout (118).

In this particular case then, S_{nc} was known and could be examined in terms of the vibrational and rotational contributions.

3.5.3. Vibrational entropy

The calculation of S_v for adsorbed molecules depends on the assignment of a reasonable value to the frequency, ν, of vibrations relative to the surface. In general, for S.H.M.,

$$\nu = \frac{1}{2}\left(f/m\right)^{\frac{1}{2}} \qquad \ldots\ldots\ldots\ldots\ldots\ldots\ldots\ldots \quad (40)$$

where f = restoring force and m = mass of vibrating particle; and, if $f \propto \Delta H$, $\nu \propto \Delta H$. This particular frequency represents the mean frequency for vibration, in 3 different directions. However, as Bratt (45) has pointed out, the available evidence suggests that ν is not so simply related to ΔH. Thus Drain and Morrison (119) showed from an analysis of adsorption data of O_2, N_2 and A on rutile that ν was proportional to ΔH rather than its square root. In view of the absence of evidence to the contrary, the equation $\nu = K\Delta H$ was used for the following analysis.

The low temperature specific heat of ice is given by

$$C = k\left(\frac{T}{\Theta}\right)^3 \qquad \ldots\ldots\ldots\ldots\ldots\ldots\ldots\ldots \quad (41)$$

where Θ, the characteristic temperature, $= \frac{h\nu_{max}}{kT}$ and $\nu_{max} = \frac{4}{3}\nu_{mean}$ (69). At 228°K, $\nu_{max} = 4 \times 10^{12}$ sec^{-1} (69) therefore $\nu_{mean} = 3 \times 10^{12}$ sec^{-1}; and applying this to vibration about a hydrogen bond of energy 6.1 kcal per mole (120), $\nu = 3 \times 10^{12}$ and $K = 5 \times 10^{11}$. Now according to Orr's data (67) for the adsorption of argon on KCl, $\nu = 1.0 \times 10^{12}$ sec^{-1} and $\Delta H = 2.5$ kcal per mole, so that $K = 4 \times 10^{11}$. For water adsorbed

on KCl, AgBr etc., the value of K was assumed to be the mean of these two values, i.e. 4.5×10^{-1}, giving $\nu = 4.5 \times 10^{12}$ sec^{-1} for the special case of AgBr, where $\Delta H = 10.0$ kcal per mole. Then, from equation (25), $S_V = 1.8$ cal per mole per ^oC. The internal vibrational entropy $S_I = 0.04$ cal per mole per ^oC (45) was assumed to be the same as in the gas phase.

3.5.4. Rotational and librational entropy

The entropy, S_R, of rotation about an axis normal to the surface may, in the absence of external interactions, be regarded as the same as in the gas phase. By equation (26), using the value of I_a given by Moelwyn Hughes (69), $S_R = 2.5$ cal per mole per ^oC, and equation (24) can now be written as,

$$S_{nc} = 3(1.8) + 0.04 + 2.5 + 2S_L = 20.5 \quad \ldots\ldots\ldots\ldots\ldots \quad (42)$$

giving the librational term $S_L = 6.28$ cal per mole per ^oC. To calculate S_L from equation (27) would have required a knowledge of the restricting potential, but in view of the uncertainty of this it was decided to do the converse, i.e., use the value of 6.28 for S_L in equation (27) in order to evaluate the restricting potential and then examine this in terms of the possible restrictive forces involved. For the values of the moments of inertia, I_b and I_c, given by Moelwyn Hughes (69) the restricting potential was 0.95 kcal per mole. This is probably related to the difference in energy of adsorption between a water molecule adsorbed normally and in the upside down position, and has some bearing on the lateral interactions between adsorbed molecules (section 3.7.2.).

Such a low value for the restricting potential might be expected in cases where the electrostatic contribution to the heat of adsorption is small. Thus, for AgBr the observed heat of adsorption of 10.0 kcal per mole is made up of the sum of the electrostatic, U_E, dispersion, U_{VDW}, and repulsion, U_R, contributions (section 1.5.) and the restricting potential should not be very different from $2U_E$, since the potential energies of a dipole in positions, (a) aligned with the field and, (b) turned through 180°, are equal but negative and positive respectively. In this case the contributions of U_{VDW} and U_R to the restricting potential can be assumed to be negligible compared with that of U_E. The calculations of section 3.6.2. showed that the water molecule was adsorbed above a lattice vacancy bordered mainly by silver atoms, so that U_E, and therefore the restricting potential, should both be low.

This will also apply to the adsorption above the centre of the lattice square of simple cubic crystals, where U_E is zero, but in other cases involving more complex adsorbents, e.g. PbI_2, where U_E is probably quite large, the complete rotation in this way would be excluded.

3.6. Calculation of the Heat of Adsorption

3.6.1. Adsorption on a cubic lattice

As stated in section 2.3. the two simplest cases are KCl and AgBr, since both have a simple cubic lattice, and, if the water molecule is assumed to be adsorbed above the centre of a lattice square, U_E is zero. The calculations of dispersion and repulsion

energies for various distances $z = \rho a$, where $2a$ = lattice constant, were made as follows:

(a) Dispersion energy

Following Orr (67), the Kirkwood equation may be written in the form,

$$U = \frac{6mc^2}{a^6} \left[\frac{\alpha_0 \alpha_+}{\frac{\alpha_0}{\chi_0} + \frac{\alpha_+}{\chi_+}} S_+(\rho) + \frac{\alpha_0 \alpha_-}{\frac{\alpha_0}{\chi_0} + \frac{\alpha_-}{\chi_-}} S_-(\rho) \right] \quad \ldots\ldots\ldots \quad (43)$$

where the subscripts $_0$, $+$, and $-$ refer to water, cation and anion, and the inverse sixth power of distance summations S_+ and S_- = $\frac{1}{2}\sum\rho$. The values of $\sum\rho$ were taken from the data of Orr. The polarisabilities were obtained from Mayer (121) and Pauling (122), and the magnetic susceptibilities from Hoare and Brindley (123) and Pauling (122).

Equation (43) then gives:-

U_{VDW} = 1638 kcal per mole for KCl,

and 4208 kcal per mole for AgBr.

(b) Repulsion energy

Using the repulsion energy constants (69) for water and the inert gases, A, Kr and Xe, with which the various ions are isoelectronic, the repulsion constants for water/KCl and water/AgBr were calculated from equation (29) as,

KCl : $A_{0+} = A_{0-} = 1.642 \times 10^{-92}$ erg cm^n

AgBr : $A_{0+} = 3.873 \times 10^{-92}$ erg cm^n

$A_{0-} = 2.307 \times 10^{-92}$ erg cm^n

The repulsion exponent n was assumed to be 10.5, i.e. the mean of 9 for inert gases and 12 for water. The summation of $U_R = Az^{-10.5}$ was made over the nearest 20 ions.

(c) The energy of adsorption

The various values of U_{VDW}, U_R and the sum $(U_{VDW} + U_R)$ = the energy of adsorption U are given in Table 16, and the potential energy curves of U as a function of distance z are shown in Fig.30. The depth of the potential well (plus zero point energy $\epsilon_0 = h\nu_0 \simeq 50$ cals per mole for $\nu_0 = 10^{12}$ sec^{-1}) represents the energy of adsorption at the equilibrium distance, z_e.

The calculated values of $\Delta H(= U + RT)$ were thus 3.55 kcal per mole for KCl and 4.3 kcal per mole for AgBr, the higher heat of adsorption on the latter being the result of the higher polarisabilities and magnetic susceptibilities of Ag^+ and Br^-. On this basis it would be expected that a simple cubic lattice of AgI would give a higher heat of adsorption than that of AgBr.

As far as the experimental results are concerned the calculated value for KCl showed fairly good agreement with the results observed at the lower temperature range (section 3.1.3.4.). Although these experimental results may have applied to the 110 plane, it was assumed, on the basis of the results of Lenel and Orr (section 1.5.), that the experimental results for the 100 plane would be much the same. This justified the initial assumption that the water molecule was adsorbed above the centre of the lattice square.

The calculated heat of adsorption on AgBr was somewhat lower than the observed value of about 6.0 kcal per mole. This was probably due to adsorption in cracks or surface irregularities

Fig. 30 Potential Energy Curves : H_2O/KCl and H_2O/AgBr

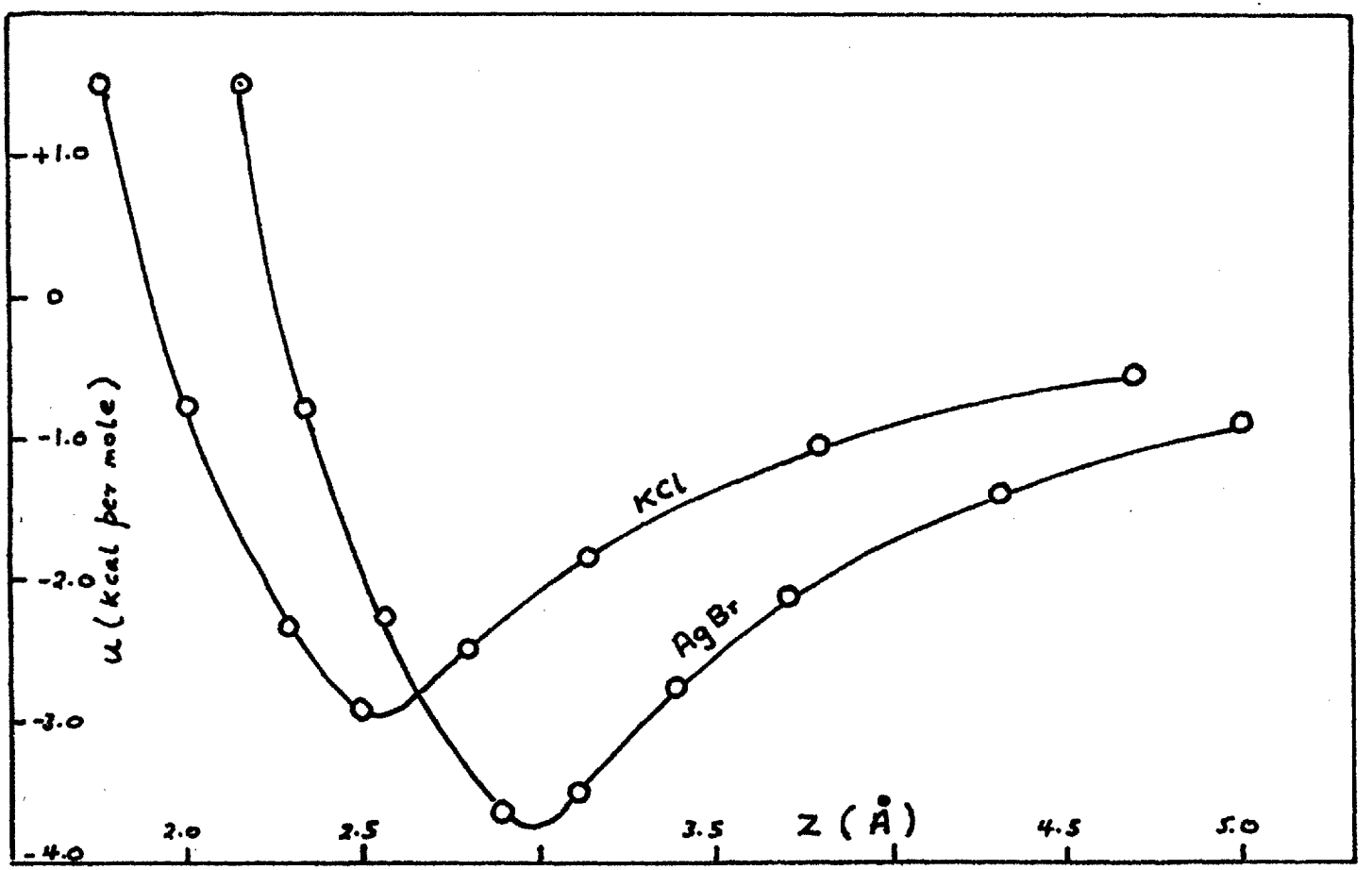

(section 1.5.) of high adsorption potential. The calculated equilibrium distance from the surface was greater (3.0 Å) for AgBr than KCl (2.5 Å), as would be expected from the smaller R-X distance (2.885 Å) of the bromide.

Table 16

	z(Å)	$\rho = \frac{z}{a}$		$-U_{VDW}$	$+U_R$	U
				cal per mole		
KCl	1.75	.56	8.132	13321	14827	+1506
a=3.14 Å	2.0	.63	6.255	10244	9438	- 806
	2.3	.73	4.315	7067	4820	-2247
	2.5	.79	3.378	5532	2565	-2967
	2.8	.89	2.358	3862	1422	-2440
	3.14	1.00	1.564	2562	713.6	-1848
	3.8	1.21	.905	1482	432	-1050
	4.7	1.50	.365	599	32	- 567
AgBr	2.12	.73	4.315	18158	21043	+2885
a=2.885 Å	2.3	.79	3.378	14215	13400	- 815
	2.6	.89	2.358	9922	7653	-2269
	2.9	1.00	1.564	6583	2884	-3699
	3.1	1.075	1.184	4982	1491	-3491
	3.4	1.18	.906	3814	1071	-2743
	3.7	1.28	.692	2913	809	-2104
	4.3	1.50	.365	1539	156	-1383
	5.0	1.73	.234	986	90	- 896

No calculations were carried out for water adsorbed above the tetrahedral zinc blende type lattice of AgI, but it was apparent that this would involve extra laborious and complex summations of the electrostatic ion-dipole and polarisation

terms, which would contribute to a higher overall heat of adsorption than that for the simple cubic crystal. However, it could be deduced from the isosteric heat curve (Fig.20) that the heat of adsorption of water on the bare surface of tetrahedral AgI was between 5 and 7 kcal per mole.

Some approximate calculations, involving the electrostatic terms, were carried out for the less difficult case of adsorption above a surface lattice vacancy of AgBr, since this was particularly relevant to the effects concerning photochemical decomposition and entropy of adsorption. The method is outlined below.

3.6.2. Adsorption above a lattice vacancy of AgBr

Fig.31 shows a water molecule (linear dipole model) adsorbed directly above a surface anion vacancy at a distance z = 2.0 Å. The position shown is that of maximum ion-dipole interaction, U_{ID}, energy as indicated by the results of Table 17. The dipole is of length = 1.2 Å and charge = 1.567×10^{-10} esu.

Table 17

z(Å)	$U_{ID}(x\ e_i e_w)$
0.8	.068
1.0	.078
1.2	.083
1.4	.087
2.0	.094
2.6	.090
3.1	.083

Fig. 31 Water Molecule adsorbed above a surface lattice vacancy of AgBr

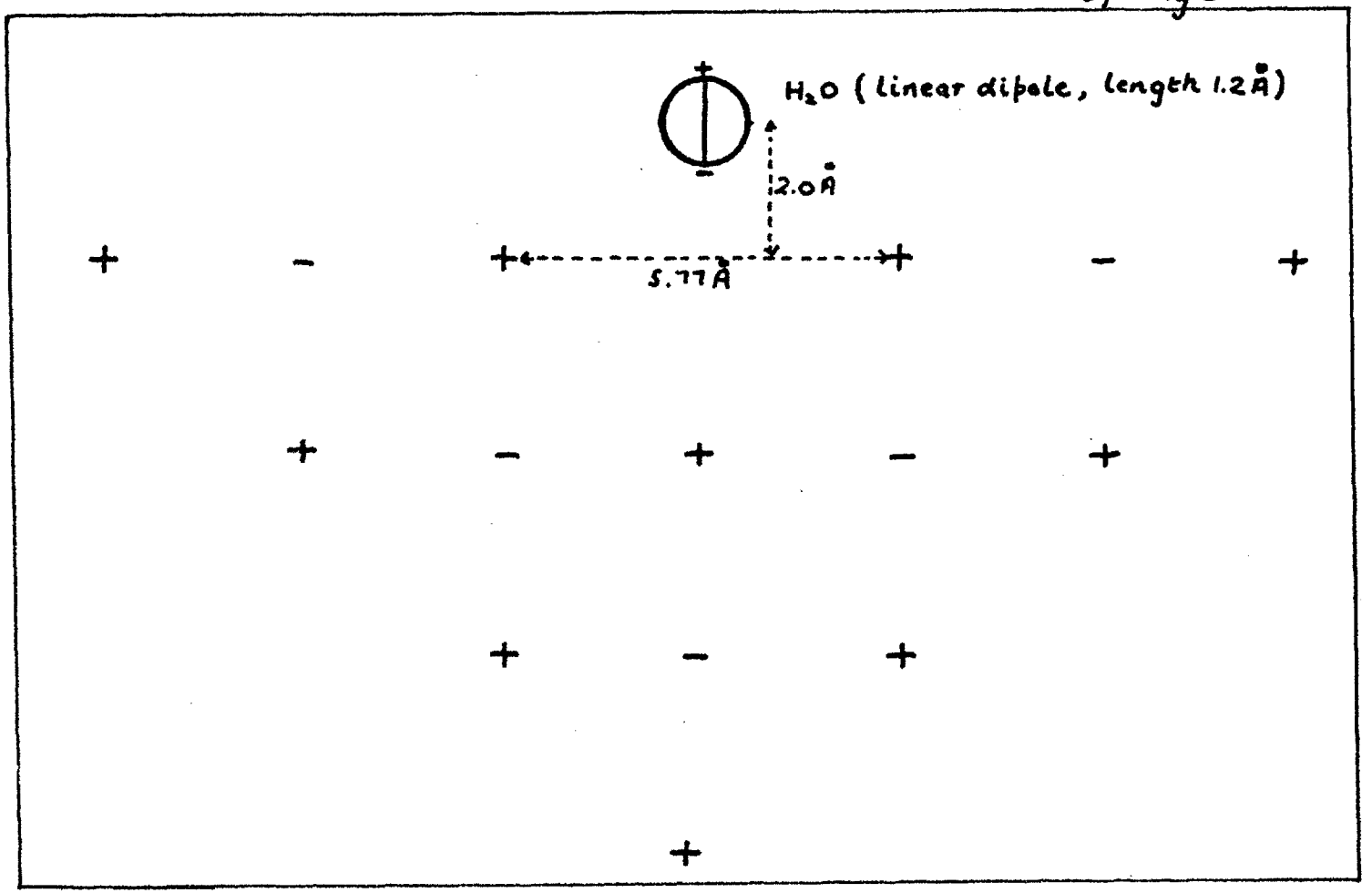

These results were obtained by summing the ion-dipole interactions, $\frac{e_i e_w}{z}$, where e_i is the charge on the ion (electronic charge) and e_w is the charge on the water dipole, over the nearest 5 ions of the plane shown, and are proportional to the complete ion-dipole interactions with the whole 3-dimensional crystal.

The complete ion-dipole term at z = 2.0 was estimated by integrating the field, F, data of Lennard Jones and Dent (65) and Orr (67) for the position above an ion of a simple cubic crystal, and then subtracting the electrostatic term due to the single Br^- ion now vacant. Thus the potential, u_1, due to the complete lattice is given by;

$$u_1 = e_w \int_{\rho = .485}^{\rho = .9} F d = \frac{.048\ e_w\ 2\pi e_1}{a^2} \quad \ldots\ldots\ldots\ldots \quad (44)$$

where the limits correspond to the ends of the water dipole; and the potential, u_2, due to Br^- alone, by;

$$u_2 = e_i e_w \left(\frac{1}{1.4} - \frac{1}{2.6}\right) = .33 e_i e_w. \quad \ldots\ldots\ldots\ldots \quad (45)$$

From this, $U_{ID} = u_1 - u_2 = 32$ kcal per mole.

In addition to the U_{ID} energy there will be interaction terms due to mutual polarisation dispersion and repulsion. The equation:

$$U_p = -\frac{1}{2}\alpha_w F^2 - \frac{\alpha_i \mu^2}{a^6} \quad \ldots\ldots\ldots\ldots\ldots\ldots\ldots \quad (46)$$

where μ is the dipole moment of water and α the polarisability, is a suitable approximation for the polarisation interaction between an ion and a water molecule (point dipole). Probably the largest contribution would be from $\frac{1}{2}\alpha_w F^2$, which, by

extrapolating the field data of Orr, and using $\alpha_w = 1.48 \times 10^{-24}$ (121) was shown to be 5.7 kcal per mole.

The $(U_{VDW} + U_R)$ sum would be expected to be somewhat greater than the value of 3.8 kcal per mole obtained from the potential energy curve for the normal case, but not greater than four times this value. Thus De Boer and Custers (72) showed that for a molecule adsorbed at distance $z = 0$ from the first layer above a hemispherical crevice, the heat of adsorption was about four times as great as for a plane surface. In this case $z = 2.0$, so $(U_{VDW} + U_R)$ would probably be nearer to 4 than 15.4 kcal per mole.

These results show that the total equilibrium heat of adsorption of water above a surface lattice vacancy in AgBr would be of the order of 40 - 45 kcal per mole, a value which is substantially higher than the experimental values. However, if the particles surrounding the vacancy were silver atoms, not ions, the electrostatic terms would be considerably reduced and, presumably, the largest contribution would then be from $(U_{VDW} + U_R)$. The restricting potential of 0.95 kcal per mole (section 3.5.4.) for stage 2 photolysed AgBr suggests that the U_{ID} is only 0.475 kcal per mole, confirming this. In actual fact there would be an extra contribution from the highly polarisable silver atoms, but the general picture as such is reasonably compatible with the observed heats of adsorption.

3.7. Treatment of Lateral Interactions

3.7.1. Nearest neighbour interaction energy

The interaction between two adsorbed water molecules should, neglecting the polarisation induced by the surface field, not be very much different from that of two isolated molecules at the same distance, a, apart in the gas phase. A combination of the Lennard Jones '6-12' equation and an angle dependent dipole term may be used, i.e.

$$u = Aa^{-12} - Ba^{-6} - (C \cos \Theta)a^{-3} \quad \ldots\ldots\ldots\ldots\ldots\ldots \quad (47)$$

Using the linear dipole model for water, it can be shown (69) that the maximum electrostatic term is $\frac{2\mu^2}{a^3}$, when the dipoles are oriented parallel and head to tail. From the values of A and B given by Moelwyn Hughes (69), the various terms corresponding to a = 2.8 Å (O - - O distance in ice) are;

U_R;	+2.1 kcal per mole
U_{VDW};	-2.42 kcal per mole
U_E;	-4.5 kcal per mole
total	4.8 kcal per mole

This may be compared with the value of 6.1 kcal per mole (120) for water-water interactions involving hydrogen bonds. Since the electrostatic term is the largest it was assumed that the interaction potential between two adsorbed water molecules is given by;

$$u = -\frac{K}{a^3} \quad \ldots\ldots\ldots\ldots\ldots\ldots\ldots\ldots \quad (48)$$

where $K = 4.5(2.8)^3 = 99.0$.

For example, for water adsorbed on AgI, a = 3.235 Å and u = 4.0 kcal per mole.

3.7.2. Higher neighbour interactions: oriented dipoles

The ideas of the previous section were extended to the higher neighbour interactions of water molecules adsorbed in a regular pattern on the surface. The simplest case is that of a square array, and if the interaction between any two nearest neighbours is attractive, by virtue of the oriented dipoles, then some of the higher neighbour interactions would be repulsive, depending on their positions. This is illustrated by the diagram below, and the various interaction energies corresponding to a = 3.235 Å are shown in Table 18.

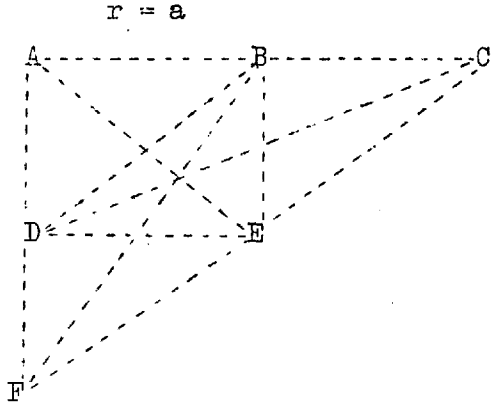

Table 18

A – B B – C A – D D – E B – E	attraction, type R_1 (nearest neighbour)	$u = \frac{k}{r^3}$ (kcal per mole) -4.0
D – C B – F	attraction, type K	-0.38
A – E B – D C – E	repulsion, type R_1	+1.47
F – C	repulsion, type R_3	+ .18
A – C A – F	repulsion, type R_2	+ .48

Using this model the average interaction energy was calculated statistically as a function of the number n of molecules adsorbed (up to n = 5) by means of the Boltzmann equation,

$$\frac{n_1}{n_2} = \exp\left(\frac{E_1 - E_2}{kT}\right) \qquad \ldots\ldots\ldots\ldots\ldots\ldots\ldots \qquad (49)$$

where n_1 and n_2 are the respective numbers of molecules adsorbed on sites of adsorption potential E_1 and E_2. The results are shown in Table 19.

Table 19

n	u(kcal per mole)
1	0
2	4.0
3	3.45
4	6.55
5	6.55

The significant feature of these results was the decrease in u accompanying entry of the third molecule into the array. Since there would be many of these arrays forming at different points on the surface at any moment, the isosteric heat should largely depend on the distribution of E over the surface. In the general case involving a heterogeneous surface there would be an inflexion in the isosteric curve at a point corresponding to the decrease in u, and, the more marked the heterogeneity, the less marked the inflexion, since the effect is an average over all the arrays. For a uniform surface, and this does not necessarily mean that the surface must be homo-ionic, there would be a decrease of 0.55 kcal per mole.

This is somewhat lower than the observed experimental decrease of 1.5 (AgI) and 1.0 (AgBr) kcal per mole. However, if the hydrogen bond energy of 6.1 kcal per mole is used instead of 4.0 kcal per mole for the nearest neighbour, R_1, interaction energy, the calculated decrease in u, corresponding to n = 3, then becomes 1.0 kcal per mole. This suggests that the lateral interactions between the adsorbed molecules may be based on hydrogen bonding rather than simple Coulombic force.

3.7.3. Higher neighbour interactions: general treatment

The above oriented dipole theory necessarily required a restricting potential less than the nearest neighbour interaction energy, otherwise the dipoles would all be pointing the same way and all the interactions would be repulsions. In this sense, then, the theory was applicable only to cases such as AgBr and KCl where the electrostatic contribution to the heat of adsorption is low or equal to zero. However, the theory could be generalised to cover all cases simply by disregarding the idea of orientation and applying a general interaction equation of the same form as equation (48)

$$\text{i.e.,} \quad u = -\frac{w}{r^3} \qquad \ldots\ldots\ldots\ldots\ldots\ldots\ldots\ldots \qquad (50)$$

In this case the results of Table 20, below, show that an interaction inflexion would occur as the fifth molecule is adsorbed outside the formed square array.

Table 20

n	u(kcal per mole)
1	0
2	0.8
3	1.1
4	1.9
5	1.25
6	2.05

The interaction parameter w in equation (50) was arbitrarily based on the total interaction energy of one water molecule inside a large 3-dimensional array. For ease of calculation the structure was assumed to be square packed, and by summing over the nearest 72 molecules of intermolecular distance 3.0 Å and equating the total to the 3-dimensional heat of liquefaction, w was shown to be 21.6 and the maximum possible value of u in a monolayer, i.e. the 2-dimensional heat of liquefaction, 5.1 kcal per mole.

3.7.4. Discussion

The above mentioned treatments of lateral interactions predicted the occurrence of a maximum at an early stage in the isosteric heat curve, as exhibited experimentally by the silver halide - lead fluoride group, but as such did not cover the whole of the curve, particularly the secondary rise towards the 3-dimensional heat of liquefaction. However, it was apparent that this rising portion could only be accounted for by one or more of the following.

(a) Multilayer in preference to monolayer formation occurs soon after the completion of square arrays.

(b) There is a phase change to a more close packed assembly.

(c) Increased interaction energy as a result of increasing numbers of square arrays forming on part of the surface. For this, the maximum energy of interaction in a monolayer, i.e. the 2-dimensional heat of liquefaction, plus the heat of adsorption on the bare surface would have to be approximately equal to the 3-dimensional heat of liquefaction.

Now significant effects due to (a) alone could largely be discounted on entropy grounds (section 3.5.1.) although it should be emphasised that there is a high probability of the fifth molecule being preferentially adsorbed above the centre of the four membered array, particularly in cases where the heat of adsorption on the bare surface is low.

As regards (b), the entropy curve showed no marked discontinuity corresponding to a two-dimensional gas-liquid phase change. This was probably because the surface was not sufficiently uniform or homo-ionic. A similar type of phase change, e.g. two-dimensional liquid - more compressed liquid, is perhaps feasible for this particular surface on which the heat of adsorption is not very different from the lateral interaction energy, but this would also be expected to be shown by the entropy.

The most likely explanation is probably that of (c) since, as shown in section 3.6.1., the heat of adsorption of water on AgI was about 6.0 kcal per mole, which agrees well with the difference between the calculated two-dimensional heat of liquefaction of 5.1 kcal per mole (section 3.7.3.) and the three-dimensional heat of liquefaction of 11.5 kcal per mole i.e. 6.4 kcal per mole. In support of this it may be pointed out that the maximum did not appear until over half the surface was covered.

With KCl, the ΔH curve drawn (Fig.12) through the various experimental points showed no inflexion corresponding to the one shown by the AgI-PbF_2 group. However, this line represented the mean of several results incorporating different stages of sintering of the film, and it is likely that the inflexion, if any, would be obscured by this. Thus, considering run W16 alone, an inflexion can, feasibly, be seen at $\theta = 0.8$.

For PbI_2, the increase in ΔH marking the onset of lateral interactions was only 1.0 kcal per mole, which is low compared with the values of 2 to 4 kcal per mole indicated by the theoretical treatment for the monolayer. This was not surprising in view of the effect of heterogeneity (section 3.6) tending to counteract any increase in ΔH; and, in any case, the mechanism for this adsorbent was different in that some multilayer adsorption was apparently involved.

3.8. The Rate of Adsorption

The variation with time, t, of the volume, v, of water vapour adsorbed on CaF_2 at 20°C is shown in Fig.32. This represents a typical rate plot for the four adsorbents studied, namely CaF_2, PbF_2, AgI and PbI_2. The general rate equation for these adsorbents was found by plotting $\log \frac{v_e}{p(v_e - v)}$ against $t^{\frac{1}{2}}$ to give straight lines, shown for CaF_2 in Fig.32.

$$\text{Thus, } \log \frac{v_e}{p(v_e - v)} = kt^{\frac{1}{2}} - \log p_o \quad \ldots\ldots\ldots\ldots\ldots\ldots \quad (51)$$

where,

v_e = volume adsorbed at equilibrium

p = pressure at time t

p_o = pressure at t = 0

k = constant

and, from equation (51)

$$v = v_e \left(1 - p_o/p \exp\left(-kt^{\frac{1}{2}}\right)\right) \quad \ldots\ldots\ldots\ldots\ldots \quad (52)$$

The results corresponding to different temperatures and values of v_e are given in Tables 22 to 25, and the resulting values of k are summarised below in Table 21.

Equation (51) was of the same form as that proposed by Bangham and Sever, and also by Isakawi (section 1.8.), but in this case the pressure term was included because the rates were not determined at constant pressure. The values of k were about the same magnitude as that reported by Isakawi for water adsorbed on MgO (k = .075 at 30°C), and the adsorption times to equilibrium were also much the same.

Fig. 32 Rate of Adsorption of Water Vapour on CaF_2

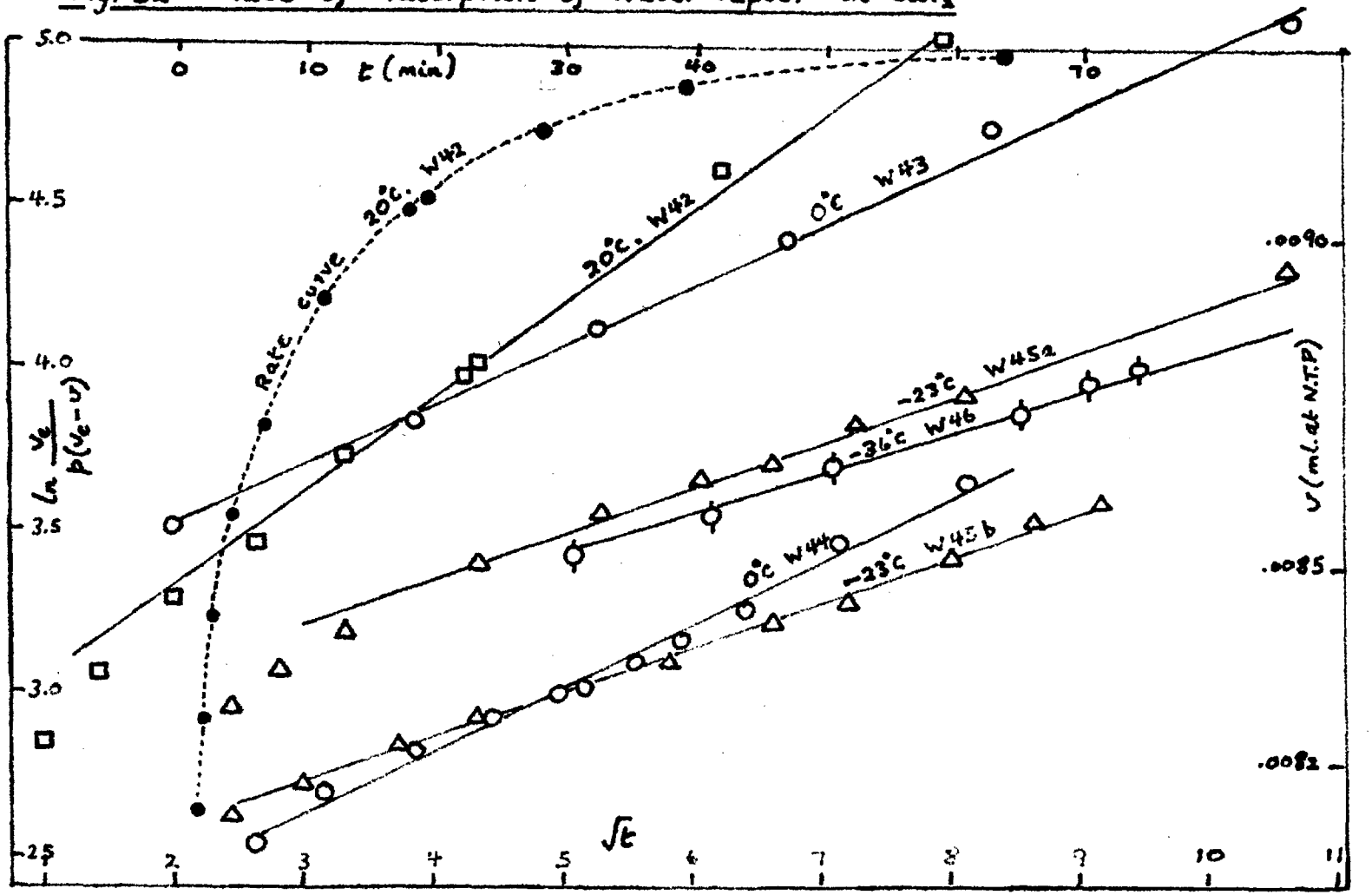

Table 21

Adsorbent	Run No.	Temp.°C	v_e (ml. at NTP)	k
CaF_2	W46	-36	.1305	.051
	W45a	-23	.056	.060
	W45b	-23	.090	.058
	W43	0	.0187	.079
	W44	0	.036	.084
	W42	20°	.027	.123
PbF_2	W37a	-23	.0282	.118
	W37b	-23	.0825	.058
	W39	0	.0365	.056
	W38	19.5	.0262	.070
AgI	W25	-23	.0415	.211
	W28	-15	.0343	.083
	W26	0	.026	.05
	W27	22	.0162	.082
PbI_2	W35a	-23	.220	.10
	W35b	-16	.189	.10
	W36	-17	.096	.093
	W35b	0	.143	.116
	W35c	22.5	.0675	.113

For CaF_2, k was independent of v_e and increased regularly with increasing temperature, indicating that k was of significance in terms of the activation energy for the adsorption process. However, such was not the case for the other adsorbents: this is illustrated by Fig.33, in which -log k is plotted against $^1/T$. With the exception of PbI_2, the behaviour seemed normal at temperatures down to 0°C, with activation energies ranging from about 1.3 kcal per mole for PbF_2 to 3.3 kcal per mole for CaF_2, but below this temperature the results were abnormal. The deviation was least marked with CaF_2, for which the activation energy in this

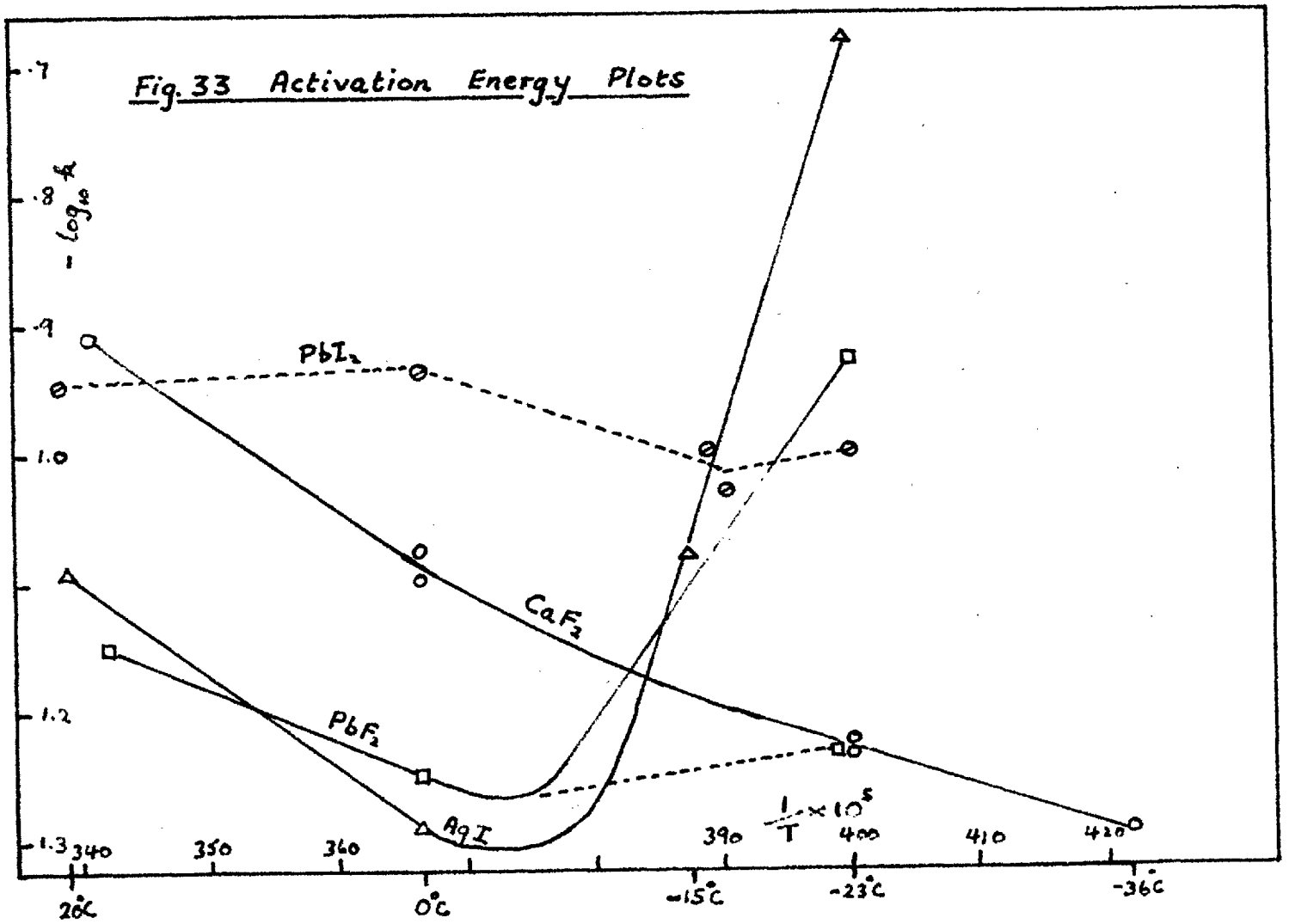
Fig. 33 Activation Energy Plots
$-\log_{10} \sigma$
·7
·8
·9
1.0
1.2
1.3
PbI_2
CaF_2
PbF_2
AgI
340
350
360
390
400
410
420
$\frac{1}{T} \times 10^5$
20°C
0°C
-15°C
-23°C
-36°C

range was 1.3 kcal per mole, but for the others the apparent activation energy was negative. This implied that a secondary process was taking place, rendering the Arrhenius equation inapplicable. PbI_2 was unique in that the abnormality was shown at both the high and low temperature ranges.

There seemed to be a parallel between these kinetic results and the adsorptive properties discussed in the previous sections. Thus PbI_2 was also shown to have a different type of heat curve than any of the others; and AgI and PbF_2 which had similar activation energy plots, both showed the same type of isosteric heat curve. Furthermore, CaF_2 was the only adsorbent for which the surface areas measured using krypton and water were the same, and was also the only adsorbent to show an almost normal activation energy plot.

Since the deviation was most marked with the silver iodide - lead fluoride group it is likely that the inversion was the result of lateral interactions as a secondary effect to that of diffusion of the adsorbate along the surface.

Table 22a. CaF_2 : Rate of Adsorption

Time, t (mins)			Pressure, p (mm x 10^{-3})			v (ml at N.T.P. x 10^{-2})			$\log_{10} \frac{v_e}{p(v_e - v)}$		
20°C	0°C W43	-36°C	20°C	0°C W43	-36°C	20°C	0°C W43	-36°C	20°C	0°C W43	-36°C
1	4	16	9.5	7.8	36.2	.79	1.79	12.8	2.842	3.498	3.207
2	28	21	7.7	5.4	34.6	.82	1.84	12.86	3.06	4.107	3.30
4	46	26	6.2	4.8	33.0	.85	1.85	12.9	3.283	4.3806	3.407
7	69	38	5.3	4.4	31.5	.87	1.86	12.93	3.458	4.719	3.531
11	114	51	4.25	4.25	30.0	.89	1.86	12.96	3.727	5.042	3.684
18	134	63	3.55	4.15	29.5	.90	1.86	12.97	3.977		3.748
19		73	3.45		28.8	.90		12.99	4.02		3.858
28		83	2.9		28.3	.92		13.0	4.104		3.940
39		89	2.6		28.0	.92		13.0	4.605		3.996
63.5		103	2.3		27.5	.93		13.03	5.017		4.132

Table 22b. CaF_2 : Rate of adsorption

Time, t (mins)			Pressure, p ($mm \times 10^{-3}$)			v (ml at N.T.P. $\times 10^{-2}$)			$\log_{10} \frac{v_e}{p(v_e - v)}$		
0°C W44	-23°C W45a	-23°C W45b	0°C W44	-23°C W45a	-23°C W45b	0°C W44	-23°C W45a	-23°C W45b	0°C W44	-23°C W45a	-23°C W45b
7	6	6	31.5	22.5	53.8	3.26	5.36	8.60	2.532	2.955	2.618
10	8	9	28.0	20.5	50.7	3.33	5.40	8.66	2.684	3.067	2.719
15	11	14	25.3	18.6	47.7	3.38	5.44	8.72	2.825	3.189	2.835
20	19	19	23.7	16.0	45.8	3.42	5.5	8.76	2.923	3.395	2.922
25	28	34	22.7	14.5	42.7	3.44	5.53	8.83	2.992	3.545	3.089
27	37	44	22.0	13.6	41.0	3.45	5.54	8.86	3.045	3.654	3.208
31	44	52	21.5	13.3	40.2	3.46	5.55	8.88	3.084	3.695	3.273
35	53	64	20.7	12.5	38.8	3.48	5.57	8.91	3.154	3.816	3.411
41	66	75	19.8	12.0	37.9	3.5	5.58	8.93	3.243	3.904	3.523
52	113	84	18.0	10.5	37.5	3.53	5.61	8.94	3.466	4.296	3.581
66			17.0			3.55			3.639		

Table 23. PbF_2 : Rate of Adsorption

Time, t (mins)				Pressure, p ($mm \times 10^{-3}$)				v, (ml at N.T.P. $\times 10^{-2}$)				$\log_{10} \frac{v_e}{p(v_e - v)}$			
19.5°C	0°C	-23°C W37a	-23°C W37b	19.5°C	0°C	-23°C W37a	-23°C W37b	19.5°C	0°C	-23°C W37a	-23°C W37b	19.5°C	0°C	-23°C W37a	-23°C W37b
6	9	6	10	51.0	47.0	9.38	42.7	1.97	2.99	2.70	7.78	1.901	2.074	3.435	2.621
12	17	12	17	38.0	34.1	7.21	37.8	2.21	3.24	2.74	7.88	2.233	2.423	3.771	2.778
21	22	16	26	30.2	30.5	6.55	33.8	2.36	3.31	2.75	7.97	2.527	2.555	3.908	2.939
32	27	22	37	25.6	27.9	5.94	31.0	2.44	3.36	2.77	8.02	2.775	2.661	4.062	3.073
42	63	27	43	23.2	20.3	5.52	30.2	2.49	3.51	2.77	8.04	2.949	3.118	4.202	3.118
55	73	32	53	21.6	19.4	5.11	28.8	2.52	3.53	2.78	8.07	3.097	3.203	4.36	3.204
67	83	37	62	20.4	18.5	4.90	27.6	2.54	3.54	2.79	8.09	3.234	3.286	4.48	3.289
82	93	40		19.6	18.0	4.89		2.56	3.55	2.79		3.348	3.349	4.481	
92	111			19.0	17.25			2.57	3.57			3.449	3.439		
	136				16.3				3.59				3.579		
	167				15.4				3.60				3.751		
	200				14.8				3.62				3.914		
	232				14.7				3.62				3.965		

Table 24. AgI : Rate of Adsorption

Time, t (mins)				Pressure, p (mm Hg x 10^{-3})				Volume, v (ml at N.T.P. x 10^{-2})				$\log_{10} \frac{v_e}{p(v_e - v)}$			
22°C	0°C	-15°C	-23°C	22°C	0°C	-15°C	-23°C	22°C	0°C	-15°C	-23°C	22°C	0°C	-15°C	-23°C
4	5	8	10	63.0	67.4	70.0	66.9	.76	1.57	2.47	3.37	1.476	1.574	1.719	1.902
8	8	14	23	48.5	54.9	55.1	39.6	1.0	1.81	2.77	3.92	1.750	1.780	1.977	2.675
14	11	25	26	38.6	48.7	43.3	37.6	1.21	1.93	3.01	3.97	2.010	1.905	2.277	2.787
32	25	33	33	27.9	35.3	39.2	33.4	1.41	2.19	3.09	4.05	2.439	2.261	2.415	3.121
46	33	43	35	24.5	31.5	34.0	32.9	1.47	2.26	3.19	4.06	2.643	2.395	2.640	3.188
53	46	51	43	23.4	27.8	32.8	30.5	1.49	2.34	3.22	4.11	2.729	2.559	2.701	3.602
67	56	61	46	21.4	26.0	31.2	30.1	1.53	2.37	3.25	4.12	2.920	2.647	2.795	3.691
84	71	78	48	20.1	24.0	28.6	30.0	1.55	2.41	3.30	4.12	3.077	2.768	2.989	3.725
104	86	81		19.0	22.3	28.3		1.57	2.44	3.31		3.263	2.880	3.015	
	104	99			21.1	26.2			2.47	3.35			2.980	3.235	
	126	120			20.0	25.0			2.49	3.37			3.08	3.429	
	152				18.7				2.51				3.223		
	201				17.5				2.54				3.40		

Table 25. PbI_2 : Rate of Adsorption

Time, t (mins)				Pressure, p (mm x 10^{-3})				Volume, v (ml at N.T.P. x 10^{-2})				$\log_{10} \frac{v_e}{p(v_e - v)}$			
22.5°C	0°C	-16°C	-23°C	22.5°C	0°C	-16°C	-23°C	22.5°C	0°C	-16°C	-23°C	22.5°C	0°C	-16°C	-23°C
7	10	15	9	17.9	25.6	28.2	15.8	6.4	13.9	18.5	21.8	3.063	3.171	3.304	3.8605
11	20	26	13.	10.1	16.8	21.9	13.3	6.5	14.1	18.7	21.9	3.568	3.613	3.619	4.068
17	29	36	21	6.6	13.7	19.2	11.3	6.6	14.2	18.75	21.9	3.940	3.853	3.811	4.294
23	35	54	32	5.2	12.2	15.9	9.9	6.65	14.2	18.82	22.0	4.159	3.993	4.140	4.503
36	45	65	49	3.6	10.5	14.9	8.4	6.69	14.2	18.84	22.0	4.494	4.198	4.275	4.829
66	51	76	59	2.0	9.8	1.42	7.8	6.71	14.2	18.85	22.04	5.034	4.307	4.406	5.003
83	56	89	65	1.5	9.6	13.3	7.7	6.72	14.3	18.87	22.04	5.305	4.349	4.634	5.059
100	60			1.2	8.9			6.73	14.3			5.516	4.464		
	67				8.4				14.32				4.576		
	73				7.9				14.32				4.699		
	80				7.6				14.33				4.812		

3.9. General Discussion : Conclusions

1. Effect of solubility

Among the several adsorbents studied, KCl is unique in that at low coverage the isosteric heats of adsorption in the lower temperature range are significantly lower than those at a higher temperature. This can be explained on the grounds that the former represents 'normal' behaviour, and on raising the temperature the surface ions at re-entrant corners or growth steps become partially hydrated. In the lower temperature range the preferred adsorption site is assumed to be above the centre of the lattice square, where the electrostatic field is zero. This is justified by the close agreement between the calculated and observed heats of adsorption.

2. Effect of the crystal structure of the adsorbent

The various insoluble adsorbents fall into two groups, i.e.

(a) CaF_2 and PbI_2

(b) Silver halides and PbF_2.

In group (a) the crystal structure of the underlying solid is an important factor in determining the adsorptive properties of water. The homo-ionic surface of fluoride ions in CaF_2 allows hydrogen bonding to the surface to occur as a precursor to two-dimensional condensation; and the heterogeneous layer lattice structure of lead di-iodide promotes the formation of liquid state clusters on a small fraction of the surface. For group (b), however, monolayer adsorption of water is largely independent of the structure of the adsorbent; the main factor being the lateral interactions (attractions) between

adsorbed molecules. Thus, although the crystal structures differ widely, from simple cubic for AgCl and AgBr, to zinc blende type for AgI, and α-$PbCl_2$ type for PbF_2, these four adsorbents show the same type of isosteric heat curve.

3. Effect of lateral interactions

The isosteric heat curve shown by the silver halide/PbF_2 group, in particular the occurrence of an inflexion in the early stages can be explained, semi-quantitatively, on the basis of nearest and higher neighbour interactions between molecules adsorbed in groups of two-dimensional square arrays. With both the groups of insoluble adsorbents the effect of lateral interactions is also reflected by,

i. its effect on rate measurements,

ii. the disagreement between water and krypton B.E.T. surface areas.

In i, the lateral interactions act as a secondary process to that of diffusion of the adsorbate along the surface, and render the Arrhenius equation inapplicable as a means of determining the energy of activation. Where this effect is least marked, i.e. for CaF_2 over the whole range of temperature, and AgI and PbF_2 above 0^oC, the observed activation energies of 2 to 3 kcal per mole agree with values obtained by other workers (section 1.8.). Since the Arrhenius equation is applicable to AgI and PbF_2 at temperatures above, but not below, 0^oC it is tentatively predicted that lateral interactions would not be important at the higher temperature.

In the case of ii, the wider the difference between the surface area values, the greater the effect of lateral interactions. This may be illustrated by the two extreme cases of PbI_2, where the water B.E.T. surface area is only about one-fifth that of krypton, and CaF_2 where the two surface areas are equal. The other adsorbents show varying differences between these two.

4. Heterogeneous nucleation and photo-decay

The nucleating efficiency of silver iodide does not seem to be related to its adsorptive properties up to the monolayer stage. Otherwise, there is no reason why AgCl, AgBr and PbF_2 should not be equally efficient. If Vonneguts hypothesis (section 1.1.) is accepted, the unique character of AgI must depend on the interaction between the adsorbent and more than one layer, perhaps in the form of a re-arrangement or phase change from square array to tetrahedral ice-like form. In contrast, the nucleating efficiency of lead iodide is apparently related to the ease of formation of liquid state clusters at an early stage.

It is known (124) that the nucleation activity of AgI is decreased by photochemical decomposition, as a result of the increase in interfacial surface energy caused by silver atoms produced on the surface. However, the experiments with silver bromide show the opposite effect, i.e. that production of surface silver is accompanied by a marked increase in heat of adsorption (decrease in interfacial energy) during the early stages of the

monolayer, although there is little change in the region of $\theta = 1$. Presumably silver iodide behaves similarly, in this respect, to the bromide, since both show the same monolayer adsorption characteristics. This further suggests, then, that the mechanism of nucleation of several layers on AgI is not related to the mechanism involved in building up the monolayer.

Bibliography

(1) **The Artificial Stimulation of Rainfall; Pergamon Press Ltd., New York (1957)**

(2) Vonnegut, Chem. Rev., 44, 277 (1949)

(3) Duran, Ann. Physik, (4), 87, 307 (1928)

(4) Frazer, Phys. Rev., 34, 644 (1929)

(5) Uhara and Nakamura, Bull. Chem. Soc. Japan, 12, 227 (1937)

(6) Brunauer, The Adsorption of Gases and Vapours, Vol.I, Oxford University Press (1943)

(7) Coulter and Candella, Z. Electrochem., 56, 449 (1952)

(8) Birstein, Journal of Meteorology, 12, 324 (1955)

(9) McBain and Bakr, J. Am. Chem. Soc., 48, 690 (1926)

(10) Halsey, J. Phys. Chem., 58, 330 (1954)

(11) Polly, Schaefer and Smith, J. Phys. Chem., 57, 469 (1953)

(12) Karasz, Champion and Halsey, J. Phys. Chem., 60, 376 (1956)

(13) Moskvitin, Dok. Akad. Nauk. SSSR, 122, 840 (1958)

(14) Jenkins, Private communication

(15) Price, Sherman and Wilkinson, Proc. Roy. Soc., 247A, 467 (1958)

(16) Papée and Laidler, Can. J. Chem., 36, 1338 (1958)

(17) Calvet and Prat, Microcalorimetric, Masson et Cie, Paris, 1956

(18) Young and Morrison, J. Sci. Instr. 31, 90 (1954)

(19) Benson, Can. J. Chem., 34, 1553 (1956)

(20) Papée, Journal of Meteorology, 16, 244 (1959)

(21) Papée, Journal of Meteorology, 16, 295 (1959)

(22) Papée, Can. J. Chem., 37, 375 (1959)

(23) Papée, Can. J. Chem., 36, 1443 (1958)

(24) Law, J. Phys. Chem., 59, 67 (1955)

(25) Theimer, Trans. Far. Soc., 48, 326 (1952)

(26) Ballou and Ross, J. Phys. Chem., 57, 653 (1953)

(27) Amphlett, Trans. Far. Soc., 54, 1206 (1958)

(28) Mays and Brady, J. Chem. Phys., 25, 583(L) (1956)

(29) Bowden and Throssel, Nature, 167, 601 (1951)

(30) Wicke, Z. Electrochem., 52, 86 (1948)

(31) Gregg, J. Chem. Soc., 563, July 1946

(32) Hickmott and Selwood, J. Phys. Chem., 60, 452 (1956)

(33) Pearce and Rice, J. Phys. Chem., 33, 692 (1929)

(34) Fiat, et al., Proc. Roy. Soc. A1302, 260, 409 (1961)

(35) Kurosaki, J. Phys. Chem., 58, 320 (1954)

(36) Langmuir, J. Am. Chem. Soc., 40, 1361 (1918)

(37) Volmer, Z. Phys. Chem., 115, 253 (1925)

(38) Fowler, Proc. Camb. Phil. Soc., 31, 260 (1935)

(39) Schwab, Catalysis, D. Van Norstrand and Co., New York, 1937

(40) Zeldowitsh, Acta Physicochim. URSS, 1,, 961 (1934)

(41) Baly, Proc. Roy. Soc., A160, 465 (1937)

(42) Polanyi, Verk. deut. physik. Ges., 16, 1012 (1914)

(43) Barrer and Brook, Trans. Far. Soc., 49, 940 (1953)

(44) Bering and Serpinsky, Dokl. Akad. Nauk, USSR, 114, No.6, 1254 (1957)

(45) Bratt, Ph.D. Thesis (1958)

(46) Brunauer, Emmett and Teller, J. Am. Chem. Soc., 60, 309 (1938)

(47) Hill, J. Chem. Phys., 15, 767 (1947)

(48) Halsey, J. Chem. Phys., 16, 931 (1948)

(49) Hüttig, Monatsh., 78, 177 (1948)

(50) Hill, J. Am. Chem. Soc., 72, 5347 (1950)

(51) Rosenberg, J. Am. Chem. Soc., 78, 2929 (1956)

(52) Beebe, J. Am. Chem. Soc., 67, 1554 (1945)

(53) Harkins and Jura, J. Am. Chem. Soc., 66, 1362 (1944)

(54) Innes and Rowley, J. Phys. Chem., 45, 158 (1941)

(55) Bangham, Trans. Far. Soc., 33, 805 (1937)

(56) Gregg, J. Chem. Soc., 696 (1942)

(57) Adamson, Phys. Chem. of Surfaces, Interscience Pub., 492 (1960)

(58) Harkins and Jura, J. Am. Chem. Soc., 66, 1366 (1944)

(59) Livingston, J. Chem. Phys., 12, 466 (1944); Loeser and Harkins, J. Am. Chem. Soc., 72, 3427 (1950)

(60) Hill, Advances in Catalysis, Academic Press Inc., New York, Vol.IV (1952)

(61) Hill, J. Chem. Phys., 17, 590, 668 (1949)

(62) Everett, Trans. Far. Soc., 46, 942 (1950)

(63) Kemball, Advances in Catalysis, Academic Press Inc., New York, Vol.II (1950)

(64) Halford, J. Chem. Phys., 2, 694 (1934)

(65) Lennard Jones and Dent, Trans. Far. Soc., 24, 93 (1928)

(66) Lenel, Z. Phys. chem., B23, 379 (1933)

(67) Orr, Trans. Far. Soc., 35, 1247 (1939)

(68) Müller, Proc. Roy. Soc. A154, 624 (1936)

(69) Moelwyn Hughes, Physical Chemistry, Pergamon Press (1957)

(70) Lennard Jones, Physica, IV, 10, 347 (1937)

(71) Rhodin, J. Am. Chem. Soc., 72, 5691 (1950)

(72) De Boer and Custers, Z. phys. chem., B25, 225 (1934)

(73) Barrer, Proc. Roy. Soc. (Lond.), A161, 476 (1937)

(74) De Boer, Advances in Colloid Sci., 3, 36 (1950)

(75) Chessick, Can. J. Chem., 33,, 251 (1955); J. Phys. Chem., 62, 489 (1958)

(76) Lennard Jones and Devonshire, Proc. Roy. Soc., 165A, 1, (1938)

(77) Fowler and Guggenheim, Statistical Thermodynamics

(78) Hill, J. Chem. Phys., 18, 988 (1950)

(79) Yang, J. Chem. Phys., 13, 66 (1945)

(80) Li, Phys. Reviews, 76, 972 (1949)

(81) Polanyi and Welke, Z. phys. chem., A132, 371 (1928)

(82) Semenoff, Z. phys. chem., B7, 471 (1930)

(83) Goldmann and Polanyi, Z. phys. chem., A132, 321 (1928)

(84) Jones and Gortner, J. Phys. Chem., 36, 387 (1932)

(85) Patrick and Kemper, J. Phys. Chem., 42, 369 (1938)

(86) Bangham, Proc. Roy. Soc., A138, 162 (1932)

(87) Harkins and Jura, J. Phys. Chem., 13, 535 (1945); 14, 117 (1946); 14, 344 (1946)

(88) Gregg and Maggs, Trans. Far. Soc., 44, 123 (1948)

(89) Ross and Winkler, J. Am. Chem. Soc., 76, 2637 (1954)

(90) Edelhoch and Taylor, J. Chem. Phys., 16, 490 (1948)

(91) Fisher and McMillan, J. Chem. Phys., 28, 549 (1958)

(92) Hodgson and McIntosh, Can. J. Chem., 37, 1278 (1959)

(93) Kawasaki, Bull. Electrotech. Lab. (Tokyo), 19, 825 (1955)

(94) Tiselius, J. Phys. Chem., 40, 223 (1936); Z. phys. chem., A174, 401 (1935)

(95) Beebe and Dowden, J. Am. Chem. Soc., 60, 2912 (1938)

(96) McBain, Z. phys. chem., 68, 471 (1909)

(97) Damköhler, Z. phys. chem., A174, 222 (1935)

(98) Bangham and Sever, Phil. Mag. (6), 49, 935 (1925)

(99) Isakawi and Kanamori, Bull. Inst. Phys. Chem. Research (Tokyo) 19, 1213 (1940)

(100) Keii, J. Chem. Phys., 25, 1283 (1956)

(101) Herzberg, Infra-Red and Raman Spectra of Polyatomic molecules, van Norstrand, New York (1945)

(102) Burnelle and Coulson, Trans. Far. Soc., 53, 403 (1957)

(103) Duncan and Pople, Trans. Far. Soc., 49, 217 (1953)

(104) Lonsdale, Proc. Roy. Soc., 247A, 424 (1958)

(105) Bernal and Fowler, J. Chem. Phys., 1, 515 (1933)

(106) van P. van Eck, Proc. Roy. Soc., 247A, 472 (1958)

(107) Handbook of Physics and Chemistry, Chem. Rubber Pub. Co., p.2324.

(108) Bennett and Tompkins, Trans. Far. Soc., 53, 185 (1957)

(109) Schulz, J. Chem. Phys., 17, 1152 (1949)

(110) Livingston, J.A.C.S., 66, 569 (1944)

(111) Huggins, J. Chem. Phys., 22, 1389 (1954)

(112) Mitchell, J. Photog. Soc., 5.

(113) Wyckoff, Crystal Structures, Interscience Pub.

(114) Bunn, Chemical Crystallography, Oxford Press, N.Y., 1946, p.59

(115) Emmett, Hill and Joyner, J.A.C.S., 73, 5102 (1951)

(116) International Critical Tables, Vol.5, p.113

(117) Guiaque and Archibald, J.A.C.S., 59, 561 (1937)

(118) Guiaque and Stout, J.A.C.S., 58, 1149 (1936)

(119) Drain and Morrison, Trans. Far. Soc., 49, 654 (1953)

(120) Coulson, Research, 10, 149 (1947)

(121) Mayer, J. Chem. Phys., 1, 270 (1931)

(122) Pauling, Proc. Roy. Soc., A114, 181, (1927)

(123) Hoare and Brindley, Proc. Roy. Soc., A159, 395 (1937)

(124) Fletcher, Faraday Society Conference, Sept. 1960